AN ABSTRACT OF THE THESIS OF

Yingxian Fu for the degree of Doctor of Philosophy in Chemistry presented on July 7, 1993

Title: Studies of Time-Resolved Fluorescence Spectroscopy and Resolved Absorption Spectra of Nucleic Acid Components

Abstract approved _ Redacted for Privacy
Malcolm Daniels

There is considerable uncertainty about dynamic aspects of the photophysics of the adenylyl chromophore, stemming from the discordant values reported for the room temperature fluorescence lifetimes (τ_1 = 5 ps, τ_2 = 330 ps for 9MeAde; τ_1 = 290 ps, τ_2 = 4.17 ns for ATP). Spectra reported in conjunction with these lifetimes create difficulties in assignment of emission. To clarify this situation I have investigated the fluorescence decay times and time-resolved emission spectra of adenylyl compounds under a variety of conditions (concentration, pH, solvent) using sub-ns laser excitation at 265 nm together with gated fast sampling (100 ps) detection and signal averaging. Multi-component decays and spectra are observed in aqueous solution. Major slow components (τ = 4.4 ± 0.2 ns) with emission maxima at 380 nm are found for all components at pH 1.1 and for ATP at pH 4.4. At pH 7 a fast component (<100 ps) predominates. There is no marked evidence for a concentration dependence, the oscillator strengths are 10^{-3} - 10^{-5} and

transitions must be classified as weakly forbidden. Single component emission is observed in acetonitrile and ethanol.

The UV absorption spectra of biomolecules d(CG) and polyd(GC)·polyd(GC) exhibit the different hypochromic effects due to different interactions between guanosine(G) and cytidine(C) in stacked form. The present work has been carried out to explain this quantitatively. To approach this problem the absorption spectra of G and C have been resolved into gaussian components using the PeakFit program. The absorption spectra (220-310 nm) of d(CG) and polyd(GC)·polyd(GC) have been fitted with gaussian components of G and C (in the order of increasing energy, G1 and G2, and C1, C2 and C3, respectively), and the contribution to both spectra from individual gaussians is estimated in terms of oscillator strengths. The fitting results suggest that the small hypochromism in absorption spectrum of d(CG) may be attributed to the interactions between G1 and C1; the large hypochromism in absorption spectrum of polyd(GC)·polyd(GC) probably originates from the interactions between G1, C1, C2 and C3.

The present work has also resolved a series of absorption spectra of cytidyl chromophore in different pH aqueous solution and various solvents.Time-resolved emission spectra of GMP, dCMP and m^5-dCMP in different pH aqueous solutions have been determined. The results show that pH affects the lifetimes and spectral characteristics of GMP significantly, but does not affect dCMP and m^5-dCMP.

STUDIES OF TIME-RESOLVED FLUORESCENCE SPECTROSCOPY AND RESOLVED ABSORPTION SPECTRA OF NUCLEIC ACID COMPONENTS

BY
YINGXIAN FU

A THESIS

submitted to

Oregon State University

in partial fulfillment of the
requirements for the
degree of

Doctor of Philosophy

Completed July 7,1993
Commencement June 1994

APPROVED

Redacted for Privacy

Professor of Chemistry in Charge of Major

Redacted for Privacy

Head of Department of Chemistry

Redacted for Privacy

Dean of Graduate School

Date thesis is presented July 7, 1993

Typed by Yingxian Fu

ACKNOWLEDGEMENTS

I would like to express my grateful thanks to my major professor Dr. Malcolm Daniels for his patient supervision, many valuable discussions and countless corrections in this manuscript.

Thanks also are due to Dr. Lucas P. Hart for his frequent assistance in experimental techniques, data analysis and useful discussions.

Finally, thanks to Mr. Dingguo Hu for his help in my initial data analysis.

To my husband and my son

TABLE OF CONTENTS

LIST OF FIGURES

List of Figures, Continued

List of Figures, Continued

List of Figures, Continued

List of Figures, Continued

List of Figures, Continued

LIST OF TABLES

List of Tables, Continued

List of Tables, Continued

LIST OF APPENDICES FIGURES

LIST OF APPENDICES TABLES

STUDIES OF TIME-RESOLVED FLUORESCENCE SPECTROSCOPY AND RESOLVED ABSORPTION SPECTRA OF NUCLEIC ACID COMPONENTS

1. INTRODUCTION

1.1 The significance of this research

It is well known that nucleic acid is the genetic material in living organisms. When solar UV irradiates human beings and animals it can have a deleterious effect due to radiation damage which causes a mutagenic effect on NA, and this eventually leading to the induction of skin cancer (Kripke and Sass, 1978). It is apparent that studying the photochemistry and photobiology of NA and searching for the molecular mechanisms of the effects of radiation on NA are very important for protecting the health of human beings and animals. In order to achieve this goal, it is necessary to have quantitative photophysical knowledge about the excited states of NA. Excited states may be detected and studied directly by their specific emission behavior -- fluorescence for singlet states and phosphorescence for triplet states. There have been difficulties in applying this approach to the nucleic acids. First, the observed fluorescence emission is usually very weak, due principally to quantum yields which are commonly ~ 10^{-4}. Second, nucleic acids contain four different chromophores (major bases), so that the emission can be heterogeneous. Third, in polymeric forms (oligonucleotides and naturely-occurring NAS), the chromophores are often arranged in closely stacked conformations in which excited states can interact leading to excimer-like states and emissions. Conventional steady state

fluorescence of NAS is thus difficult to study and complex in its interpretation. Furthermore steady-state methods of absorption and fluorescence spectroscopy, being primarily concerned with energy aspects of the molecule-radiation interaction, give only indirect access to the other characteristic of excited states, their dynamic behavior. This situation changed with the development of laser sources of excitation, particularly those with sub-nanosecond pulse widths, capable of undergoing second-harmonic generation to give UV radiation below 300 nm. These excitation capabilities, in conjunction with fast gated detection, have led to the extensive development of multi-component lifetime analysis and time-resolved spectroscopy in which complex emissions are resolved according to their individual component fluorescence lifetimes (Lakowicz, 1988, 1990). In this thesis these methods will provide us with information about emission lifetimes, time resolved emission spectra, electronic transitions and oscillator strengths.

1.2 General photophysics of organic molecules

The absorption of UV or visible light by a molecule produces an electronically excited state. Since both ground and excited states possess multiple vibrational levels, the transitions from the ground state to excited state (photoabsorption) or vice versa (photoemission) take place to various vibrational levels either in the excited state or in the ground state. In the case where a molecule is excited to higher electronic levels, transitions from the higher energy state (S_n) to the lowest excited state (S_1) (internal conversion) occur with

dissipation of the excess vibrational energy to solvent. This process usually occurs within a much shorter time than the fluorescence lifetime, particularly in condensed phases, so that fluorescence is usually observed only from the lowest singlet excited state.

The photophysical pathways which dissipate the energy of the singlet S_1 state are classified into radiative and non-radiative processes. For our purposes, the most important and informative decay process is fluorescence ($S_1 \rightarrow S_0 + h\nu$). Other processes include intersystem crossing to the triplet state ($S_1 \rightarrow T_1$ + heat), radiationless decay and intramolecular chemical reaction pathways. The lowest triplet excited state decays by a radiative path (phosphorescence, $T_1 \rightarrow S_0 + h\nu$) or radiationlessly (intersystem crossing, $T_1 \rightarrow S_0$ + heat) to the ground state. These photoprocesses are illustrated in the Jablonski state diagram in Figure 1.1.

The yield of each of these emission processes is expressed as a quantum yield ϕ, which is defined as:

ϕ = number of photons radiated / number of photons absorbed

Following the Einstein formulation of the absorption/emission processes (Einstein, 1917) an intrinsic emission lifetime τ_0 is defined as the reciprocal of the rate constant k_r for emission. The relationship between ϕ and τ_0 can be described as $\phi = \tau/\tau_0$ where τ is the actual emission lifetime in the presence of intramolecular quenching. Thus measurement of the singlet lifetime τ_f and quantum yield ϕ_f for fluorescence makes it possible to obtain the radiative lifetime τ_0. τ_0 also can be calculated from spectral data using the Strickler-Berg equation (Strickler and Berg, 1962):

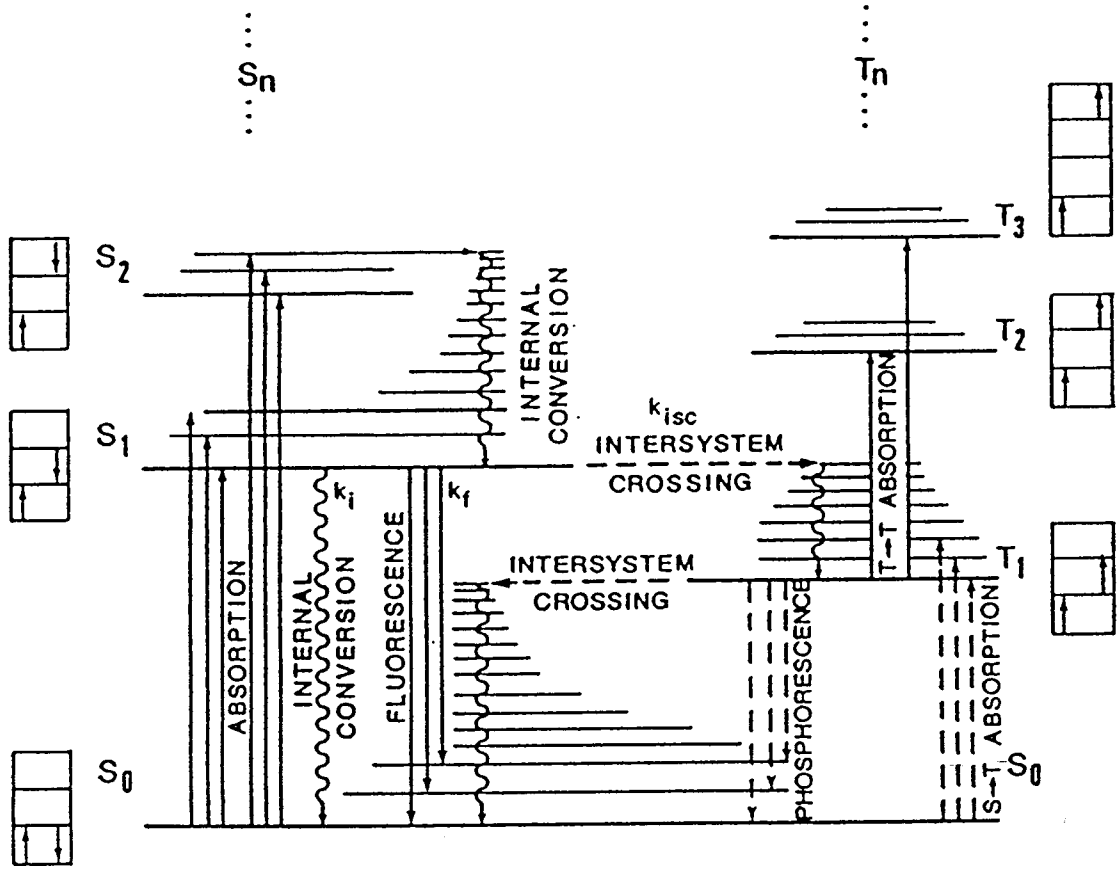

Figure 1.1 A Jablonski diagram showing the lowest singlet and triplet states of a typical molecule and identifying the various transitions.

$$1/\tau_0 = 2.880 \times 10^{-9}\, n^2 \langle \bar{\nu}^3 \rangle^{-1} (g_l/g_u) \int \varepsilon \, d\ln\bar{\nu}$$

where n is the refractive index of the medium; $\langle \bar{\nu} \rangle$ is the average wavenumber of the transition; g_l and g_u are the degeneracies of the lower and upper states respectively, and ε is molar extinction coefficient.

This relation, obtained by extending the 2-level atomic model to molecules, is applicable to isolated and correlated transitions. It holds true only if most of the intensity in the absorption is due to single electronic transition. These conditions usually are indicated when the absorption and fluorescence spectra show a mirror image relationship. Errors are introduced into the calculated lifetimes if there are weaker bands lying in the same region as the observed absorption band and if the emissions are composite (a topic in my thesis work).

The oscillator strength f has been developed to provide a theoretical reference for comparing the intensities of the spectroscopy transitions (Mulliken, 1939). The oscillator strength is the ratio of the strength of a transition to the strength of a transition for an electron oscillating harmonically in three dimensions. The oscillator strength for an actual transition may be calculated from the measured absorption coefficient integrated over the absorption band

$$f = 4.32 \times 10^{-9} \int \varepsilon \, d\bar{\nu}$$

where ε is extinction coefficient and $\bar{\nu}$ is wavenumber. Allowed transitions yield oscillator strengths of approximately unity. Forbidden transitions have oscillator strengths (orders of magnitude) much less than unity. The oscillator strength is inversely proportional to the radiative lifetime τ_0:

$$f = 1.47/\bar{\nu}^2\tau_0$$

Accordingly, a weak transition, which possesses a small oscillator strength, has a long intrinsic lifetime and vice versa.

From a theoretical viewpoint the intensity of a transition can be described in terms of a transition moment having both magnitude and direction with respect to the molecular geometry because in principle this can be calculated from approximate MO theory. Electromagnetic radiation is able to induce a transition between two molecular energy states provided that there exists a molecular electronic or magnetic moment with which the radiation field can interact. Restricting attention to the dominant interactions between electrical dipoles and the electric field component of the radiation, the molecular quantity of relevance is the expectation value of the dipole operator between the two states called the electric dipole transition moment:

$$\mu_{if} = \langle\psi_f|\mu|\psi_i\rangle,$$

where ψ_i and ψ_f are the wavefunctions associated with the initial and final state. The strength of the interaction between the electric field and this vectorial molecular quantity will depend on the orientation of the transition moment relative to that of the field as well as the magnitude of the moment.

The transition dipole moment can be related with the oscillator strength through:

$$f = (8\pi^2 mc)/3h\nu)\,|\mu_{if}|^2$$

where m is mass of the electron, c is velocity of light in vacuum, hν is the

energy used for excitation, and $|\mu_{if}|$ is the magnitude of transition dipole moment.

1.3 Photophysics of NA monomers

The electronic structure and excited state dynamics of NA and its components have been studied extensively since the period 1960-70. The absorption spectra of monomeric nucleic acid components (NAC) such as nucleobases, nucleosides, nucleotides (structures and names shown in Figure 1.2) in aqueous solution are known to exhibit broad overlapping bands with λ_{max} in the range 250-270 nm (Voet, et al, 1963). By comparing these spectra with those of ribose and ribose-phosphates one can see that absorption spectra of nucleosides and nucleotides in this wavelength range above 220 nm is mainly determined by the absorption of the bases: the NA chromophores. The absorption of NA bases in this spectral region is mainly due to allowed $\pi\pi^*$ electronic transitions of pyrimidine and purine rings. When a NAC molecule absorbs a photon in the linear regime, it passes to the first excited electronic singlet state S_1. Along with photochemistry (by which is meant bond deionization, rearrangement or isomerization), vibrational and many possible electronic deactivation processes of excited states can occur(see Jablonski diagram in Figure 1.1).

The first report of room temperature fluorescence from the NA bases was by Daniels and Hauswirth (1971) who reported both quantum yields ϕ_f's and

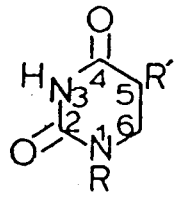

PYRIMIDINES

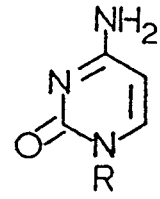

U, R'=H R=H
Urd, R'=H R=ribose
UMP, R'=H R=ribose phosphate

T, R'=Me R=H
Thd, R'=Me R=deoxribose
TMP, R'=Me R=deoxribose phosphate

C, R=H
Cyd, R=ribose
CMP, R=ribose phosphate

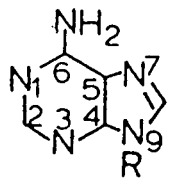

PURINES

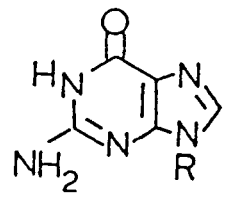

A, R=H
Ado, R=ribose
AMP, R=ribose phosphate

G, R=H
Guo, R=ribose
GMP, R=ribose phosphate

Figure 1.2 Structure and names of nucleic acid monomers. Bases: U, uracil; T, thymine; C, cytosine; A, adenine. Nucleosides: Urd, uridine; Thd, deoxythymine; Cyd, cytidine; Ado, adenosine. Nucleotides: UMP, uridine monophosphate; TMP, deoxythymidine monophosphate; CMP, cytidine monophosphate; AMP, adenosine monophosphate; GMP, guanosine monophosphate.

excitation spectra as well as corrected fluorescence spectra. Since then both their emission and absorption spectra at low and room temperatures have been widely studied (Daniels, 1976; Callis, 1983; Nikogosyan, 1990; Cadet and Vigny, 1990).

Conventional luminescence methods were used in conjunction with digital signal sampling and averaging to measure the true (corrected) fluorescence spectra and thence the quantum yields of NAC in aqueous solutions (Daniels and Hauswirth, 1971; Vigny and Ballini 1977; Callis, 1979; Morgan and Daniels 1980). The fluorescence spectra together with the absorption spectra allowed τ_0's to be estimated, and this together with the quantum yields showed that actual fluorescence lifetimes must be in the picosecond (ps) range. Currently available quantum yields and emission maximum for the S_1 levels of NAC molecules in aqueous solutions at room temperature are listed in table 1.1. The ϕ_f's which are on the order of 10^{-4}, are considered correct today. Between pyrimidine bases and corresponding nucleotides no major differences in ϕ_f are observed although they are not identical, whereas for the purines the bases fluoresce several time more intensely than nucleosides or nucleotides. One explanation for this is that the fluorescence of adenine and guanine occurs from the minor 7-H tautomer form, which fluoresces several times more strongly (Eastman, 1969; Wilson and Callis, 1980).

The first room temperature excitation spectra of the NA bases (Daniels and Hauswirth, 1971) exhibited significant deviations from their respective absorption spectra. The excitation maxima were all shifted 5-10 nm to wavelength

Table 1.1 Quantum yields and emission maxima of excited electronic state S_1 of NAC molecule in aqueous solutions at room temperature*

Molecule	$\phi_f \times 10_4$	$\lambda_{f,max}$(nm)
Adenine	2.6	321[a]
7-MeAdenine	8.2	310[b]
Adenosine	0.5	310[b]
AMP	0.5	312[c]
ApA	1.8	315,(360,400,440)*[,d]
polyA	2.7	315,405[d]
Guanine	3.0	328[e]
GMP	0.8	340[c]
GpG	1.3	350[c]
polyG	4.7	342[c]
Cytosine	0.8	313[a]
Cytidine	0.7	324[b]
CMP	1.0	320[d]
CpC	1.9	320[d]
polyC	1.6	335[d]
Thymine	1.0	338[e]
Thymidine	1.0	327[b]
TMP	1.2	330[c]
polyT	1.0	328, 400**[,c]
Uracil	0.5	309[a]
UMP	0.3	320[c]
polyU	0.4	322,(380)[c]
polyA-T	1.8	(330),415[c]
polydG.polydC	1.3	335, 395[c]
DNA	0.2	349[a]

*Taken from Callis, 1983 and Nikogosyan 1990.
*Parentheses indicate shoulder.
**Believe due to photoadducts.
[a]Daniels and Hauswirth, 1971; [b]Knighton, 1980; [c]Vigny and Ballini, 1977; [d]Morgan and Daniels,1980; [e]Hauswirth and Daniels,1971.

longer than the corresponding absorption. Because of the low ϕ_f's it was recognized that a minor tautomeric or impurity species could dominate the fluorescence, provided it was intrinsically much more fluorescent than the main species.

A fundamental quantity of interest is τ_0. This in general can not be directly determined by experiment. It may be estimated indirectly in two ways. First, as indicated above, it may be calculated from absorption and emission spectra (Strickler-Berg). Second, it may be obtained from the experimental quantum yield and experimental fluorescence lifetime by the relation $\tau_0 = \tau_f/\phi_f$.

The S-B method was first used (Daniels & Hauswirth, 1971) when emission spectra had been measured. These estimates depend on limits of integration which were chosen to approximate the first excited state. Table 1.2 lists the estimated τ_0 calculated from different authors. Column (a) corresponds to the integration over the entire absorption band; column (b) refer to the partial absorption based on fluorescence excited spectra (attributed at that time to possible tautomers). The different values obtained by Callis (1978) may reflect his use of uncorrected emission spectra and possible different limits on integration. The values used by Vigny and Duquesne (1976) have been determined from their own quantum yields (relatively to that reported by D and H for adenine) and their estimated fluorescence lifetimes.

Estimation of τ_0 by the second method requires determination of τ_f. This has proved to be very difficult, as it was early shown that these fluorescence lifetimes must be in the low ps range. At the time of writing, only a few actual

Table 1.2 Estimated intrinsic radiative lifetimes τ_0 of various NAC molecules in aqueous solution at room temperature by Strickler-Berg method

Compound	τ_0 (ns)			
	D & H[a]		Callis[c]	Vigny[b]
	(a)	(b)		
Ade	3.8	34	3.9	
AMP				6.0
Gua	4.7	10	7.8	
GMP				6.3
Cyt	2.5	11	7.7	
CMP				10
Thy	14	28	7.0	
TMP				6.7
Ura	7.1	14		
UMP				10

[a]Daniels and Hauswirth, 1971.
[b]Callis, 1978.
[c]Vigny and Duquesne, 1976.

lifetimes of NAC have been determined (Rigler, 1985; Yamashita, 1987) by picosecond laser spectrophotofluorometry. Rigler and co-workers used time-correlated single-photon counting with additional refinements to improve time resolution, which appears to be the most sensitive method for fluorescence decay measurement. However, it still suffers from the FWHM of the detector response limitation (43 ps). Yamashita et al. performanced decay time analysis by the use of a very expensive streak camera. The streak camera can directly registers the ultrafast high decay. The basic principle is to transform a time-dependent signal into a space-dependent optical image. But, this temporal technique is also restricted on the FWHM limitation (60 ps) of the instrument response time (Yamashita, 1986).

Direct measurement of relative transition moment directions can come from polarized crystal absorption spectra. Unfortunately this has only been carried out for the adenylyl system, specifically 9-methyladenine (Stewart and Davison, 1963). Most work has utilized linear dichroism of molecules or systems partially oriented by flow (Matsuoka and Nordén, 1982), circular dichroism studies (Sprecher and Johnson, 1977), and polarized reflection spectra of crystals (Novros and Clark, 1986). Recent compilation of transition moment directions of $\pi \rightarrow \pi^*$ transition in NA bases are listed in table 1.3. These remain some uncertainties for three of the chromophores as follows: i) G; There are some discrepancies between experimental data (polarized reflection spectra (Clark, 1977)) and theoretical calculations. A number of MO calculations predict a reverse ordering of band I and II with regard to polarization and intensity (Hug

and Tinoco, 1973; Ito and I'Haya, 1976; Srivastava and Mishra, 1979). ii). A; The directions and relative strengths of the two lowest energy transitions have not been settled. There currently are three resolutions of this band available (Stewart and Davison, 1963; Fornasiero et al., 1981; Clark, 1989, 1990). As this relates to a main topic of this thesis (Part III) it will be presented and discussed at a later stage. iii). C; The experimental result (table 1.3) shows that there exist four electronic transitions in the range of 200-270 nm, while the MO calculations predict that there are only three transitions in that range. The discrepancy between experimental and theory is not yet resolved and will be discussed in Part IV.

1.4 Photophysics of dinucleotides and polynucleotides

The dinucleotides have been drawn a lot of attention in the past twenty years as the simplest polymeric form of monomer constituent of nucleic acids, and the elucidation of their structures and conformation in aqueous solution are of great interest. It was early recognized that the stacking forces which stabilized the characteristic helical structures lead to an equilibrium distribution of partially ordered structures in the dinucleotides and the existence of such ordered structures has been inferred from NMR shift (Hosur et al., 1981) and hyposhromism in UV absorption changes (Cantor and Schimmel, 1980).

The room temperature fluorescence of dinucleotides and polynucleotides was first reported by Vigny and co-workers (Vigny and Duquesne, 1976; Vigny and Ballini, 1977). In addition to monomer fluorescence ApA exhibits a second,

Table 1.3 Absorption transition moment directions of $\pi \rightarrow \pi^*$ transition in NA bases*

Adenine					
λ/nm	290	263	230 or 200	-	Matsuoka & Nordén, 1982
θ/deg	?	10 or 25	-75 or -45	-	Clark,1990
Guanine					
λ/nm	280	248	<220	<200	Clark, 1977; Matsuoka &
θ/deg	4	-88	90	0	Nordén, 1982
Cytosine					
λ/nm	270	260	220	200	Matsuoka & Nordén, 1982
θ/deg	5	-40	75	-27 or 86	Clark,1986
Thymine					
λ/nm	260	210	-	-	Matsuoka & Nordén, 1982;
θ/deg	-30	60	-	-	Novros & Clark,1986
Uracil					
λ/nm	260	210	-	-	Matsuoka & Nordén, 1982;
θ/deg	-10	60	-	-	Novros & Clark,1986

*Taken from Norden et al, 1992.

long wavelength fluorescence with a peak near 410 nm. CpC and GpG apparently show only monomer-like (unstacked form) fluorescence (Table 1.1). The long wavelength band of ApA is very temperature independent and seems to be connected with increasing stacking, and it has been assigned as excimer fluorescence. The polynucleotides polyA and polydA-T exhibit predominant excimer-type fluorescence near 410 nm, which is also very temperature-dependent. It also can be seen from Table 1.1 that ϕ_f's generally increase slightly in the order of monomer → dinucleosides → polynucleotides. It is suggested that the internal conversion process may be slowed down by delocalization of excitation.

Ballini et al. (1991) studied the sequence isomer d(AT) and d(TA) using synchrotron excitation. Two-component analysis for both d(AT) and d(TA) gave identical very fast component (τ<100 ps) spectra which were considered to originate from unstacked fraction; ns components, τ = 4.7 ns for d(AT) and 3.7 ns for d(TA), which were successfully analyzed as sum of the gaussians and it was suggested that they originate in different stacking geometry. Daniels et al. (1988) studied ApC and CpA systems by cw spectroscopy and polarization analysis and found the similar characteristics of stacking form as above. Another interesting thing they found is the evidence for left-handed stacked conformation by comparison with circular dichroism and NMR literature (Bobruskin et al, 1980; Doornbas et al, 1983). Following this, direct experimental evidence of the left-handed helical Z form from the emission spectra of the trimer of dinucleotides $d(GC)_3$ was observed (Daniels et al., 1990). The interest in this is

that the Z-structure offers a precisely characterized stacking geometry which is quite different from the right-handed helical B-structure. They reported that there are three components in emission, a weak shoulder near onset with ps lifetime which was considered to be attributed to a monomer-like emission, a clear peak at 360 nm and broad longer-wavelength component which were considered to be stacked emissions. The striking feature which distinguishes the spectrum from B-DNA is the strength of the long-wavelength component, and this may be a distinguishing characteristic of Z form.

In summary, work over the last three decades has yielded considerable progress, yet today our understanding of excited states structure and dynamics of nucleic acids remains fragmented and incomplete. In the present work, I made my effort to study the time-resolved fluorescence spectroscopy and resolved absorption spectra of some nucleic acid components. In contrast to the conventional CW fluorescence spectroscopy, quite distinctive information on the nature of emitting states can be obtained by studies of time-resolved fluorescence spectroscopy. The measurement of the fluorescence lifetimes can lead to values for intrinsic radiative lifetimes and hence to oscillator strength for transitions from the excited states to ground. The time-windowed fluorescence spectral studies also allow the resolution of multicomponent emission spectra into individual components.

Resolved absorption spectra of monomers can provide the information about the number of the electronic transitions, which may be used to fit the absorption spectra of their dimer and polymer, and then, along with the

conformation parameters of DNA and experimental transition moment orientations and oscillator strengths the interactions between monomers in the dimer and polymer may be clarified.

2. EXPERIMENTAL METHODS

2.1 Materials

Compounds: ATP, ADP Ado, GMP, CMP AND ^{5}m-CMP were purchased from Sigma; AMP was obtained from Calbiochem.

Solvents: Acetonitrile (MeCN, spectroscopically Pure) is a product of Matheson $ Bell, and ethanol (EtOH, Analytical Pure) is a product of USI Chemical Co.

Phosphate-buffered solutions (pH 7.0) were prepared using water triple-distilled over alkaline permanganate and acid dichromate in a stream of purified oxygen. Unbuffered solutions was made in triply-distilled water. Acidic solutions (pH 1.1) were obtained using 0.1 M $HClO_4$.

The fluorescence impurities of all above solvents and blank solutions were very low. This was demonstrated by measuring ratios of Raman scattering (solvent) to fluorescence signal in one time-windowed spectrum (delay 0) observing the ratios to be larger than 50:1. Addition of buffer decreases the ratio to 22:1 (Figure 2.1). It is recognized that Raman scatter is intrinsically a very weak process (Herzberg, 1945) and thence this demonstrates the purity of the system and the low background to which it gives rise.

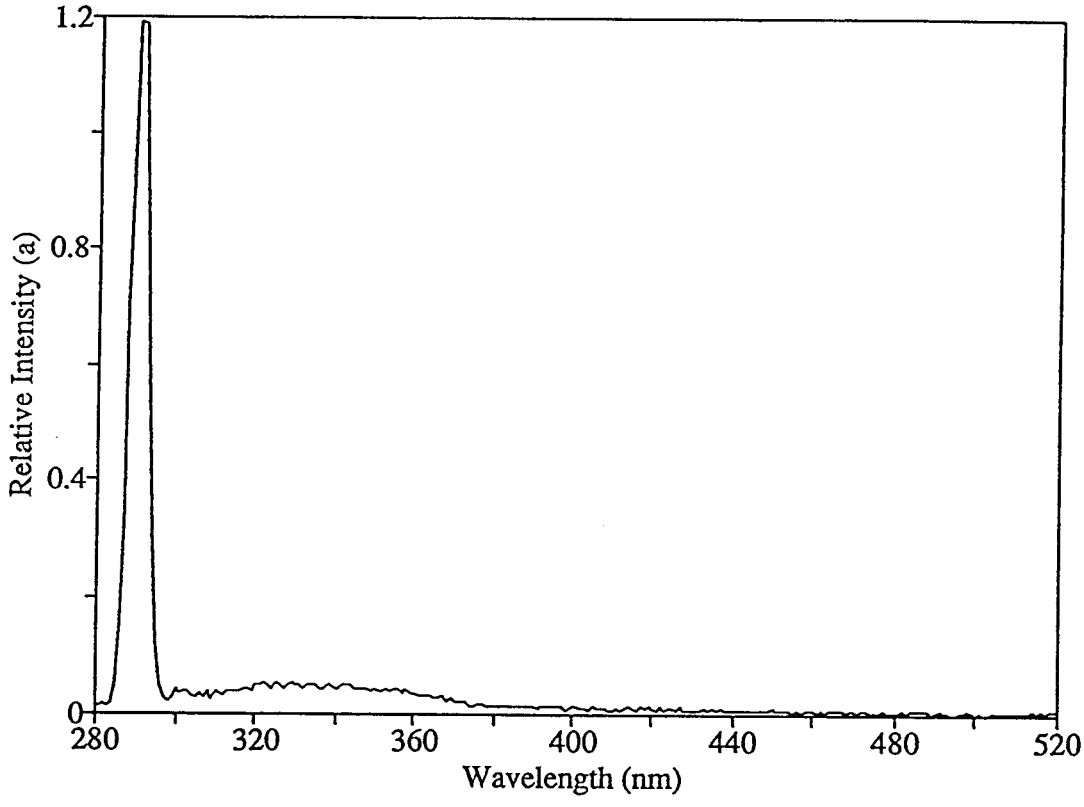

Figure 2.1 Time-windowed emission spectra of phosphate buffer ($4x10^{-3}$ M) solution (pH 7.0). Delay time: 0 ns.

2.2 Instruments

Samples for excitation were contained in 1 cm x 1 cm high-purity silica cuvette. Pulsed excitation radiation at 265 nm (band width 0.04 nm) was produced by frequency-doubling the output from a nitrogen-pumped dye laser (Coumarin 485 (Exciton) at 10 Hz, with a pulse width of 600 ps and pulse energy (at 265 nm) of ~ 2 J. Fluorescence was monitored at the appropriate wavelengths through an f/3.5 holographic-grating monochromator (ISA H-10, bandwidth 8 nm), by a Hamamatsu R2055 photomultiplier (0.7 ns rise time and 0.8 ns transit time jitter). Data was acquired by a computer-scanned fast sampler (SRS 255) with a 100 ps gate width and SRS 245 computer interface module into an IBM PC-XT. The system allows digital averaging of the signal by accumulation to any desired extent during the acquisition stage. Typically decay waveform were measured by scanning over a delay range of 25 ns, with a 0.1 ns delay increment and averaging 64 or 128 scans. A baseline was obtained subsequent to each decay waveform. If the fluorescence signal of the sample is not strong, such as ATP in buffer system, the fluorescence of the blank solution will be measured immediately following sample measurement and subtracted from the sample signal. Emission spectra were acquired with a wavelength scan in 1 nm increments, typically averaging 64 or 128 samples at each wavelength. The schematic diagrams of optical system and data acquisition are shown in Figure 2.2 and 2.3 respectively. The detailed technical information about this instrument was described by Hart and Daniels (1992).

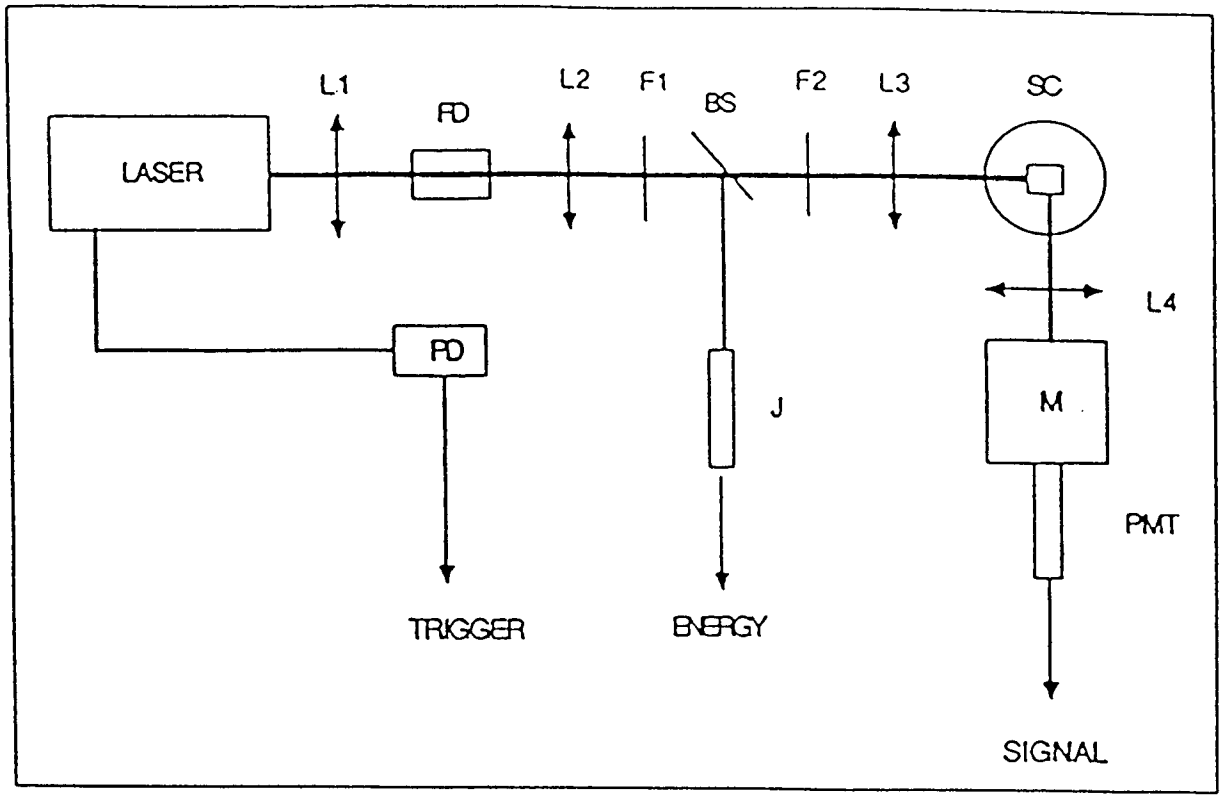

Figure 2.2 Schematic diagram of time-resolved fluorescence detection system. Legend: **BS**, beam splitter; **F**, filter (1, UV pass; 2, neutral density); **FD**, frequency doubler; **J**, pyroelectric joulemeter; **L**, lens; **M**, monochromator; **PD**, photodiode; **SC**, sample chamber (taken from Hart & Daniels, 1992).

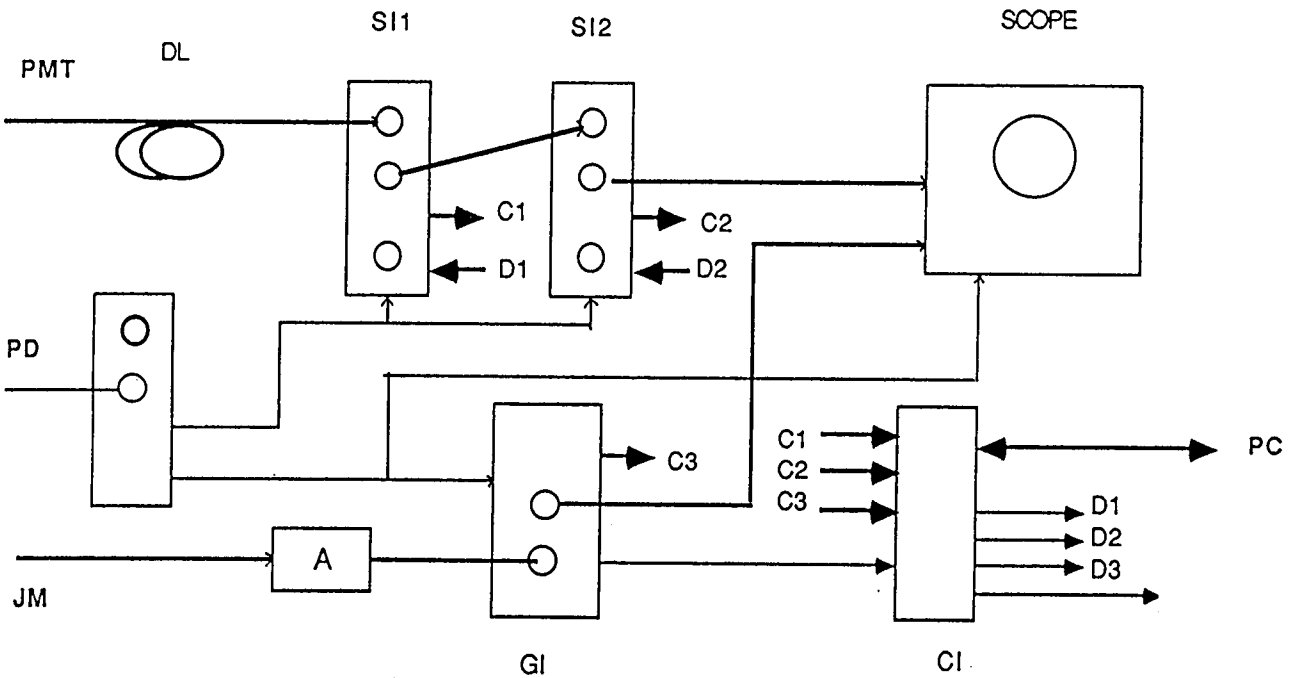

Figure 2.3 data acquisition system.

A---Amplifier
C#---Channel number in the computer
CI---Computer interface
D#---Delay times for different samplers
DL---Delay line
GI---Gate integrator
JM----Joule meter
PC----Computer
PD----Photodiode
PMT---Photomultiplier
SI#---Sampler

2.3. Data Analysis

2.3.1 The non-linear least squares reiterative convolution program for lifetime analysis

Non-linear least squares analysis (NLLS) using iterative convolution is the most commonly used and widely accepted method for determining lifetimes from noisy data. The fluorescence lifetimes in present work were determined with a NLLS program SPLMOD from European Molecular Biology Laboratory (Vogel, 1986). There are several features in this program:

1. It uses a cubic B-spline approximation to the fitting function; this approximates the model function within 4 significant figures (Provencher and Vogel, 1983), so that, after some preliminary computation, the analysis is independent of the number of data points and the number of exponential terms. Thus the program runs considerably faster than conventional NLLS programs.

2. The program runs repeatly a number of times (typically 20 times) for each model using different starting values until the termination criterion (see later) is reached.

3. A separable modified Gauss-Newton algorithm is used for the estimation of the parameters of the model function and this facilitates the inclusion of linear terms in the model function parameters to account for background signal, scatter, and correction for small time shift errors.

4. Global analysis can be carried out, i.e. several decay curves can be analyzed simultaneously with the requirement that they have lifetimes in

common; this can result in improved estimates because of decreasing the number degrees of freedom.

The program is based on the convolution:

$$Y(\lambda,t) = E(t) * F(\lambda,t) + \varepsilon(t)$$

where $Y(\lambda,t)$ is the measured waveform (observed signal).

$E(t)$ is instrumental system impulse response function (IRF).

$F(\lambda,t)$ is the function to be determined.

* represents convolution.

$\varepsilon(t)$ is the noise signal.

$F(\lambda,t)$ is in general taken to be a sum of independent exponential terms

and $$F(\lambda,t) = \sum_{i=1}^{N_i} \alpha_i(\lambda)\exp(-t/\tau_i)$$

where α_i and τ_i are preexponential coefficient and lifetime for component i, respectively, in condensed phase. Both of them are parameters of interest for N_i components. The instrument response function may be estimated using a scattered light signal under the same experimental conditions as the sample measurement. The SPLMOD provides the option of including linear terms which might contribute to the observed signal, i.e.:

$$Y(\lambda,t) = E(t) * F(\lambda,t) + G(t) + \varepsilon(t)$$

where $G(t) = \sum_{j=1}^{N_j} g_j(t)$, N_j is the number of linear correlation terms.

Examples of gi(t) used include:

$g_1(t) = 1$, i.e. a constant background in the sample.

$g_2(t) = E(t)$, a contribution from scatter, or a very fast decay.

$g_3(t) = E'(t)$ a small time shift error term.

The best parameters α_i and τ_i are estimated by iterative convolution with the system impulse response using trail values for the parameters, and comparing the result with observed waveform. The process is continued, using new trial values determined by particular NLLS method employed until goodness-of-fit or other criteria such as standard error for the lifetime, randomness of residuals and their auto-correlation are satisfied.

The evaluation criteria can be expressed as:

Standard Deviation of fit = Stdfit = $[VAR/(N_y-2N_a-N_r)]^{1/2}$

and $$VAR = \sum_{k=1}^{N_y} W_k(Y_k - \hat{Y}_k)^2$$

where VAR is the variance, W_k is an optional weight, Y_k is the observed signal, $\hat{Y}_k$ is the model function, and N_y, N_a and N_r correspond to the total number of data points, non-linear terms (α_i and τ_i), and linear terms in the model function, respectively. $(N_y-2N_a-N_r)$ is the number of degrees of freedom.

The termination criterion for stopping the iterative search for the minimum of VAR is

$$|VAR - VAR_{old}| \leq \max \{VARMIN, VAR_{old} \cdot CONVRG)$$

where VAR_{old} is the variance from the last iteration and

$$VARMIN = \sum_{n=1}^{N_D} \sum_{k=1}^{N_{yn}} (w_{kn} y_{kn} \cdot CONVRG)^2$$

where N_D, N_{yn} correspond to the number of different data sets and number of data point in each set respectively; w_{kn}, y_{kn} denote the optional weight and observed signal respectively for kth data point and nth data set; and CONVRG defines the maximum relative accuracy of the data. The default value CONVRG = 5×10^{-5} is designated, i. e., the data has at most four figures accuracy.

The apparatus and procedures have been validated (Hart and Daniels, 1992) using several extensively investigated reference compounds viz NADH (reduced nicotinamide adenine dinucleotides) with a lifetime of 0.4 ns, L-tryptophan with a two-component decay, $\tau_1 = 0.7$ ns, $\tau_2 = 3.2$ ns in which the fractional emission $\alpha_1\tau_1/(\alpha_1\tau_1+\alpha_2\tau_2) \sim 0.06$ at 320 nm, and p-terphenyl with $\tau =$ 0.9 ns.

For all models the standard deviation of the fit have been determined as a function of an arbitrary time shift (in 0.2 channel increment, i.e. 20 ps) and the results have usually been selected for the time shift at which the standard deviation of fit was a minimum. The effect of positive or negative shift can result in appearance or disappearance of fast component. Although sometimes a smaller standard fit may be obtained at larger shift the numerical lifetime analysis may not reflect the true situation but result in an artefact. In principle, the intrinsic lifetime should not be changed with the time shift, if it has a significant change after a large positive or negative time shift, the lifetime result

will be suspected and eliminated, and then the second best standard fit at a smaller time shift will be carried out until a reasonable solution is reached.

2.3.2 Time-resolved emission spectra (TRES) program for time-windowed spectra analysis

In a mixture of two fluorophores, time-windowed spectral (TWS) measurements can directly yield the emission of the separate components only if their lifetimes are quite different and lie within the time range of the measurement. The successful extraction time-resolved spectra (TRS) from TWS depend on i) operational parameters (delay time Δt and width δt) relative to lifetimes and lifetime difference of the species. ii) width of lifetime distribution (standard error or standard deviation). iii) relative intensities of emissions. If the fluorophore lifetimes are similar a deconvolution separation of the TWS is required in order to obtain spectra characteristic of the individual species. Such `time-resolved' spectra are also commonly termed decay-associated spectra (DAS) or species-associated spectra (SAS) in the literature and may be derived from experimental TWS in the following way (Knutson et al, 1982). Suppose the observed emission result from two components, having decay times τ_1 and τ_2, and spectral distribution $f_1(\lambda)$ and $f_2(\lambda)$. The directly measured TWS will then consist of two contributions:

$$I(\lambda,\Delta t) = f_1(\lambda)\, i_1(\Delta t_j) + f_2(\lambda)\, i_2(\Delta t_j)$$

in which $i_i(\Delta t_j) = \int_{\Delta t_j}^{\Delta t_j+\delta t} I_i(t)\, dt$

(see Figure 2.4), where Δt_j is the jth time-delay window, δt is the width of the window, and I_i is the relative intensity of the ith emission component. $i_i(\Delta t_j)$ can be estimated from the indicated areas in the convoluted decay curves, which are constructed with τ_1 and τ_2 obtained from deconvolution of decay curves.

Suppose now we measure TWS at two delay time Δt_1 and Δt_2. Then, we will have the equations:

$$I(\lambda,\Delta t_1) = f_1(\lambda)\, i_1(\Delta t_1) + f_2(\lambda)\, i_2(\Delta t_1)$$

$$I(\lambda,\Delta t_2) = f_1(\lambda)\, i_1(\Delta t_2) + f_2(\lambda)\, i_2(\Delta t_2)$$

It is clear that the removal of the convolution effects from TWS and determination of the contribution from each component to the TWS becomes a linear problem. The task for TRES program is just to determine the two unknowns $f_1(\lambda)$ and $f_2(\lambda)$ with two linear equations above. The ratio of $f_1(\lambda)$ to $f_2(\lambda)$ should be equal to the ratio of pre-exponential $\alpha_1(\lambda)$ to $\alpha_2(\lambda)$.

Some examples of lifetime and TRES analysis in technical detail as well as the detection of lifetime resolution limit can be found in Appendix.

2.4 Gaussian Curve Resolution

2.4.1 The model of gaussian

The gaussian fit program "PEAKFIT" (Jandel Corporation, 1990) was used to resolve the absorption bands of monomer G and C's.

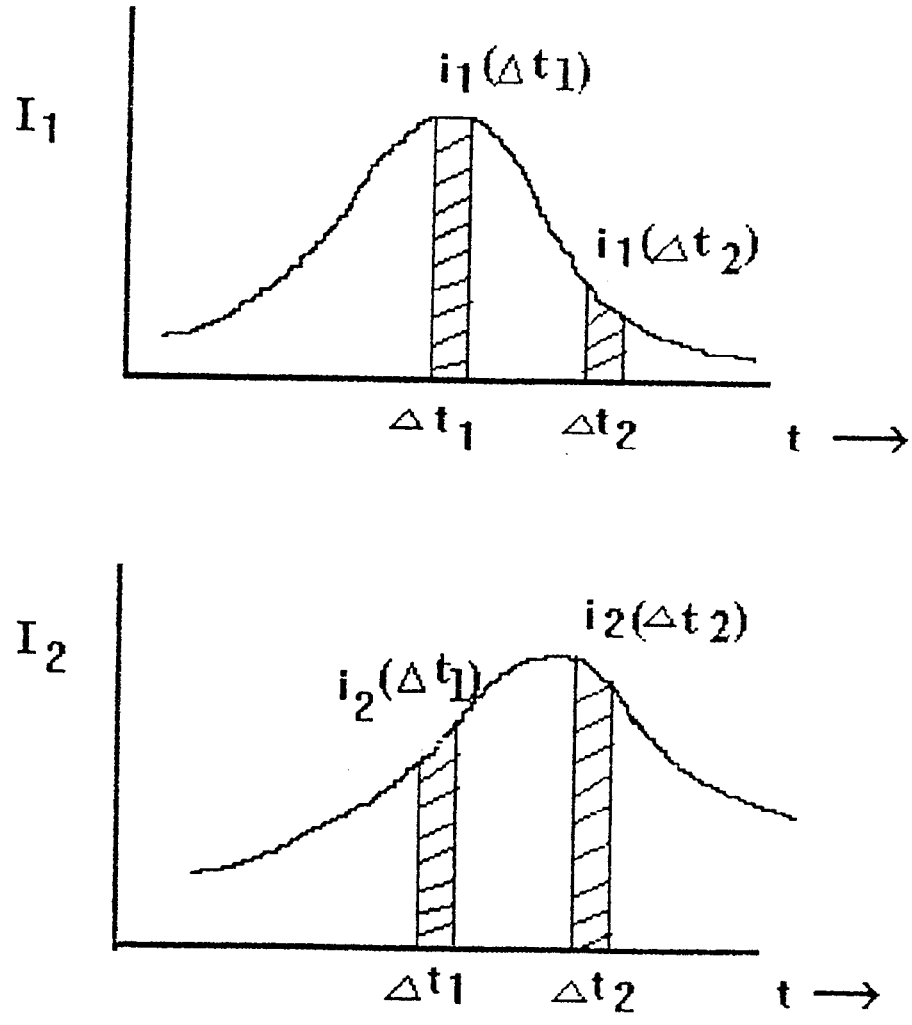

Fig 2.4. Deconvolution of decay curves.

The gaussian function in PEAKFIT program is expressed as:

$$G(\lambda) = A_0 \exp [-0.5(\lambda-\lambda_0)^2/\delta^2]$$

or $$G(\bar{\nu}) = A_0 \exp [-0.5(\bar{\nu}-\bar{\nu}_0)^2/\delta^2]$$

where λ and $\bar{\nu}$ are wavelength and wavenumber respectively, A_0, λ_0 (or $\bar{\nu}_0$) and δ are three basic fit parameters:

A_0 = Amplitude, λ_0 (or $\bar{\nu}_0$) = Center position, δ = width

2.4.2 Fit processes

There are two types of fit procedures in PEAKFIT: Curve Fit and Step Fit. Curve Fit lets one go through the fit program completely after presetting the initial fit parameters until the best sum of residuals χ^2 (minimum) and the coefficient of determination r^2 (nearest to 1) are reached. Step Fit allows one to run the fit program iteration by iteration after presetting. Step Fit is especially useful when one desires to control the width of gaussian in a reasonable range.

The termination criterion for stopping the fit process is when the χ^2 is unchanged within eight significant figures for five full iterations.

The statistic terms in PEAKFIT are included:

$$\chi^2 = SS_r = \sum_{1}^{n} (y_i - \hat{y}_i)^2 = \text{sum of squares of residuals}$$

$$r^2 = SS_r / SS_y = \text{coefficient of determination}$$

where $SS_y = \sum_{1}^{n} (y_i - \bar{y}_i)^2 = \text{sum of squares about the mean}$

y_i = y value of ith data point
$\hat{y}_i$ = y value of curve fit at ith data point
y_i = average value of y
n = number of data point

2.4.3. Calculation of oscillator strengths

The absorption intensity is proportional to oscillator strength f, which is defined as:

$$f = 4.32 \times 10^{-9} \int \varepsilon(\bar{\nu}) d\bar{\nu}$$

The area of experimental absorption data is approximately estimated by dividing the area into small rectangulars and summing them together:

$$\text{Area (experimental)} = \Sigma (y_i + y_{i+1})(x_i - x_{i+1})/2$$

where y_i and y_{i+1} denote the molar extinction coefficient of the ith and (i+1)th data, respectively; x_i and x_{i+1} represent the wavenumber of the ith and (i+1)th data respectively; $x_i - x_{i+1}$ corresponds to 2 nm interval.

Area of absorption for a gaussian shaped function can be analytically determined as:

$$\text{Area (gaussian)} = A_0 \times \delta_{1/e} \times \sqrt{2}$$

where A_0 is amplitude and $\delta_{1/e}$ is full width at 1/e maximum in cm^{-1}. The relation between $\delta_{1/e}$ and δ is

$$\delta_{1/e} = \sqrt{2}\delta.$$

3. TIME-RESOLVED FLUORESCENCE SPECTROSCOPY OF ADENYLYL CHROMOPHORE

3.1 Introduction

After more than thirty years of work the major features of the electronic transitions and absorption spectra of the NA chromophores are reasonably well characterized and understood (Callis, 1986; Cadet and Vigny 1990). Yet some characteristics of the excited states of the adenylyl chromophore remain uncertain. One of these problems is the description of the electronic transitions involved in the lowest energy absorption band of adenosine, λ_{max} 259 nm, in aqueous solution. Most of the experimental evidence shows that this band contains two overlapping $\pi\pi^*$ transitions but the distribution of oscillator strength between the two are still uncertain, as are the directions of the transition moments. The polarized absorption work for single crystal of 9-methyladenine (Stewart and Davison, 1963; Stewart and Jensen, 1964) assigned the lowest energy transition as the dominant component, polarized close to the short molecular axis (-3°, 97%, $f_1 = 0.28$, $\lambda = 267$ nm), and second weak transition ($f_2 = 0.008$, $\lambda = 255$ nm) polarized along the long molecular axis (they are illustrated in Figure 3.1a). After 25 years, during which these assignments seemed to be in agreement with other techniques and calculations (Callis, 1983), they have been brought into question by Clark (1989,1990). Examining together the crystal reflection spectra of two different methylated adenines (9-methyladenine and 6-

(methylamino) purine), Clark suggested that the previous assignments of transition moment direction should be revised. It was concluded that the 270 nm absorption region was dominated by a slightly shorter wavelength transition polarized +25° away from the short molecular axis (f_2 = 0.20, λ = 265 nm), while another slightly weaker transition was polarized close to the long molecular axis (+85°, f_1 = 0.10, λ = 275 nm) and this heavily overlapped the first transition (see Figure 3.1b), and the third transition was well separated from the first two (f_3 = 0.25, λ = 213 nm)). Apparently, the assignments of the first two transitions by Clark are inversely ordered to those by Stewart et al. Nevertheless, both concluded that the lowest transition is allowed ($f_1 \geq 0.10$). However, Fornasiero et al (1981) came to a different conclusion. Differing from above two group's work on crystals (aggregated state), they co-analyzed isotropic absorption, linear dichroism and circular dichroism for dilute solutions (isolated and solvated state) of AMP and adenosine as well as its complexes with cis- and trans-diamminedichloroplatinum (II), a condition which is more relevant to DNA. They found that whereas the great bulk of the intensity was in one transition similar to the first transition of Stewart et al and Clark (f_2 = 0.30, λ = 269.5 nm), it was necessary to include a very weak transition 700 cm^{-1} lower in energy (the f value was not given by Fornasiero but it was indicated to be ~ 10^{-4}). This assignment is compared with the crystal work in Table 3.1. The striking feature of this work is that the lowest energy transition is both very

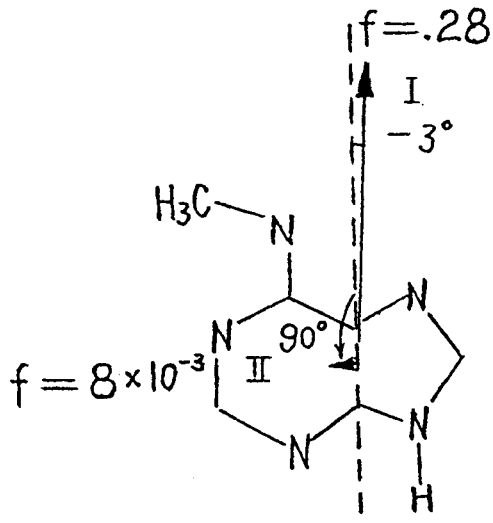

a. From Stewart and Davidson

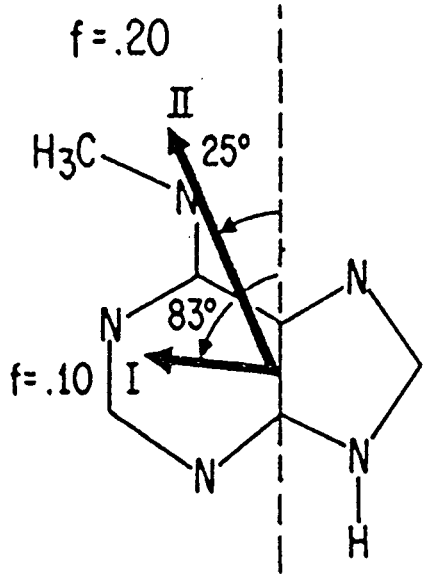

b. From Clark

Figure 3.1 Transition moment directions for the two transitions in the first absorption region of adenine chromophore.

Table 3.1 Assignments of the two electronic transitions in the first absorption region adenine chromophore

	f_1	λ_1 (max)	θ_1	f_2	λ_2 (max)	θ_2
Stewart & Davidson (1965)	0.28	267	-3°	$8x10^{-3}$	255	~90°
Clark (1990)	0.10	275	+83°	0.20	265	25°
Fornasiero et al (1981)	0.30[a]	270[a]				
	10^{-4}[,a]		271[b]			

[a]Main transition, E(0-0') = 37,037 cm^{-1}.
[b]Lowest energy transition, E(0-0') = 36,000 cm^{-1}.

weak and hence quite forbidden, yet it is implied to be in-plane polarized $\pi \rightarrow \pi^*$ transition. There are weak and hence quite several other spectroscopic results which also suggest the existence of a lower energy, weak transition (Fucaloro and Forster, 1971, Matsuoka and Norden 1982).

A lowest energy transition which is weak would be expected to have a longer intrinsic lifetime than an allowed transition with an oscillator strength of 0.28, which would be expected to have τ_0 of 3.5 ns. Blumberg et al (1968) first reported at an American Physical Society meeting a lifetime about 4.3 ns for adenosine at 77K, anomalously long because the quantum yield is 8.8 x 10^{-3} (Hønnas and Steen, 1970). Seventeen years later Rigler et. al. (1985) measured the fluorescence lifetimes of ATP in aqueous solution at room temperature with ps single photon counting and found there to be two lifetimes, a fast one with τ_1 of 290 ps, along with a slow (major) component with τ_2 of 4.17 ns (96% of total emission). The emission spectrum was apparently mostly a single strong component with λ_{max} 390 nm with a weak shoulder at 330 nm. However using the sychroscan streak camera technique, Yamashita et al (1987) studied 9-methyl adenine aqueous solution at room temperature and observed τ_1 of 5 ps (λ_{max} ~ 320 nm), and a second component with τ_2 of 330 ps (λ_{max} 380 nm). The results of those two groups contradict each other both in lifetime and spectra. Ballini et al (1983) detected the synchrotron-excited states decay profiles of NA chromophore at room temperature and observed an unexpected "tail" for adenosine fluorescence, indicating a weak contribution of some long lived emission. Detailed

investigation led to the collusion that there are three emissions from adenosine, a very fast one with $\tau < 100$ ps and λ_{max} 320 nm, and two 'slow' emissions with similar lifetimes ~ 4 ns in the range of 350-390 nm. Further insight has come from laser lifetime studies at 77K by Hart and Daniels (1989). Compared to the room temperature report (Ballini et al), they found the decay of emission at 340 nm excited at 290 nm to be described best as a sum of only two exponential with lifetimes 1.2 and 7.0 ns, and they suggested that the room temperature 390 nm emission comes from a state which is produced post-excitation by an activation-controlled solvation process, which is inhibited at 77K and too fast to resolve at room temperature. For comparison with each other the life times and oscillator strengths of adenyl group from previous work are summarized in Table 3.2.

This constitutes fairly strong evidence that the lowest electronic transition of adenosine is weak and does not correlate fundamentally with the major features in absorption spectra. It must be emphasized that the nature of the electronic transitions in the adenyl group remains a little uncertain pending further characterization. The present work studying the time-resolved spectroscopy of adenylyl chromophore in aqueous solution with sub-nanosecond laser excitation is an extension of the above time-domain research. The reasons for us to concentrate on ATP are as follows. First, because ATP and adenosine contain the same chromophore we expect that the intrinsic lifetimes and oscillator strengths of ATP and adenosine will be very similar and if so, this may add to evidence for the existence of the weak

Table 3.2 The lifetimes and oscillator strengths of adenylyl chromophore[*]

compound	measurement	τ_{1f} (λ_{max})	τ_{2f} (λ_{max})	$\tau_{0(1)}$	f_1
Ado	absorption	(259)		3.5 ns[*]	0.28
ATP[a]	fluoresc.	290 ps	4.17 ns (390)	320 ns	
9m-Ade[b]	fluoresc.	5 ps (~320)	320 ps (380)	100 ns	$1x10^{-2}$
Ado[c]	fluoresc.	<100 ps (320)	4 ns (350,390)	<2000 ns	$>1x10^{-3}$
Ado[d]	fluoresc.	1.2 ns (320)	1.7 ns (340)	130 ns	$1x10^{-2}$

[*]Using equations $\tau_0 = \tau_f/\phi_f$; f(abs.) = $4.3 \times 10^{-9} \int \varepsilon d\nu$ and f(fluoresc.) = $1.47/\bar{\nu}^2\ \tau_0$
where τ_0 and τ_f are intrinsic lifetime and fluorescence life respectively, ϕ_f is quantum yield of fluorescence, f is oscillator strength, and $\bar{\nu}$ is wavenumber in the transition.

[*]Calculated from the oscillator strength for the entire first absorption band.

[a]Rigler et al, 1985, at room temperature and in H_2O. τ_0 is calculated using an estimated $\phi_{ATP}(H_2O) \approx 5\ \phi_{ATP}$(acid). ($\phi_{ATP}$(acid)= $4.6x10^{-3}$ (Börresen,1967)).

[b]Yamashita et al 1987, at room temperature and in neutral aqueous solution. τ_0 is calculated using $\phi_{Ado} = 5x10^{-5}$ (Vigny, 1971).

[c]Ballini et al, 1988, at room temperature and neutral aqueous solution. τ_0 is calculated using $\phi_{Ado} = 5x10^{-5}$ (Vigny, 1976).

[d]Hart and Daniels 1988, at 77K. τ_0 is calculated using $\phi_{Ado} = 8.8x10^{-3}$ (Hønnas and Stten, 1970).

transition in adenyl group. Second, it can be noticed that the τ_1 which Rigler measured was anomalously large (compared to Yamashita's), and third, the spectrum he measured disagreed with the steady-state emission spectrum reported by everyone else for Ado and AMP. It is expected that measuring several time-windowed spectra and obtaining the time-resolved spectra, some assignments of lifetimes and spectra can be made so that the current understanding of excited states of ATP can be improved. A comparable situation holds for adenosine and other adenyl nucleotides.

The present work investigates the problem of the anomalous results of Rigler and Yamashita, elaborates the spectral characteristics of protonated and unprotonated ATP by altering the pH of the solutions, researches the spectroscopic aspect of the stacked form of ATP by changing the concentration, clarifies the phosphate group effects on adenyl group by measuring systematically the spectroscopy of ATP, ADP, AMP and Ado and studies some solvent effects on the adenyl group absorption and emission.

3.2. Results

3.2.1 ATP in neutral phosphate buffer solution

i) Lifetime analysis

The decay profiles for ATP fluorescence at various emission wavelengths were collected following excitation at 260 nm together with Rayleigh scatter at 290 nm. The results of the lifetime analysis of aqueous ATP neutral solution in three different concentrations are listed in Table 3.3 (detailed data treatments by NLLS reiterative convolution program can be found in Appendices).

The $f(\alpha)$ denotes the fraction of initial magnitude α; $f(\alpha\tau)$ represents the fraction of total emission intensity. The value immediately following the lifetime is the standard error. From Table 3.3 we can get the following:

1. In the whole system, there are at least two emission components, the fast component with a lifetime τ_1 ~ 60 ps (the instrument limit in lifetime resolution, see Appendix), and the slow component with a lifetime τ_2 of 2.5 ns.

2. At the emission wavelength 320 nm, the major component is the fast one since $f(\alpha)$ and $f(\alpha\tau)$ are around 100%.

3. On increasing emission wavelength to 350 nm and then to 390 nm, more and more slow component is observed in addition to the fast one.

4. Increasing the ATP concentration, the two lifetimes are basically unchanged, but the contribution of slow component to the total emission

Table 3.3 Lifetime analysis of ATP in phosphate buffer solution (pH 7.0)

Conc., M	λ_{em}, nm	τ, ns	f(α)	f($\alpha\tau$)
1×10^{-4}	320	0.090	100%	100%
	350	0.13	>99%	87%
		2.38 ± 0.2	<1%	13%
	390	0.132	97%	63%
		2.40 ± 0.06	3%	37%
5×10^{-4}	320	0.060	>99%	90%
		3.0 ± 0.27	<1%	10%
	350	0.060	99%	70%
		2.5 ± 0.06	1%	30%
	390	0.126	96%	56%
		2.3 ± 0.03	4%	44%
1×10^{-2}	320	0.080	100%	100%
	350	0.050	99%	66%
		2.9 ± 0.12	1%	34%
	390	0.070	98%	51%
		3.0 ± 0.08	2%	49%

$f(\alpha_2\tau_2)$ is increased a little (10%). 5. There is no indication of a component with lifetime of 290 ps as reported by Rigler et al (1985).

The presence of the third component is possible although the standard fit of the decay curve and the standard error of the lifetime from three exponential (Appendices) are worse than those from the two exponential analysis.

ii) Time-resolved emission spectra

To investigate the spectral characteristics of ATP emission components in neutral aqueous solution, the time-windowed spectra were measured at 0, and 1.0 ns (and/or 2.0 ns) delay time relative to the time of the maximum of Rayleigh scatter as time zero with 100 ps width for each window. These time-windowed spectra were analyzed into time-resolved spectra by TRE program and corrected for the spectral sensitivities of the detection system (Fu, 1989). The corrected time-resolved smoothed spectra (in terms of α) at three different concentrations of ATP in neutral buffer solution with τ_1 = 0.060 ns, and τ_2 = 2.5 ns are shown in Figures 3.2, 3.3 and 3.4, respectively.

It can be seen clearly that the convoluted spectra have been successfully separated into two distinct spectra in each system. The fast component (C1) with the peak ~ 310 nm is predominant and the slow component (C2) with the peak at 385 nm is much smaller in magnitude than the fast one. Three-windowed spectra analysis was also attempted, but the results were not satisfactory.

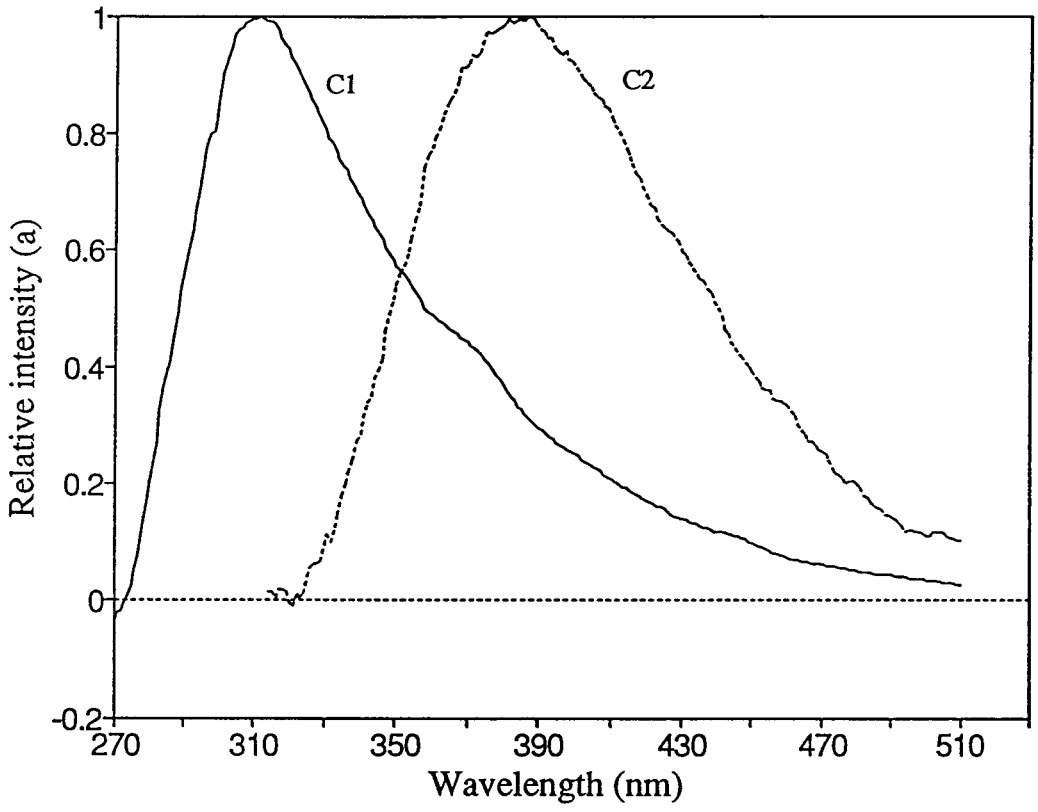

Figure 3.2 Corrected time-resolved emission spectra of ATP ($1x10^{-4}$ M) in phosphate buffer solution (pH 7.0). τ_1 = 0.06 ns, τ_2 = 2.5 ns are used. (C1) fast component, (C2) slow component. $[\alpha_1/\alpha_2]$ = 101.

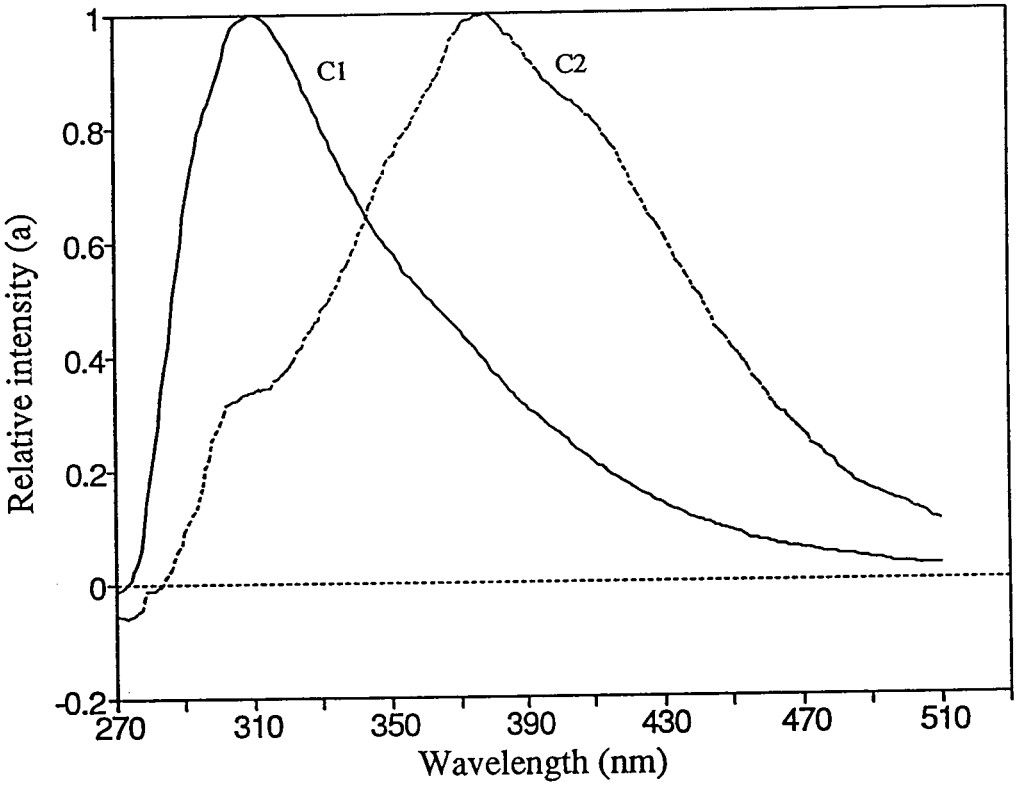

Figure 3.3 Corrected time-resolved emission spectra of ATP ($5x10^{-4}$ M) in phosphate buffer solution (pH 7.0). τ_1 = 0.06 ns, τ_2 = 2.5 ns are used. (C1) fast component, (C2) slow component. $[\alpha_1/\alpha_2]$ = 55.

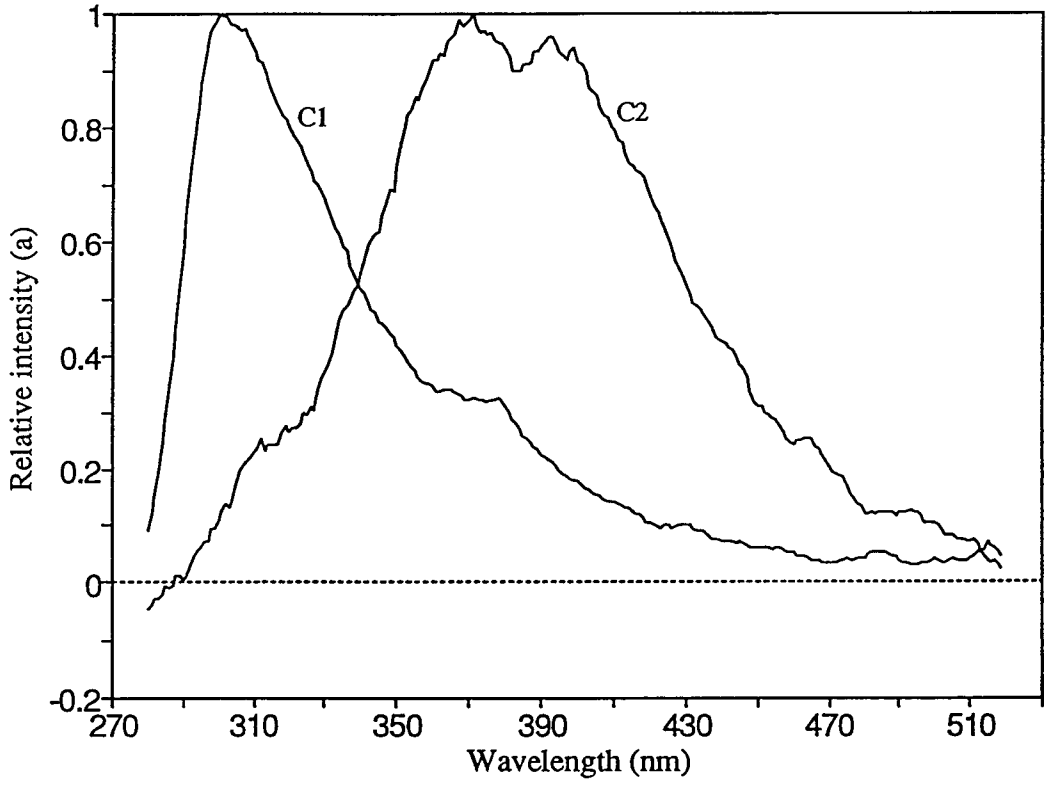

Figure 3.4 Corrected time-resolved emission spectra of ATP ($1x10^{-2}$ M) in phosphate buffer solution (pH 7.0). τ_1 = 0.06 ns, τ_2 = 2.5 ns are used. (C1) fast component, (C2) slow component. $[\alpha_1/\alpha_2]$ = 27.

Comparison of the corrected TRES for the fast and slow component in different concentration of ATP are shown in Figures 3.5 and 3.6 respectively.

There are some similarities and differences between the spectra at different concentrations of ATP. The similarities are that the lifetime, the shape and the peak positions for each component are almost the same, which suggests that the emitters are identical in different concentrations. The differences are that the ratio of the fast component to the slow $[\alpha_1/\alpha_2]$ (integrated from $\int\alpha(\lambda)d\lambda$) is decreased a few times by increasing the concentration from 0.1 to 10 mM, which may not be significant due to the existence of the experimental error.

3.2.2 ATP in unbuffered aqueous solution (pH 4.4)

i) Lifetime analysis

From the time-resolved spectroscopy of ATP in neutral aqueous solution the lifetimes are determined as $\tau_1 < 100$ ps and $\tau_2 = 2.5$ ns, which are quite different from the results obtained by Rigler for ATP in aqueous solution, $\tau_1 = 290$ ps, $\tau_2 = 4.17$ ns. In an attempt to search for the origin of this difference the conditions under which Rigler's experiments were carried out were carefully inspected. The most obvious differences in data acquisition are that Rigler excited ATP at 290 nm, below the 0-0' level, i.e. in the range of 'hot' absorption. This would not be expected to cause a difference in lifetimes.

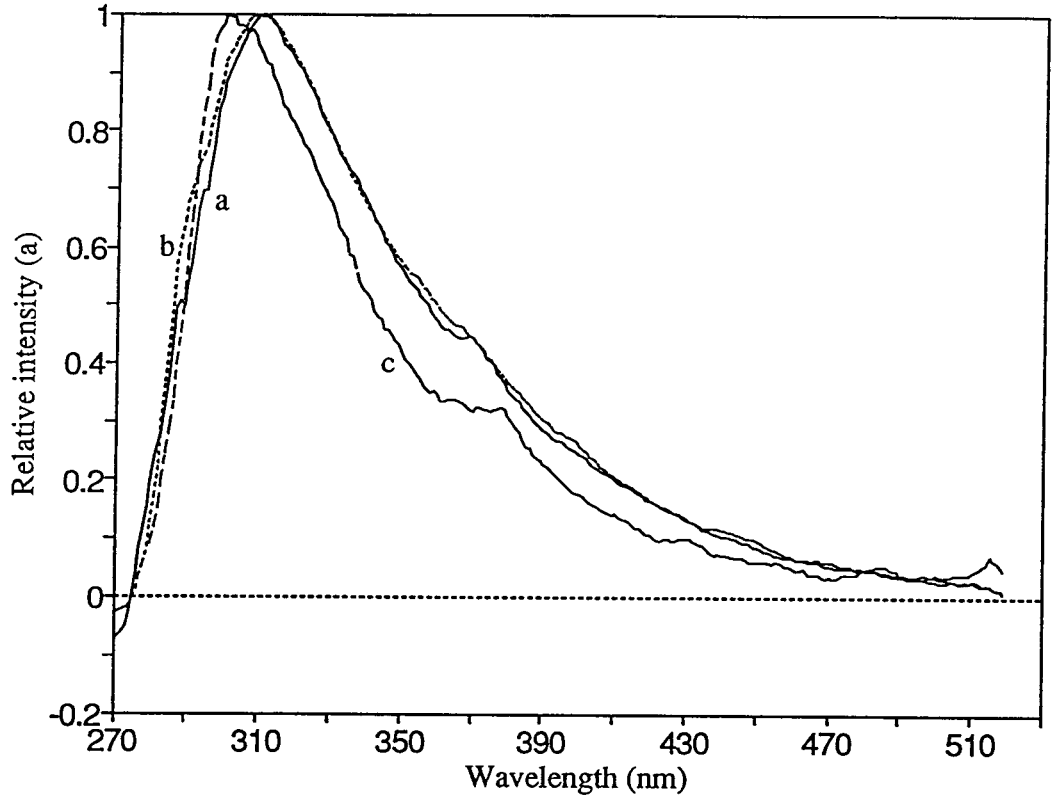

Figure 3.5 Comparison of fast component at different concentrations of ATP in neutral buffered solution. τ_1 = 0.06 ns. (a) $1x10^{-4}$ M, (b) $5x10^{-4}$ M, (c) $1x10^{-2}$M.

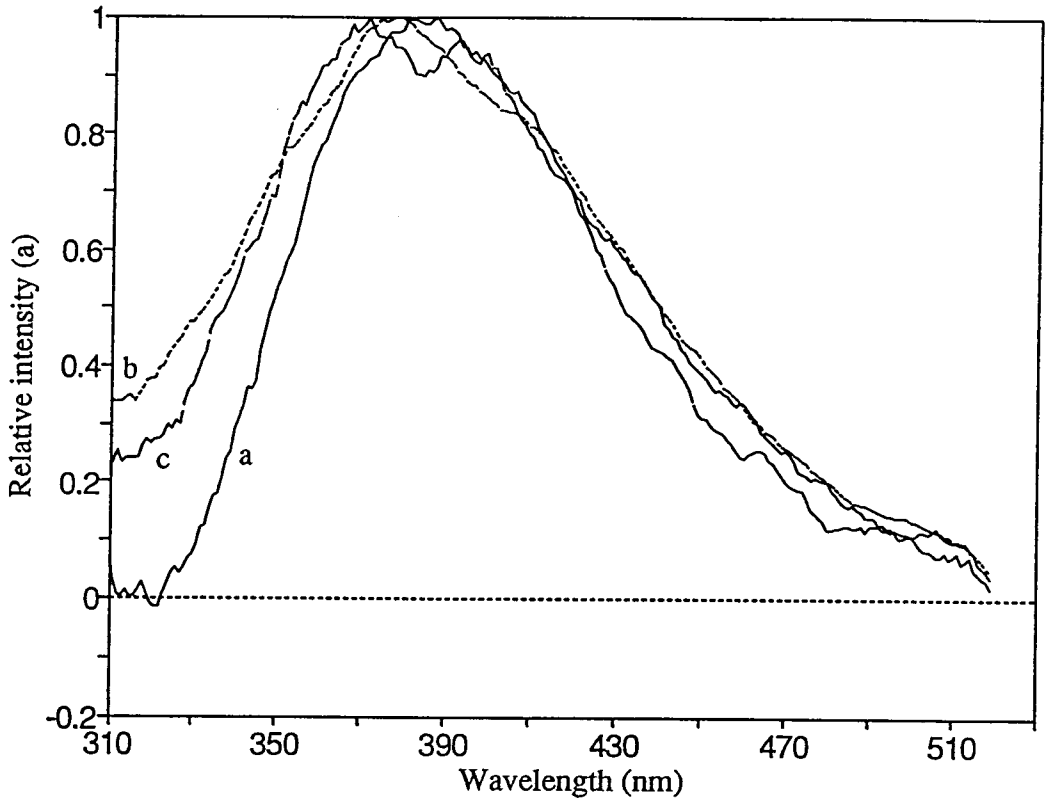

Figure 3.6 Comparison of slow component at different concentrations of ATP in neutral buffer solution. τ_2 = 2.5 ns. (a) $1x10^{-4}$ M, (b) $5x10^{-4}$ M, (c) $1x10^{-2}$M.

The other difference, not apparent at first and not explicitly statedis that Rigler's sample was in an unbuffered solution with a pH of 4.4. As ATP has a pK = 4.26 (Christensen, 1971) this implies that the solute is approximate 50% protonated under his condition and this could obviously affect the fluorescence lifetimes. Accordingly, to investigate the lifetimes and time-resolved spectra the experiments were carried in unbuffered solution. The lifetime results are listed in Table 3.4. The following can be reached:

1. There are at least two emission components in ATP unbuffered aqueous solution with a lifetime for fast component $\tau_1 \approx$ 60-100 ps and a lifetime for slow component τ_2 of 4.4 ns.

2. Contrary to the aqueous neutral solution, the major component is now the slow component at all emission wavelengths (see values of $f(\alpha\tau)$). The contribution of the fast component decreases until it is absent totally at 390 nm. The $f(\alpha\tau)$ for fast component is decreased from 10% at 320 nm to 2% at 360 nm, and only the slow component left at $\lambda_{em} \geq 390$ nm.

3. The lifetime of slow component (4.4 ns) is very similar to Rigler's (4.17 ns).

4. There is still no evidence for 290 ps component reported by Rigler et al. (1985).

Table 3.4 Lifetime analysis of aqueous ATP in unbuffered solution (pH 4.4)

Conc., M	λ_{em}, nm	τ, ns	f(α)	f($\alpha\tau$)
2×10^{-4}	320	0.050	91%	10%
		4.36 ± 0.01	9%	90%
	360	0.105	53%	3%
		4.40 ± 0.01	47%	97%
	390	4.37 ± 0.01	100%	100%

It is possible for existence of the third component although the standard error of the lifetime for the third component is unreasonably large and the standard fit of three exponential has no significant improvement.

ii) Time-resolved emission spectra

Successively, the time-windowed emission spectra were measured by setting three delay times at 0, 1.0 and 2.0 ns all with 100 ps window width. Through TRE program analysis, only the two-exponential model gives more reasonable spectra (no large negative values and ratios of α are close to those from lifetime analysis) than one or three-exponential model. The corrected time-resolved emission spectra with different τ_1 (0.1 ns and 0.29 ns (Rigler's result, 1985)) and same τ_2 (4.4 ns) are shown in Figures 3.7a and b respectively.

As we see from Figure 3.7 that Changing τ_1 from 100 ps to 290 ps does not change the shape of the emission components significantly, and only changes the fraction $f(\alpha)$ of the component a few times. This indicates that the TRE spectra are not sensitive to a change of short lifetime when τ_2 is large.

There are two striking spectroscopic distinctions of ATP in unbuffered aqueous solution with those in neutral buffered solution. First is the difference in lifetime for slow component, τ_2 = 4.4 ns for the former and 2.5 ns for the latter although the shape of spectra remains unchanged. Second is

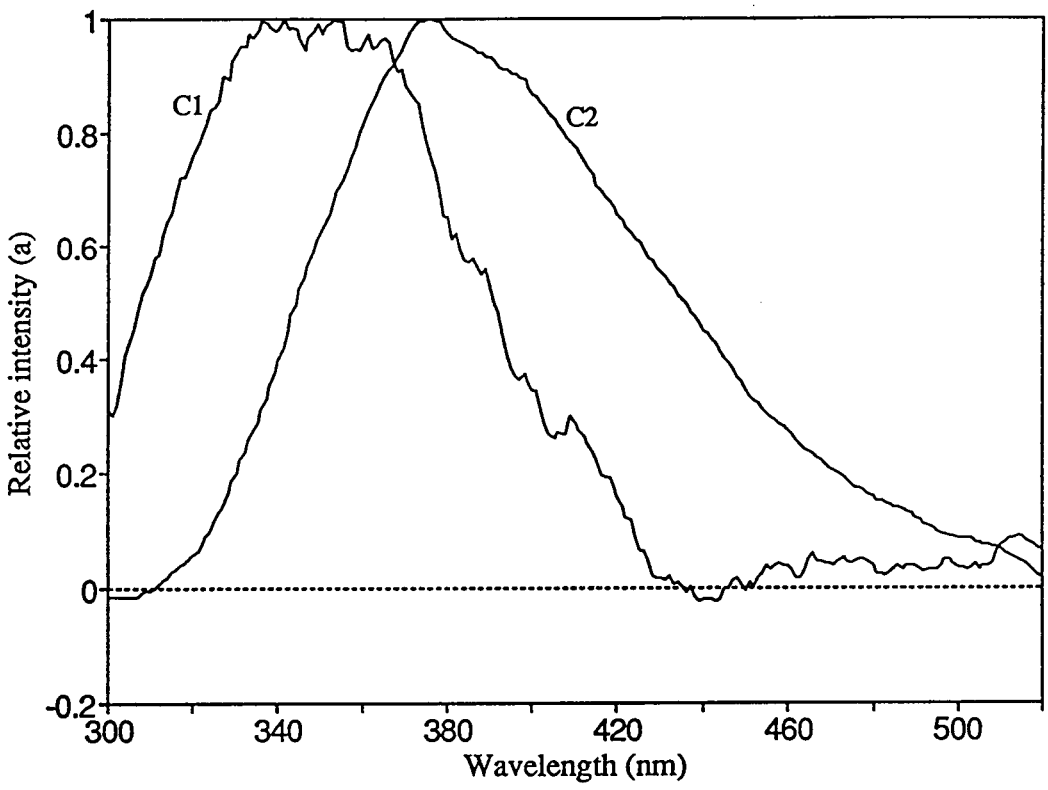

Figure 3.7a Corrected time-resolved emission spectra of ATP ($2x10^{-4}$ M) in unbuffered aqueous solution (pH 4.4). τ_1 = 0.1 ns, τ_2 = 2.5 ns are used. (C1) fast component, (C2) slow component. $[\alpha_1/\alpha_2]$ = 0.9.

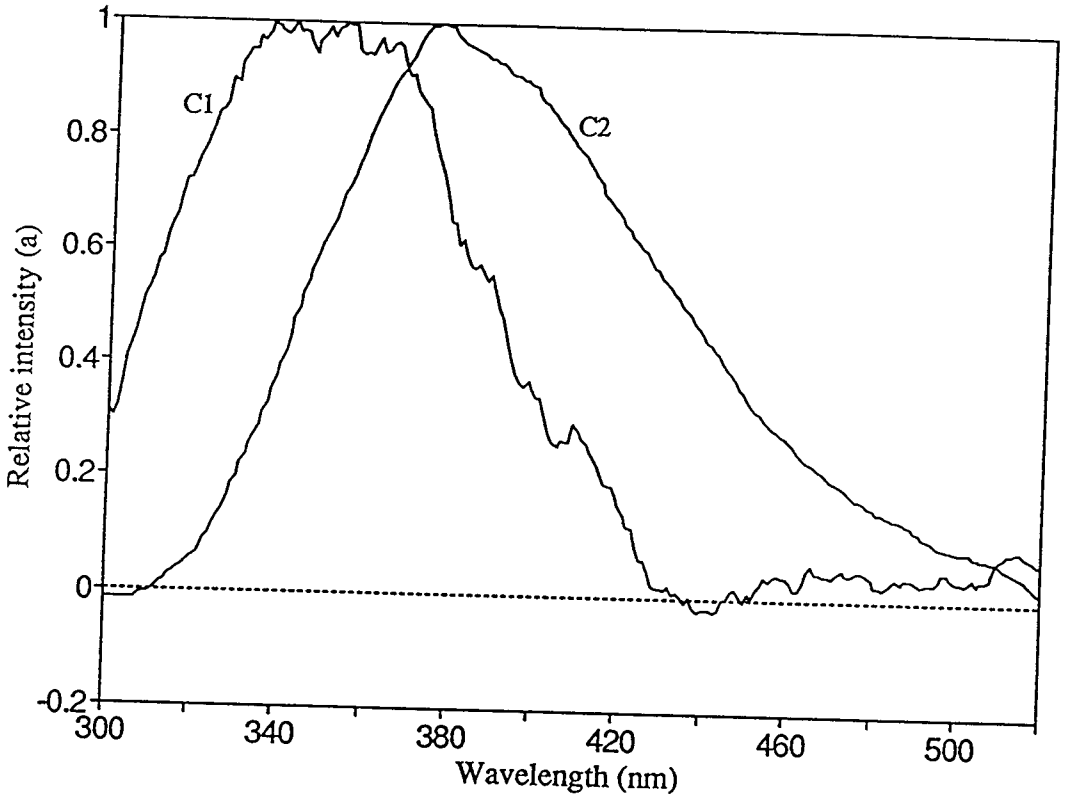

Figure 3.7b Corrected time-resolved emission spectra of ATP ($2x10^{-4}$ M) in unbuffered aqueous solution (pH 4.4). τ_1 = 0.29 ns, τ_2 = 2.5 ns are used. (C1) fast component, (C2) slow component. $[\alpha_1/\alpha_2]$ = 0.42.

the considerable peak shift for the fast component, i. e. 340 nm for the former and 310 nm for the latter.

3.2.3 ATP in acidic aqueous solution (pH 1.1)

From the previous section it is possible to see that the slow component with the lifetime τ_2 of 4.4 ns in ATP unbuffered aqueous solution (pH 4.4) originates from protonated $ATPH^+$ present in this solution. In order to confirm this point and also investigate the effects of pH on ATP spectroscopy, we measured the decay profiles and time-windowed spectra of ATP in $HClO_4$ solution (pH1.1).

i) lifetime and TRES analysis

The decay profiles of ATP ($1x10^{-4}$ M) in $HClO_4$ aqueous solution were detected at four different emission wavelengths and the results from reiterative convoluted lifetime analysis for ATP are given in Table 3.5. Time-windowed spectra were measured at delay 0 and 1.0 ns and the corrected time-resolved spectra are shown in Figure 3.8.

Similar to ATP in unbuffered (pH 4.4) solutions, there are at least two components in the acidic (pH 1.1) solution with τ_1 ~ 100 ps and peak at 350 nm and τ_2 of 4.4 ns and peak at 375 nm. The major component is the slow one. Two components exist at 320 nm, and with increasing emission wavelength, the contribution of the fast component decreased, and finally only the slow component presents at 390 nm. There is still no sign of 290 ns

Table 3.5 Lifetime analysis of ATP in $HClO_4$ aqueous solution (pH 1.1)

Conc., M	λ_{em}, nm	τ, ns	f(α)	f($\alpha\tau$)
1×10^{-4}	320	0.050	89%	8%
		4.41 ± 0.03	11%	92%
	340	0.131	60%	4%
		4.44 ± 0.02	40%	96%
	390	4.47 ± 0.02	100%	100%

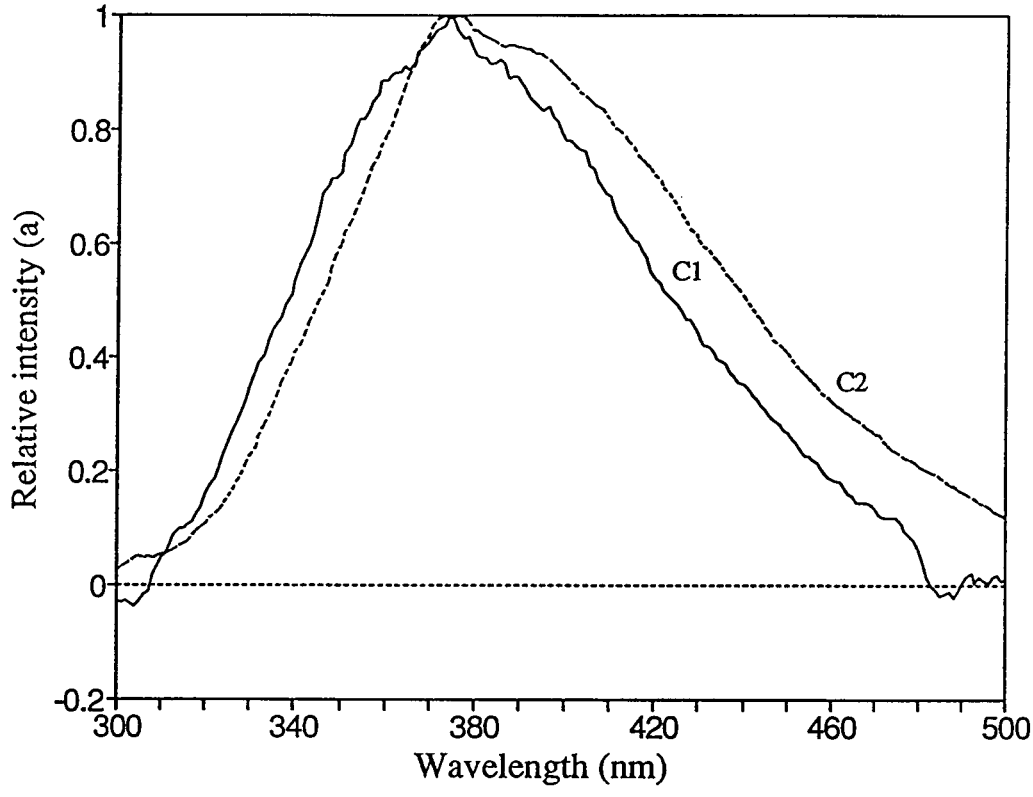

Figure 3.8 Corrected time-resolved emission spectra of ATP in $HClO_4$ aqueous solution (pH 1.1). τ_1 = 0.1 ns, τ_2 = 4.4 ns are used. (C1) fast component, (C2) slow component. $[\alpha_1/\alpha_2]$ = 2.9.

ns component. The existence of three components is possible from the lifetime analysis (see Appendices) but its TRE analysis is not satisfactory.

ii) pH dependence of resolved ATP spectra

The dependence of the fast and slow component spectra of ATP on pH are illustrated in Figures 3.9 and 3.10 respectively. Figure 3.9a is normalized TRE spectra as usual, and Figure 3.9b presents the relative intensities in terms of relative quantum yields in different pH (see section iii), i.e. the ratio of the integrated intensities (α). It is obvious that whereas the spectra of the slow component are independent of pH, those of the fast components shift successively from λ_{max} 310 nm at pH 7 to λ_{max} 370 nm at pH 1.1.

iii) pH dependence of ATP relative quantum yields

It is a common fact that the quantum yields of NAC are dependent of pH (Gill, 1971). At the early stage, the fluorescence measurements only applied to acidic solution of NAC, but not to neutral solution. The main reason is that the quantum yields of NAC in acid solution (10^{-3}) are much larger than those in neutral solution (10^{-4}-10^{-5}), hence are the emission intensities.

What is the situation at the middle pH, such as that in above unbuffered solution of ATP at pH 4.4? Is the quantum yields of ATP linearly related to pH? There is no report so far mentioning this. For examining pH effect on ATP spectroscopy, the present work uses Raman scatter as an

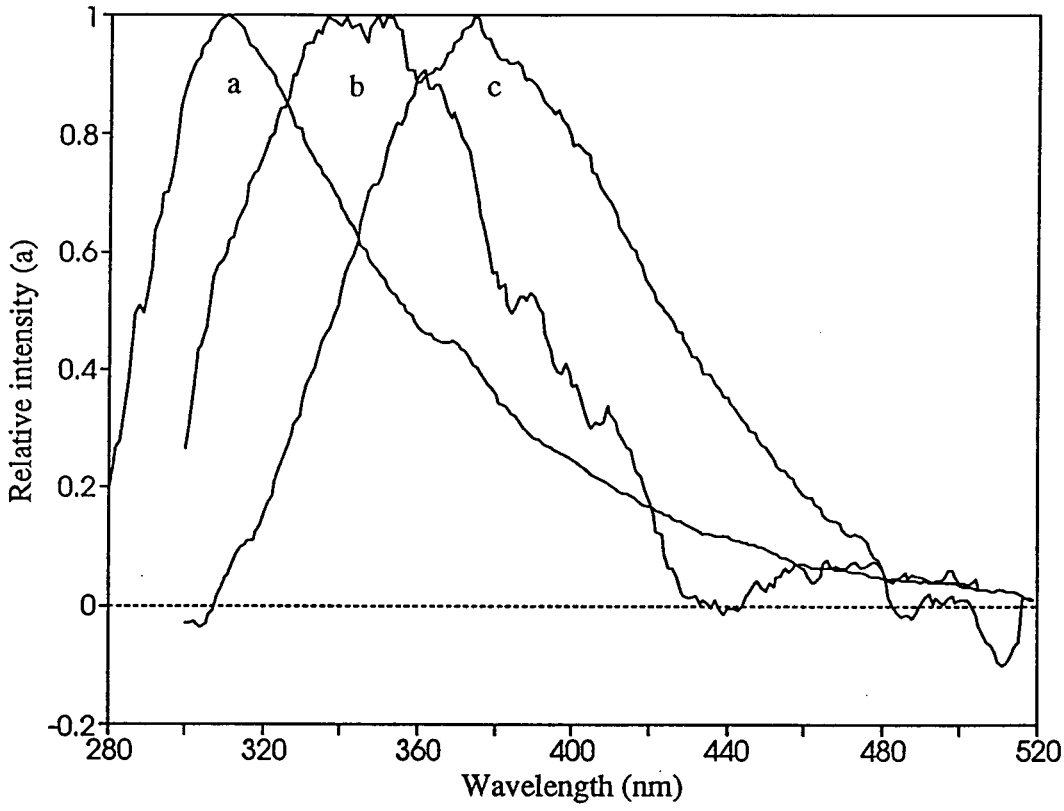

Figure 3.9a pH effect of TRE spectra of the fast component of ATP. (a) pH 7, (b) pH 4.4, (c) pH 1.1.

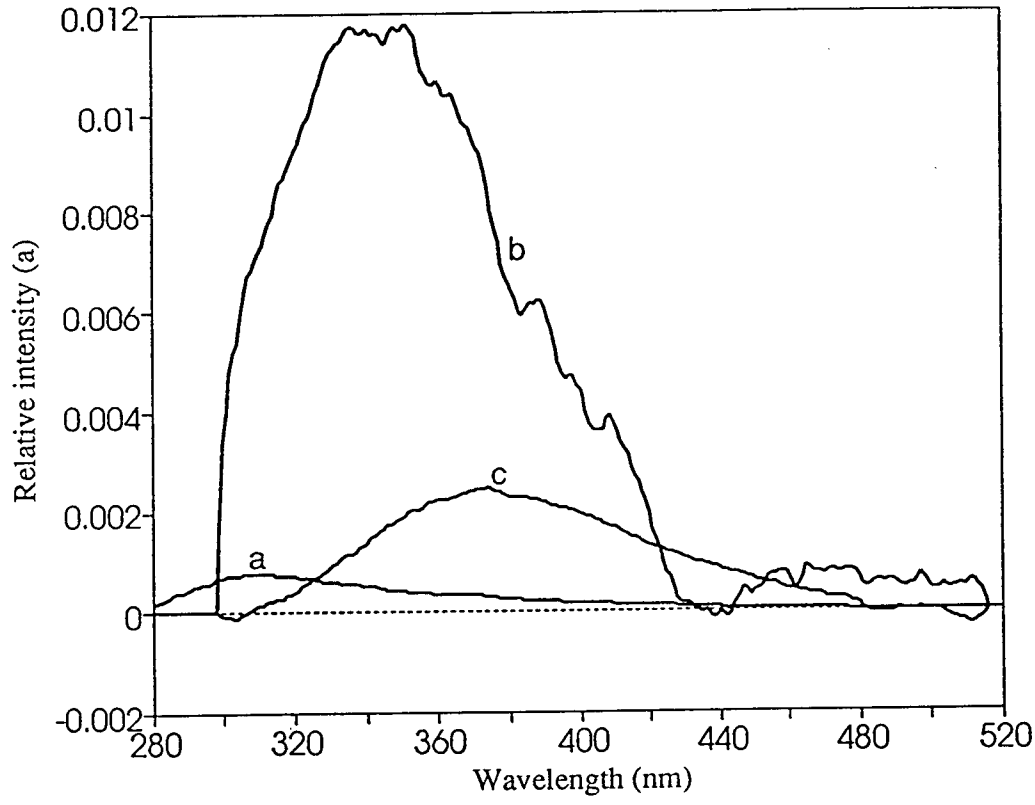

Figure 3.9b pH effect of the relative integrated intensities (see text) of the fast component of ATP. (a) pH 7, (b) pH 4.4, (c) pH 1.1.

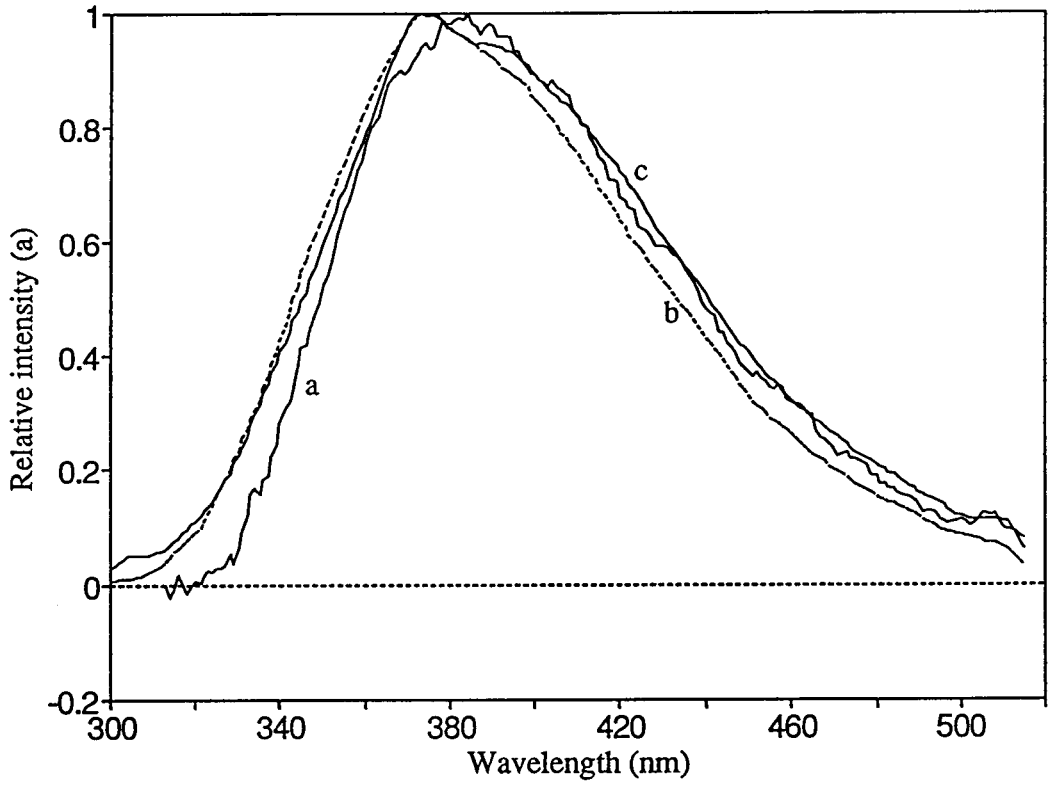

Figure 3.10 pH effect of TRE spectra of the slow component of ATP. (a) pH 7, (b) pH 4.4, (c) pH 1.1.

internal monitor to determine the relative quantum yields by comparing the ratio of fluorescence to Raman. The time-windowed spectra with delay time zero at three different pH are shown in Figure 3.11.

A striking characteristic found by comparing the above three graphs is that the highest ratio of fluorescence signal to Raman is in unbuffered (pH4.4) solution rather than in acidic (pH1.1) solution as generally believed. The tendency is the same for late windowed spectra with delay 1.0 ns. The carefully measured ratios of fluorescence signal to Raman by integrating the corresponding areas are included in Table 3.6 and illustrated in Figure 3.12. It is apparent that the ratios at pH 4.4 are about five fold higher than those at pH 1.1, which is the same as stating that the fluorescence quantum yield of ATP in unbuffered aqueous solution is five times higher that in acidic solutions.

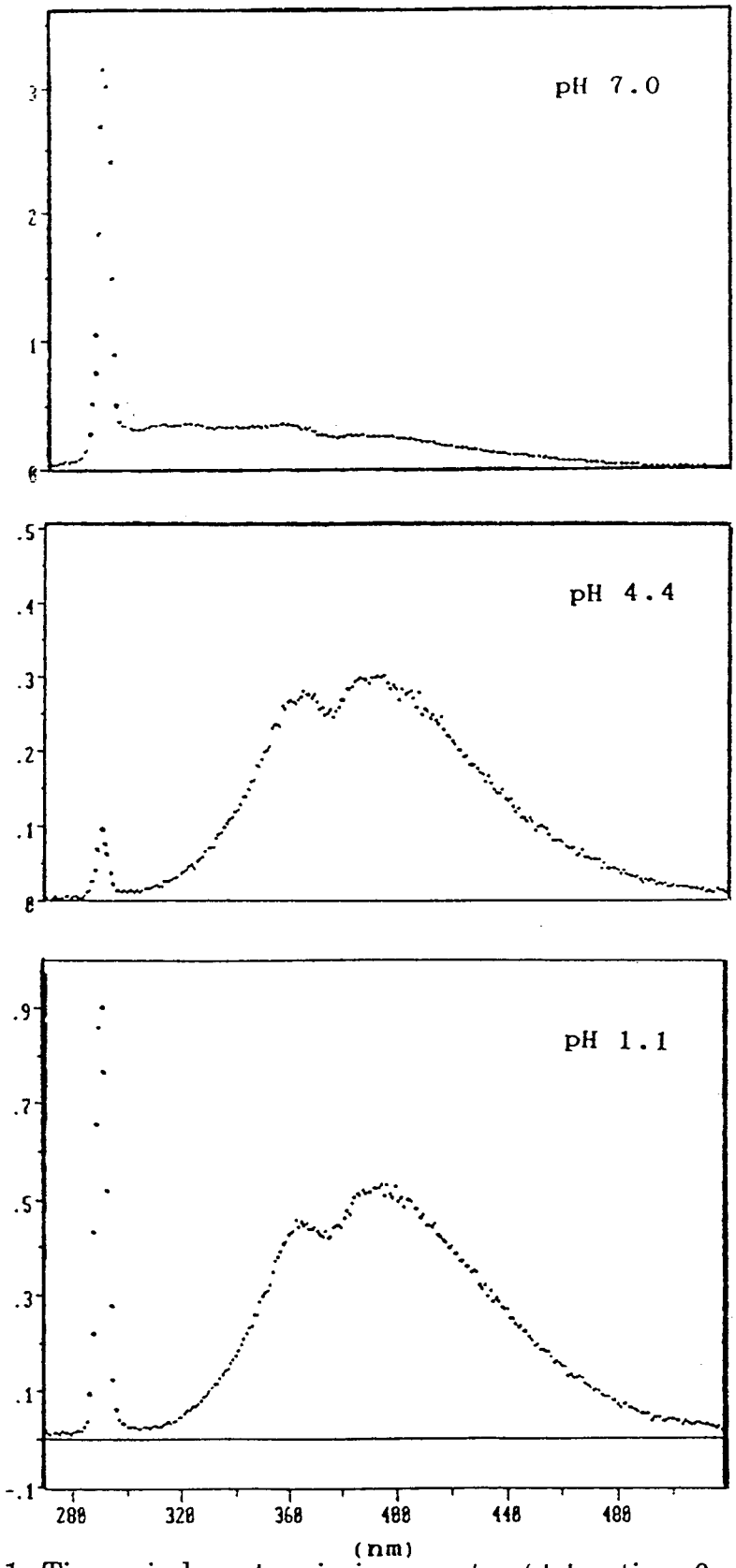

Figure 3.11 Time-windowed emission spectra (delay time 0 ns) of ATP at different pH aqueous solutions.

Table 3.6 Ratios of integrated fluorescence signal to Raman in two time-windowed emission spectra

	Early window (0 ns delay)			Late window (1 ns delay)		
pH	fluor.	Raman	Ratio	fluor.	Raman	Ratio
7.0	47.3	16.3	2.90	36.4	8.67	4.20
4.4	29.7	0.66	44.8	46.8	0.14	330
1.1	48.9	4.92	9.90	77.5	1.30	59.5

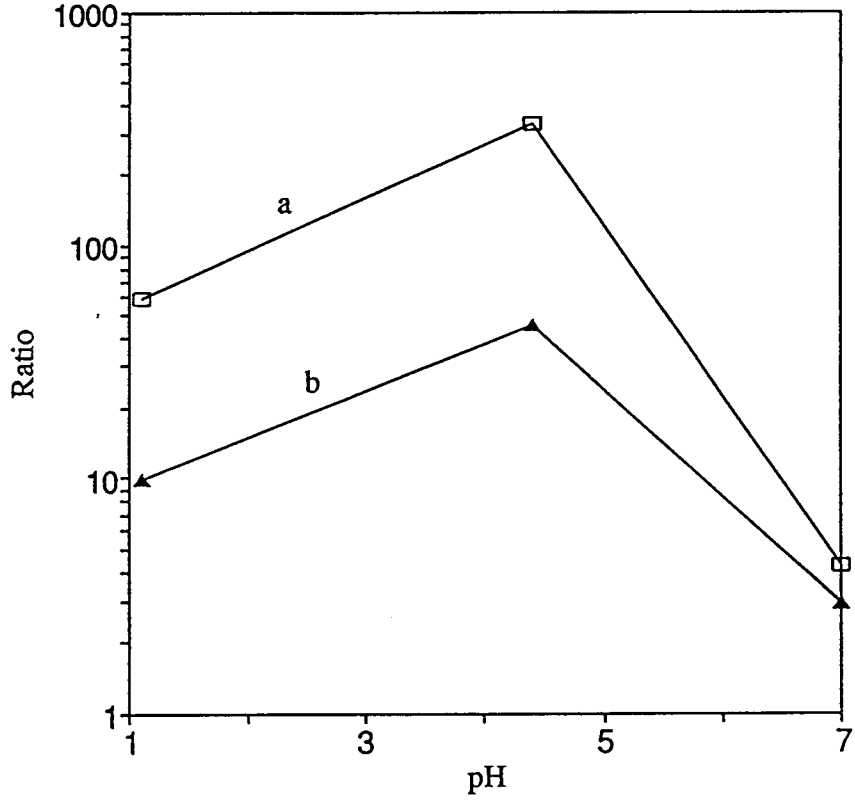

Figure 3.12 Ratios of integrated fluorescence signal to Raman in different pH aqueous solutions. (a) early window (0 ns delay), (b) late window (1 ns delay).

3.2.4 ADP, AMP and Ado in acidic aqueous solution (pH 1.1)

The results described above are the emission spectroscopy of ATP. However, as was noticed in previous work (Table 3.2), most measurements were done on adenyl compounds not containing a phosphate group such as adenosine. Yet early work (Börresen, 1967) showed some difference in quantum yields among ATP, ADP, AMP and Ado. So it became appropriate to compare the results in a series of different adenyl molecules and to study the effects of phosphate group on adenylyl chromophore. The results of a systematic studies of the spectroscopy of ADP, AMP and Ado in acidic solutions follows. Their lifetime analyses are given in Table 3.7a, b and c. The corrected TRES of the fast and slow components for four adenylyl chromophores (ATP, ADP, AMP and Ado) are shown respectively in Figures 3.13 and 3.14.

It is obvious that all three nucleotides ATP, ADP and AMP (see Tables 3.5, 3.7 and Figure 3.13 and 3.14) in acidic solution basically possess similar spectroscopic characteristics. They contain at least two emission components. They all have a fast component with the lifetime $\tau_1 \leq 100$ ps and the peak at 370 nm, and a slow component with the lifetime τ_2 of 4.4 ± 0.2 ns and the peak at 375 nm. This suggests that changing the number of phosphate groups does not affect the spectroscopy of the adenyl group. However, it is worth noticing that fast lifetime for adenosine may be significantly larger than those of adenyl nucleotides, also larger than those of adenyl nucleotides and

Table 3.7 Lifetime analysis of ADP, AMP and Ado in $HClO_4$ aqueous solution (pH 1.1)

a. ADP

Conc., M	λ_{em}, nm	τ,ns	f(α)	f(ατ)
1 x 10^{-4}	340	0.050	61%	2%
		4.16 ± 0.02	39%	98%
	360	4.06 ± 0.01	100%	100%
	390	4.19 ± 0.01	100%	100%

b. AMP

Conc., M	λ_{em}, nm	τ, ns	f(α)	f(ατ)
2 x 10^{-4}	320	0.050	94%	16%
		4.32 ± 0.03	6%	84%
	360	0.081	80%	7%
		4.58 ± 0.03	20%	93%
	390	4.44 ± 0.02	100%	100%

c. Ado

Conc., M	λ_{em}, nm	τ, ns	f(α)	f(ατ)
2 x 10^{-4}	320	0.174 ± 0.01	87%	21%
		4.32 ± 0.03	14%	79%
	360	0.597 ± 0.06	20%	3%
		4.58 ± 0.02	80%	97%

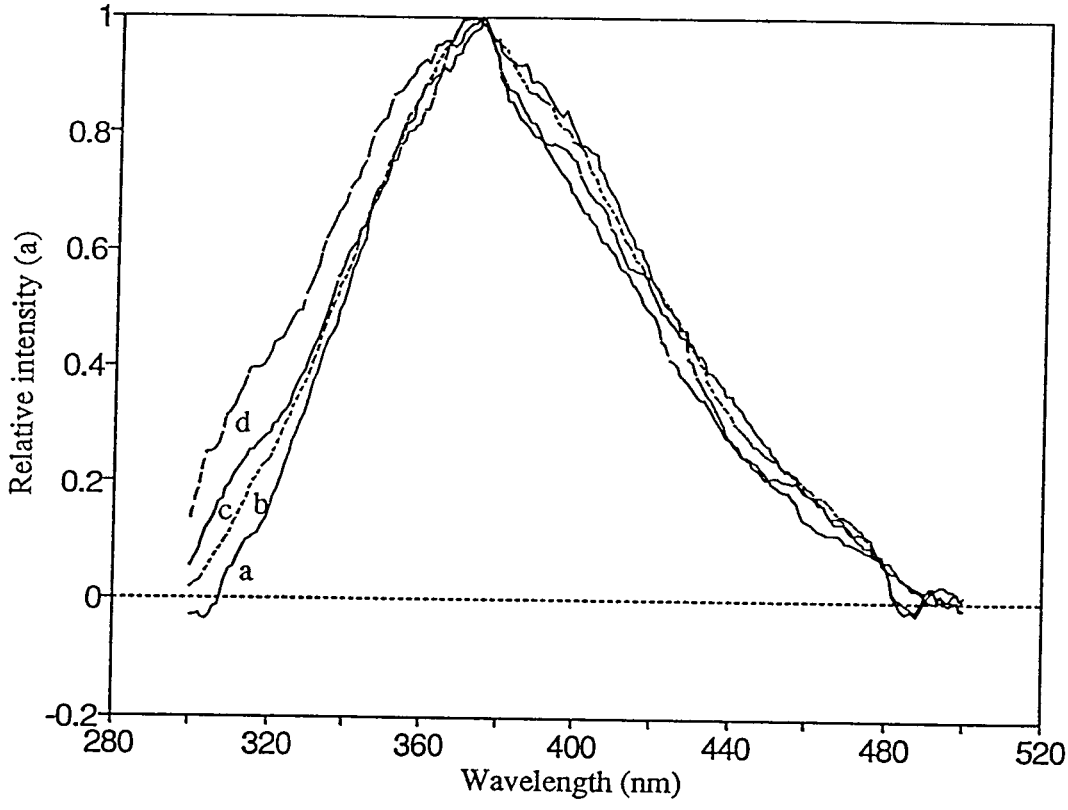

Figure 3.13 The effect of phosphate group on fast component of adenylyl chromophore in aqueous acidic solution (pH 1.1). τ_1 = 0.1 ns is used. (a) ATP, (b) ADP, (c) AMP and (d) Ado.

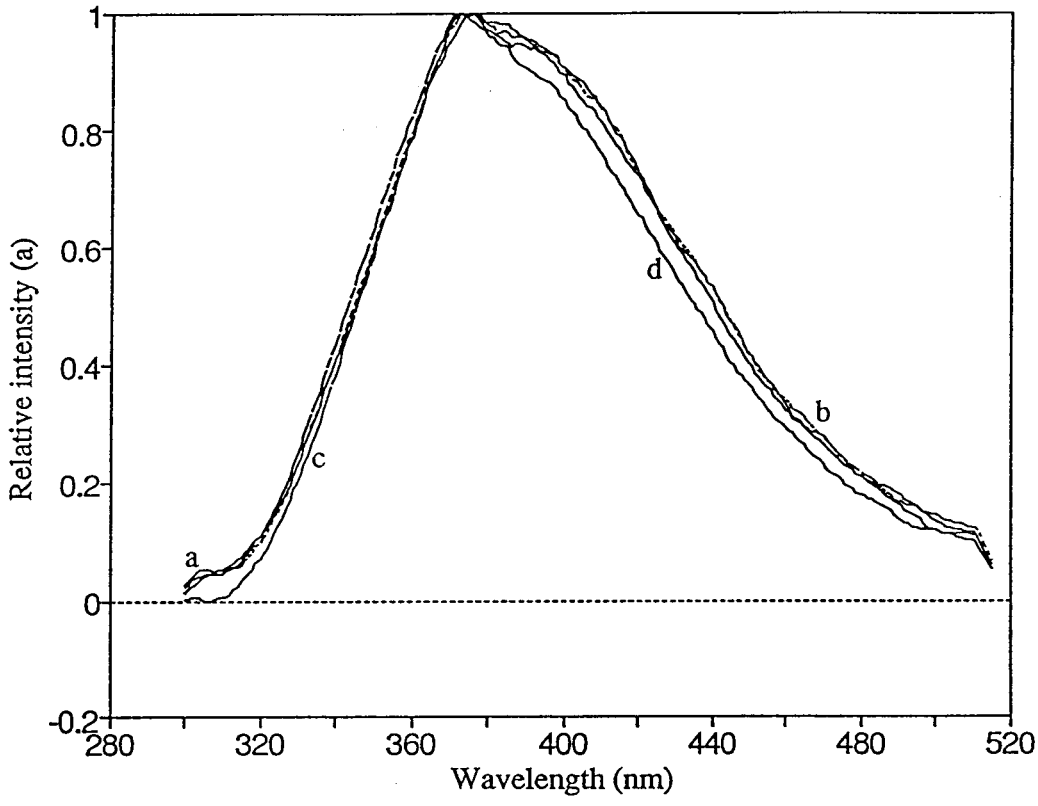

Figure 3.14 The effect of phosphate group on slow component of adenylyl chromophore in aqueous acidic solution (pH 1.1). τ_2 = 4.4 ns (for ATP) and 4.2 ns (for the rest) are used. (a) ATP, (b) ADP, (c) AMP and (d) Ado.

also its spectrum (Figure 3.13) is slightly different from the adenyl nucleotides, which may either arise from the experimental error or attribute to a small effect of phosphate group.

The relative quantum yields of above four adenyl compounds basically agree with Börresen's result, i.e. the quantum yields increase with increasing the number of phosphate group. ATP has highest value and Ado has lowest value.

3.2.5 ATP in acetonitrile and Ado in ethanol solutions

It is well known that displacements of fluorescence spectra can often be related to the solvent-medium interactions. The previous four sections have dealt with the emission spectroscopies of adenyl group in aqueous solutions with different concentrations and pH values and it was found that there were at least two components even in limiting systems of low concentration and high acidity where only one component would have been anticipated. Börresen's early work studied some solvent effects. It was stated that with addition of methanol, the fluorescence intensities of the adenylyl chromophore were either not greatly influenced or somehow augmented, the latter effect being notable in the case of ATP. However, there was no discussion of this solvent effect and no emission spectra measurement with this solvent. In an attempt to investigate the solvent effects on emission characteristics of adenyl chromophore; to examine if the fluorescence emitters are involved in H-bonding and if the polarity of the solvents effect the

spectroscopy, an aprotic polar solvent acetonitrile (D = 36) and a H-bonding polar solvent ethanol (D = 24) were chosen to examine such effects. The lifetime analysis for ATP ($1x10^{-4}$ M) in acetonitrile neutral aqueous solution (7:3 (v/v), pH 7) and Ado ($4x10^{-4}$ M) in pure ethanol solution are listed in Tables 3.8 and 3.9 respectively (ATP is insufficiently soluble in 100% acetonitrile for the purpose of the present work, consequently 70% acetonitrile aqueous solution is used).

It is clear that in both acetonitrile and ethanol solution only a fast component with τ < 100 ps and λ_{max} 305 nm at short wavelengths exists, while the slow component which was observed in other aqueous solutions is not present. As the ratio of the solvent to water was changed from 7:3 to 3:7 for MeCN/H_2O and from pure EtOH to 1:1 for EtOH/H_2O the results remained unchanged.

As there is only one component in the systems, the corresponding corrected time-windowed spectra with τ = 0.06 were obtained by dividing simply the time-windowed spectra by spectral sensitivity. The solvent effect on the fast component of adenylyl chromophore is shown in Figure 3.15. It can be seen that the fast components in three different solvents have similar shape (although the one in buffer is 10 nm wider than the other two in HWHM) and approximate peak position (within 5 nm difference), which indicates that they are identical emitters, and changing the polarity of the solvents does not change the character of their spectra.

Table 3.8 Lifetime analysis of ATP ($1x10^{-4}$M) in MeCN-H_20^* (7:3)

λ_{em}, nm	τ, ns	f(α)	f($\alpha\tau$)
320	0.064	100%	100%
350	0.061	100%	100%

*Aqueous component is buffer solution (pH 7).

Table 3.9 Lifetime analysis of Ado ($4x10^{-4}$M) in pure EtOH solution

λ_{em}, nm	τ, ns	f(α)	f($\alpha\tau$)
320	0.055	100%	100%
350	0.090	100%	100%

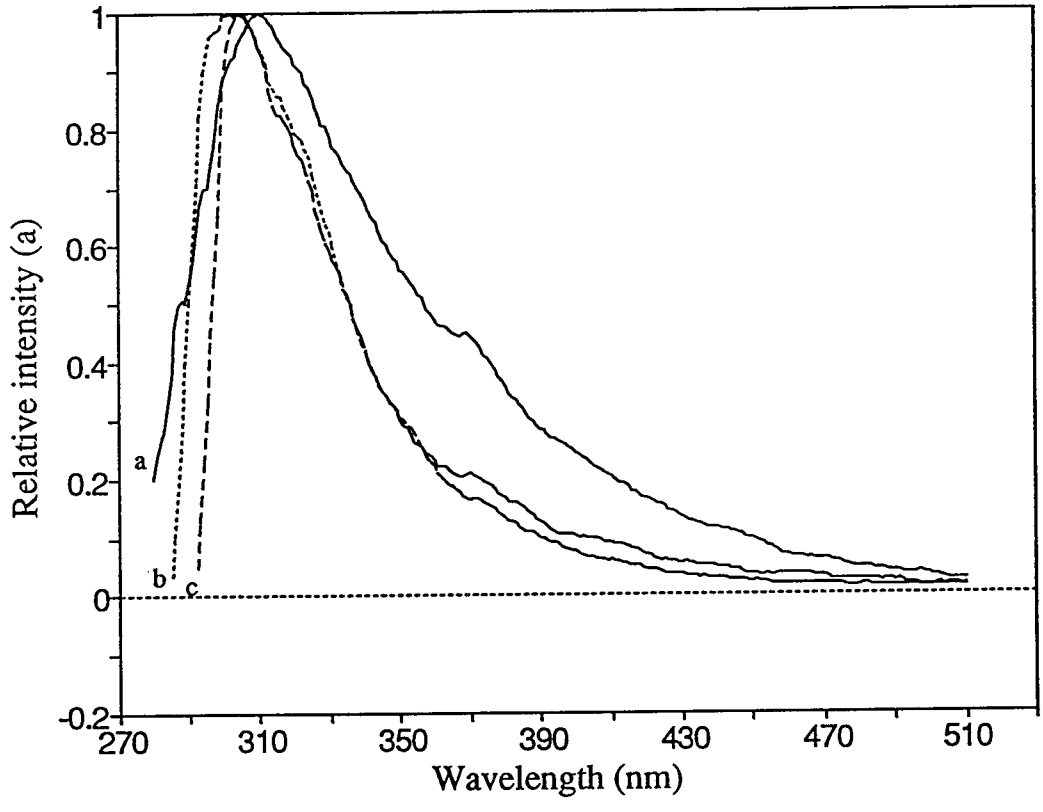

Figure 3.15 Corrected emission spectra of the fast component of adenylyl chromophore in different solvents. (a) ATP/buffer (pH7), (b) ATP/MeCN (7:3), (c) Ado/EtOH.

The entire results for emission spectroscopic properties of adenylyl chromophore in the present work are summarized in table 3.10, and their oscillator strengths in acidic solutions and ATP in neutral aqueous solution are estimated and given in Tables 3.11 and 3.12 respectively.

Table 3.10 Emission spectroscopic characteristics of adenylyl chromophore

compounds	pH or solvent	Conc. (mM)	τ_1 (ns)	$\lambda_{1,max}$	τ_2 (ns)	$\lambda_{2,max}$	$[\alpha_1]/[\alpha_2]^*$
ATP	7.0	0.1	~0.06	310	2.5	385	101
	7.0	0.5	~0.06	310	2.5	385	55
	7.0	10.0	~0.06	305	2.5	385	27
	4.4	0.2	~0.06	350	4.4	375	0.9
	1.1	0.1	~0.10	370	4.4	375	2.9
ADP	1.1	0.1	~0.10	370	4.2	375	3.0
AMP	1.1	0.2	~0.10	370	4.2	375	2.6
Ado	1.1	0.2	~0.17	370	4.2	375	2.5
ATP	MeCN/H_2O	0.1	~0.06	305			
Ado	EtOH	0.4	~0.07	305			

*From integrated time-resolved emission spectra, i. e. $\int\alpha(\lambda)d\lambda$.

Table 3.11 Intrinsic radiation lifetimes and oscillator strengths of adenylyl chromophore in acidic aqueous solutions (pH 1.1)

Compound	ϕ[a]	τ (ns)	λ_{max}	f($\alpha\tau$)[b]	τ_0[c]	f[d]
ATP	0.0046	~0.10	370	0.06		
		4.4	375	0.94	1018	$2x10^{-3}$
ADP	0.0038	~0.10	370	0.07		
		4.2	375	0.93	1184	$1x10^{-3}$
AMP	0.0015	~0.10	370	0.06		
		4.2	375	0.94	2632	$7x10^{-4}$
Ado	0.0008	~0.17	370	0.09		
		4.2	375	0.91	577	$4x10^{-3}$

[a] Cited from Börresen (1965).
[b] $f(\alpha_1\tau_1) = \tau_1\int\alpha_1/(\tau_1\int\alpha_1 + \tau_2\int\alpha_2)$.
[c] τ_0 = intrinsic radiative lifetime = $[\tau/(\phi\ f(\alpha\tau)]$.
[d] f = oscillator strength = $1.47/(\bar{\nu}^2\tau_0)$.

Table 3.12 Intrinsic radiation lifetimes and oscillator strengths of ATP in neutral aqueous solutions (pH 7.0)

ϕ[a]	Conc.(M)	τ (ns)	λ_{max}	f($\alpha\tau$)	τ_0	f
$5x10^{-5}$	$1x10^{-4}$	~0.06	310	0.70		
		2.5	385	0.30	$2x10^{5}$	$1x10^{-5}$
	$5x10^{-4}$	~0.06	310	0.54		
		2.5	385	0.49	$1x10^{5}$	$2x10^{-5}$
	$1x10^{-2}$	~0.06	305	0.37		
		2.5	385	0.63	$8x10^{4}$	$3x10^{-5}$

[a] $\phi_{(Ado)}$ is used from Vigny (1973).

3.3 Discussion

The results of the time-resolved spectroscopy of adenylyl chromophore in the previous section can be summarized as follows. There are two classes of spectra (short and long-lived) in all aqueous solutions. The long-lived spectra are independent of pH, but the lifetimes change from 2.5 ns (at pH 7) to 4.4 ns (at pH 1 and 4). The short-lived spectra change considerably with pH. pH affects the relative quantum yields of ATP dramatically (ϕ(pH 4.4) > ϕ(pH 1.1) > ϕ(pH 7.0)). In neutral solution increasing concentration increases the ratio of the integrated intensities of C2 to C1 of ATP very slightly, and this is probably due to a change in the slow component. The solvent effect shows single fast emission behavior.

3.3.1 Assignment of the emission components in neutral aqueous solution

i) Fast component

The predominant emitting component of ATP in neutral aqueous solution is the fast one with the lifetime < 100 ps and λ_{max} of 310 nm. To assign this, one needs to examine its spectrum carefully. Comparing this emission spectrum (Figure 3.2) with its absorption spectrum (P.L. Inc, 1976), it can be observed that they are mirror images. And also this is further confirmed by comparison with other closely related compounds. Vigny (1977) measured the steady state emission spectrum of AMP and found that it

possessed mirror image character to the absorption. Ballini and coworkers (1988) used time-windowed excitation and emission correlation technique on adenylyl chromophore and recognized that fast emission of Ado in neutral solution is correlated with excitation at 258 nm, the peak of the first absorption band of Ado. Since there is no essential difference in absorption between ATP and Ado, and the emission of ATP in present work is identical to that of Ado, this suggests that the fast component in neutral ATP solution is also attributable to the corresponding transition.

From the structure of adenylyl chromophore one knows that ATP is an analog of Ado because in both the N-9 position is fixed by bonding to a sugar ring. Since there are three possible tautomeric forms of N^9-substituted adenine, such as Ado or ATP (Figure 3.16) the fast emission of ATP in neutral solution may in principle arise from any one of these three tautomers (N-6, N-1 and N-3), while the possibility of the N-7 and N-9 tautomers is eliminated.

Figure 3.16 Tautomeric structures of adenosine

To clarify the tautomer assignment, the present work is compared with N^6, N^6-dimethylated Ado (DMA), a completely fixed form of tautomer of A (Ballini et al, 1988). It is noticed that relative to unmethylated form, a red shift occurs in both absorption and emission spectra of DMA, but the Stokes' shifts are the same. Similar to unmethylated form, the excitation spectrum of DMA does not differ from its absorption spectrum, the emission is very fast, and the absorption correlates with its emission. These imply that the fast component in ATP has the methylated bond structure. Accordingly, it can be stated that the fast emission component of ATP in neutral solution originates from the canonical type of tautomer (amino form).

As illustrated in Figure 3.15, the emission spectrum of ATP in acetonitrile is similar to that of the fast component of ATP in neutral aqueous solution although somewhat narrower (50 nm in MeCN vs. 70 nm in H_2O). This implies that there is no tautomeric change involved prior to the emission of ATP neutral solution since tautomeric change usually requires participation of a protic medium.

ii) Slow component

The minor emitting component of ATP in neutral aqueous solution is the slow one. Its spectrum is the same as the major emission in acid solution (Figure 3.10), and change in its lifetime from acid solution (~ 2 ns to 4 ns) is minor. To assign this, it is necessary to consider the situation in acid solution.

The steady state emission spectrum of adenylyl chromophore in acid solution (Börresen, 1967; Knighton et al, 1982) has a Stokes shift of 11,800 cm^{-1} from the absorption, where in neutral solution it is much less (~ 8000 cm^{-1}) (Hauswirth and Daniels, 1971; Vigny and Ballini, 1977). Its absorption spectrum is only slightly changed on protonation, but the mirror symmetry is lost. The emission is much more intense than neutral solution and it is depolarized, and the excitation spectrum (λ_{max} 275 nm) is also quite different (Börresen, 1967) from the absorption spectrum (λ_{max} 258 nm). The lifetime analysis shows it is quite long lived (> 4 ns)(Ballini et al, 1988) and the time-resolved spectrum shows the excitation spectrum for this emission is the same as that in steady state. The emission characteristics in acid solution are different from those of the major component in neutral solution, and the origin for this is still uncertain.

The discrepancy between the excitation and absorption spectra of adenylyl chromophore has suggested that either a minor tautomeric form is involved or tautomeric change following excitation. Attempting to resolve these questions, the methylated derivatives were used but the results are not entirely unambiguous principlely because the entirely fixed derivatives have rarely been used (Börrensen, 1963; Knighton et al, 1982). Most work was done by using substituted adenine with N^7-H ⇌ N^9-H ambiguity, plus other uncertain tautomers. This early work concluded that the fluorescent tautomer for adenine is protonated in N^1 or N^7 (Börresen, 1967) or only N^7 (Knighton et al, 1982) for N^9-substituted adenine, such as ATP or Ado.

However, this can not account for all facts because if it is the case, the emission spectra of the protonated species should be the same, which is not true. In addition, this interpretation ignores the important role of the exocyclic amino group (Ward and Reich, 1968). Two amino- purine isomers exhibit some distinct spectral characteristics. Adenosine (6-aminopurine ribonucleoside) in neutral solution possesses a pK_a of 3.7, λ_{max} of 258 nm, Stokes' shift of 6.8 k cm^{-1}, $\tau \sim 5$ ps and ϕ_f of 4×10^{-5}. On increasing acidity, ϕ_f is significantly increased and Stokes' shift doubles. In contrast to adenine, its isomer (2-aminopurine ribonucleoside) shows the similar pK_a (3.4) and Stokes' shift (5.9 km^{-1}), but the ϕ_f (0.68) is dramatically increased by four orders of magnitude and the fluorescence lifetime is much longer (~ 7 ns). In acid solution, fluorescence is quenched. These striking characteristics indicate that the exocyclic amino group and its location plays a very important role in the emission of adenyl chromophore in neutral solution, as has been proposed earlier (Ballini et al, 1988), who suggest the interactions between amino group and 7-N.

3.3.2 Origin of slow component in neutral aqueous solution

i) Via ground state

Because of the previous sections, it is reasonable to assume that the fast and slow emission components in neutral aqueous solution are attributed to unprotonated and protonated ATP respectively. At first, supposing these

unprotonated and protonated species originate via the ground state, the dynamic scheme can be expressed as:

$$ATPH^+ \overset{K_a}{\rightleftarrows} ATP + H^+ \qquad (pK_a = 4.3)$$

$$ATP \overset{h\nu}{\longrightarrow} ATP^*$$

This unprotonated species will give rise to `320' nm emission.

$$ATP^* \longrightarrow ATP + \text{fast fluoresc. } (\lambda_{max} \text{ 310 nm})$$

Excitation of the acid protonated ground species will give the acid fluorescence.

$$ATP^+ \longrightarrow (ATPH^+)^*$$

$$(ATPH^+)^* \longrightarrow ATPH^+ + \text{slow fluores. } (\lambda_{max} \text{ 380 nm})$$

Accordingly, the total fluorescence intensity should be

$$I_{fl}(ATP)_{pH7} = \phi_1(ATP)_{pH7} \times f_1(ATP) + \phi_2(ATP^+) \times f_2(ATP^+)$$

where ϕ_1 and ϕ_2 denote the quantum yields of fast and slow components respectively, and f_1 and f_2 represent the fractions of fast and slow components in the system respectively. Since ϕ(ATP) in neutral solution is not available, 3 $\phi(AMP)_{pH7}$ is used as a trial value based on the fact that the quantum yield of ATP in acid solution is about three fold greater than AMP. Since $pK_a = 4.3$,

at pH 7 $f_1 \sim 1$ and $f_2 \sim 10^{-3}$, Along with the value of $\phi(ATP^+)$ from Table 3.11 the total fluorescence intensity of ATP in neutral solution can be estimated.

$$I_{fl}(ATP)_{pH7} \simeq (3 \times 5 \times 10^{-5} \times 1) + (4.6 \times 10^{-3} \times 0.001)$$

$$= 1.5 \times 10^{-4}$$

It leads to the fraction of the emission of the fast component ~ 3% from this model. This is not in agreement with the experimental value of 30-50% (Table 3.12) and the model is inadequate.

ii) Via excited state

An alternative way to interpret the origin of the slow component in neutral solution is via excited state reaction.

$$ATP \xrightarrow{h\nu} ATP^*$$

$$ATP^* \longrightarrow ATP + \text{fast fluoresc. } (\lambda_{max} \text{ 310 nm})$$

$$ATP^* + H_2O \longrightarrow (ATPH^+)^* + OH^-$$

$$(ATPH^+)^* \longrightarrow ATPH^+ + \text{slow fluores. } (\lambda_{max} \text{ 380 nm})$$

This mechanism may occur to a significant extent if the ATP^* is a stronger base than ATP. This has been indicated by earlier work. At the early stage, Börresen (1963) studied the pH dependence of the fluorescence of NAC

aqueous solutions at room temperature and found that the pK_a's of fluorescence activation were higher than those in ground state for all adenylyl chromophore. For ATP, the difference was 0.6. Low temperature measurements (Longworth et al, 1966) showed the same tendency with larger differences (between 1 and 2). More recently, Parkanyi et al (1984) calculated pK_a from the spectral shifts, and found that the basicity of most of the purines and pyrimidines is increased in the excited singlet state and triplet state compare to the ground state. All of this evidence indicates the excited adenylyl chromophore is a stronger base than the ground state. This supports to some extent the model for the origin via an excited state.

Above model assumes that the reaction

$$ATP^* + H_2O \longrightarrow (ATPH^+)^* + OH^-$$

can take place. Its validity can be tested by comparing the magnitudes of individual rate constants in the following reactions:

$$ATP^* \xrightarrow{k_f} ATP + h\upsilon$$

$$ATP^* + H_2O \underset{k_r}{\overset{k_a}{\rightleftarrows}} (ATPH^+)^* + OH^-$$

where k_f, k_a and k_r are the rate constants of fluorescence, protonation and recombination process respectively, and $k_a/k_r = K_a^*$, the ionization constant of the excited state of ATP. For above two reactions to be competitive and to

take place at same time, the magnitude of the rate of fluorescence should be comparable to that of protonation process within an order of magnitude.

$$k_f [ATP^*] \approx k_a [ATP^*][H_2O]$$

$$k_f \approx k_a [H_2O]$$

Supposing the intrinsic radiative lifetime of ATP is several nanoseconds (Section I), say, 5 ns, then $k_f = 1/\tau_0 \approx 2 \times 10^8\ s^{-1}$ and we have

$$k_a \approx k_f/[H_2O] \approx 2 \times 10^8 / 55 \approx 4 \times 10^6\ M^{-1}s^{-1}$$

Consequently,using Börresen's estimate of pKa_a^*

$$k_r \approx k_a / K_a^* \approx 4x\ 10^6 / 2.5 \times 10^{-5} \approx 1.6 \times 10^{11}\ M^{-1}\ s^{-1}$$

This estimate of k_r is reasonable based on known results for proton-anion recombination reactions.

3.3.3 Behavior in acid solution

As exhibited in Figure 3.8, the time-resolved emission spectra of the fast and slow component in acid solution are almost completely overlapped. They have a same peak position (380 nm) and similar shape but the fast one has slight blue-shift (~ 10 nm at half-maximum on high energy side and 20 nm on the low-energy side) relative to the slow; this is very different from the spectrum of the fast emission in neutral solution. In order to account for this spectral behavior, it is necessary to consider the solvation process. The origin of the spectral shift of adenylyl chromophore does not lie only on the tautomeric forms and the role of the exocylic amino group. It has been reported that at low temperature (77°K), the emission spectrum (Figure 3.17)

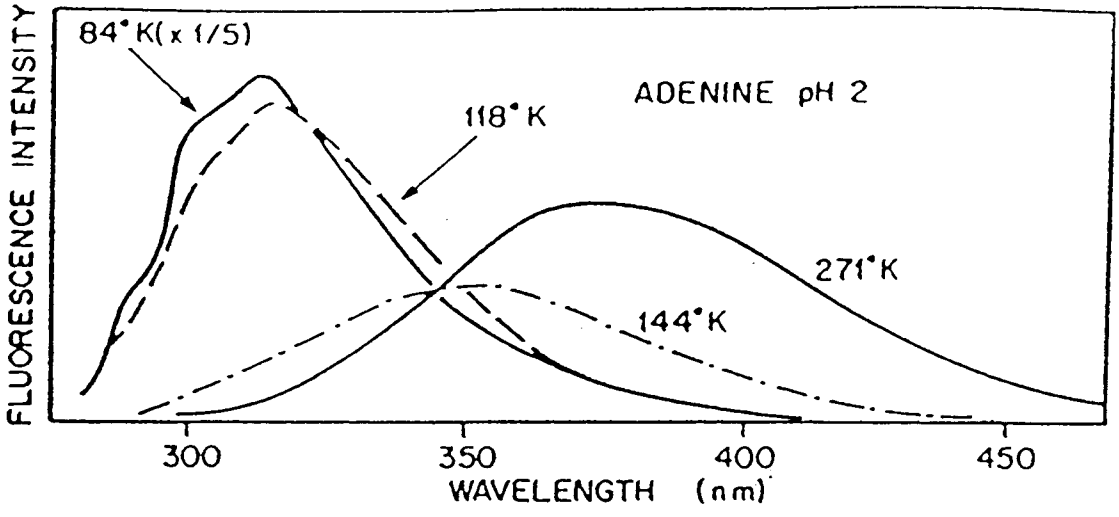

Figure 3.17 Fluorescence spectra of protonated adenine in EGW at various temperatures. (Taken from Eisinger and Lamola, 1971.)

of the protonated adenine (Eisinger and Lamola, 1971) is practically identical to the unprotonated and to the fast component of ATP in neutral solution (Figure 3.2). In view of the similarity of emission spectrum of adenine to ATP, this implies that the protonation of ATP does not change the fundamental spectral characteristics. However, on warming up the spectrum is shifted to the red successively. This raises some questions: what is happened in the system? Clearly, the spectral shift (from the 258 nm absorption peak to 380 nm) emission peak is too large to be due to changed Frank-Condon distribution. Probably this shift is involved in a solvation process, which is activation or diffusion controlled and hence inhibited at 77K.

Above model may rationally interpret why spectrum of the fast component in acid solution shows a small blue shift relative to the slow. This is because the fast component may be a residual of the original excited state which emits fluorescence before it is completely solvated. This in turn implies that the solvation process at room temperature occur on a time-scale comparable to the emission process.

3.3.4 pH effect on quantum yields

It is has been mentioned earlier that in the work from Rigler's laboratory (1985), pH is not explicit. In fact, the `390' nm component with lifetime of 4.17 ns is due to protonated ATP because in ATP/H_2O solution (pH 4.4), ATP is 44% protonated and its lifetime and spectrum are identical to those of the slow component in acid solution (Table 3.5 and Figure 3.8). The other component with a lifetime of 290 ps is not consistent with this work. Most possibly it is a stacking-form species, probably the same as the concentration-dependent species which Yamashita (1987) found in neutral solution with a lifetime of 320 ps and a peak position of 380 nm. The second possible reason is because the emission spectrum he collected is "gated" with a 2 ns delay so that a considerable proportion of the fast component may be lost. Since measured lifetime is an average value, this consequently may lead to his value (290 ps) larger than mine. The third possible reason for the discrepancy between his and my work may be caused by using the different excitation wavelength (290 nm vs. 265 nm).

A striking characteristics of pH effect observed in this research is that the relative quantum yield of ATP in unbuffered aqueous solution (pH 4.4) is greater than that in acid solution (pH 1.1) and much greater than that in neutral buffer solution (Figure 3.12). This is contrary to the common expectation. It is known that the quantum yield of the protonated ATP is one to two order larger than unprotonated one. With decreasing pH the fraction of the $ATPH^+$ is getting larger, and the quantum yield should be increasing monotonously getting greater all the way through pH 1. But it is not the case here. The maximum of the relative quantum yields at pH 4 rather than pH 1 suggests there may exist an other form of the emitting species. For simplification, A is used standing for ATP. The possible form of emitting species may be generated by combining the protonated ATP with unprotonated one.

$$AH^+ + A \overset{K_c}{\rightleftarrows} (A\ H\ A)^+$$

where the resultant $(AHA)^+$ is complex ion, whose concentration depends indirectly upon pH, reaching a maximum at pK_a. If $\phi(AHA)^+ > \phi(AH)^+$, this model will reflect the experimental results.

3.4 Conclusions

We can draw the following conclusions from the present work of adenylyl chromophore:

1. There are at least two emission components in all aqueous solutions. The long-lived spectra are independent of pH, but the lifetime change from 2.5 ns (pH 7) to 4.4 ns (pH 1-4), and the oscillator strengths (10^{-3}-10^{-5}) confirm the existence of the weak transition in adenyl group.

2. The fast emission in neutral solution is a mirror image of its absorption, and may originate from the canonical tautomer.

3. The slow emission in neutral solution may be attributed to protonated ATP origining via the excited state. The difference in lifetime from acid (4.4 to 2.5 ns) probably arise from acid/base catalysis.

4. The small difference between the short- and long-lived spectra in acid solution may be due to an incomplete solvation process.

5. Results of Rigler at el seem to pertain to unbuffered solution having a pH 4.4. The dominance of emission at λ_{max} 390 nm with lifetime 4.17 ns can be understood as the consequence of direct excitation of protonated ATP. The shorter-lived emission with lifetime 290 ns, which is not found in the present work, may be a concentration-dependent species.

6. pH affects the relative quantum yields dramatically (ϕ(pH 4.4) > ϕ(pH 1.1) > ϕ(pH 7.0)). This may be attributed to the formation of a complex $(ATPHATP)^+$ at pH 4.4.

7. Phosphate group does not affect spectroscopic characteristics of adenylyl chromophore.

8. The non-aqueous solutions show single fast emission.

4. RESOLVED UV ABSORPTION SPECTRA OF G, C'S, D(GC) AND POLYD(GC)·POLYD(GC), AND TIME-RESOLVED EMISSION SPECTROSCOPY OF G AND C

4.1 Introduction

Detailed knowledge and understanding of the electronic structure of nucleic acids is one of the natural goals of science. One way to obtain the information about this is to study the UV absorption and emission spectra of nucleic acid component, especially biopolymers.

There is considerable interest in the spectroscopic characteristics of G, C, G-C dimers and polymers because of their importance for high G-C content DNAs, which form the left-handed helix, Z form, under certain conditions (Lafer et al, 1981). It has been noticed that the UV absorption spectra of dimer d(CG) and polymer polyd(GC)·polyd(GC) (Wells et al., 1970) are quite different from each other. There are two overlapping bands in d(GC) with a maximum at 256 nm and a shoulder at 272 nm, respectively, which are very close to the peaks of the main absorption bands of G and C (Voet et al, 1963). However, polyd(GC)·polyd(GC) has only one peak, λ_{max} at 256 nm and the half-width is narrower compared to d(CG). In addition, the dimer exhibits hypochromism (7%) in the wavelength range of 255-285 nm and slight hyperchromism in the longer wavelength range of 285-300 nm. In the case of the polymer, the hypochromism (14%) covers almost the whole absorption range of 230-290 nm. All of above the facts imply that the GC pairs interact more strongly and perhaps differently in the polymer compared with the

dimer. Although d(CG) is single-strand it is a self-complementary dinucleoside phosphate, thus, there exists the possibility of it being in duplex conformation, depending on concentration.

These bring us some interesting questions: How do GC pairs interact in the dimer and polymer? Why is hypochromism in the dimer different from that in the polymer? How do the interactions relate to electronic transitions of G and C and the orientations of stacking forms of G and C? How can the contribution to the absorption from individual monomer G and C be described in terms of oscillator strengths?

No work has been done so far to answer these questions. The present work is an attempt to account for the different hypochromism of the absorption spectra of d(CG) and polyd(GC)·polyd(GC) in terms of the oscillator strengths of the transitions of the monomers and changes in those oscillator strengths when the monomers interact in d(CG) and polyd(GC)·polyd(GC).

The approach is as follows: The first stage is to determine the number and strengths of electronic transitions in the monomers G and C. This has been done here by resolving their UV absorption bands using gaussian functions. The second is to fit the absorption spectra of dimer and polymer with an appropriately weighted sum of the individual gaussians of G and C and obtain their contributions to the absorptions. (The third, not presented here, is to relate the fitting results to the orientations of experimental transitions in G and C and to the molecular geometry of DNA.)

The absorption spectra of d(CG) and polyd(GC)·polyd(GC) used in the present work is in the range of 230-310 nm (Ballini et al, 1984a and 1984b). To fit these spectra, the resolved spectra of monomer G and C must be properly accounted for in this range. For guanosine, it is acceptable to present the components simply as two transitions in the range of 230-310 nm because the minimum extinction coefficient (3100 M^{-1} cm^{-1} is almost reached at 230 nm ($\varepsilon \sim 4000$). For cytidine, the situation is not such simple because of the quite high extinction coefficient (~8000) at 230 nm. Thus, the higher transitions must be taken into account and data for analysis are extended below 200 nm. Inspection of the spectra and comparison with the literature shows that three peaks can be recognized below 6.3 eV (all spectra and calculations show a strong transition 196 nm (6.3 eV). Consequently, this is taken as a benchmark and later discussion is carried out in terms of the number of the transitions below this benchmark).

In addition, because the $\pi\pi^*$ bands of C show more solvent dependence than those of the other NAC chromophores (Callis, 1983), the present work studies and determines the number of electronic transitions of the monomer cytidyl chromophore in different solvent conditions, a problem which is still unsettled, and at the same time probes the solvent interactions.

There are several papers on the fluorescence spectroscopies of guanyl and cytidyl chromophores. In the early work, Vigny et al (Vigny 1973; 1974; Vigny and Duquesne, 1976) measured quantum yields of guanosine and cytidine as well as GMP and CMP utilizing a photon-counting

spectrophotometer, and calculated the fluorescence lifetimes of GMP and CMP by using the Stricker-Berg equation. Callis (1979) measured polarized fluorescence of guanine and cytosine both in neutral aqueous solution at room temperature and in ethylene glycol-water at -125°C and estimated their lifetimes with the Stricker-Berg equation. However, there are no direct experimental measurements of the lifetimes of C at room temperature and only a few of G (Rigler et al, 1985; LeBreton et al, 1989) and there is no report of time-resolved spectra of G and C. It was desired that by utilizing sub-ns time-resolved fluorescence spectrometer in the present research, some information about the lifetimes and time-resolved emission spectra of G and C could be obtained, thereby extending current knowledge on spectroscopic characteristics.

4.2 Results

4.2.1 Hypochromism and electronic transitions in d(CG) and polyd(GC)·polyd(GC)

The UV absorption spectra of guanosine and deoxycytidine (Voet et al, 1963) in aqueous solution were digitized manually (typically at 2 nm intervals). The digital absorption spectra of d(CG) and polyd(GC)·polyd(GC) were obtained from Ballini et al (1984a; 1984b). The experimemtal conditions under which these absorption spectra were collected and their characteristic parameters are listed in Table 4.1.

These digitized monomer absorption spectra were fitted by multiple electronic transitions using gaussian functions in the PeakFit computer program (Jandel Corperation, 1990). The automatic presetting by the program and the Curve-fit process (see section II) were used for fitting the absorption spectra of guanosine from two different sources (Figures 4.1a and 4.1b). The sum of squares of residuals χ^2 and coefficient of determination r^2 are shown above the graph and the gaussian parameters are included in Table 4.2, where λ_0, A_0 and δ represent the center wavelength, amplitude and width (δ = 0.707 $\delta_{1/e}$) respectively, and the number in parenthesis designates the gaussian in the order of increasing energy. The small χ^2 and r^2 close to one indicate that the fit is very successful. The number of gaussians in both figures suggest that there are two electronic transitions in the range of 230-310 nm. In Figure 4.1a, the first transition is at λ_{max} 278.9 nm with an

Table 4.1 The properties of absorption spectra of G, C, d(CG) and polyd(GC)·polyd(GC)

Compound	source	pH	range, nm	f	λ_1,nm	ε_1	λ_2,nm	ε_2
guanosine	P.L. Inc., 1976	7	230-310	0.38	276	8980	252	13600
guanosine	Voet et al, 1963	5.5	230-310	0.376	276	8900	252	13700
deoxycytidine	Voet et al, 1963	7.8	190-310	0.837	272	8865	197	22450
d(CG)	Ballini et al, 1984a	7.2	230-310	0.33			260	9000*
polyd(GC)·polyd(GC)	Ballini et al, 1984b	7.2	230-310	0.24			254	8400**

*Data were normalized using $\varepsilon(254) = 9.85 \times 10^3$ from P.L. Biochemical catalog, p.26(1976).
**Data were normalized using $\varepsilon(254) = 8400$ from Wells, et al, 1970.

Table 4.2 Gaussian parameters for fitting the absorption spectra of guanosine

Source	pH	λ_0 (1), nm	A_0 (1), M^{-1},cm^{-1}	δ (1), nm	λ_0 (2), nm	A_0 (2), M^{-1},cm^{-1}	δ (2), nm
P.L. Inc, 1976	7	278.9	6.586×10^3	8.875	251.2	3.66×10^3	13.92
Voet et al, 1963	5.5	278.6	6.260×10^3	8.243	251.7	13.66×10^3	13.98

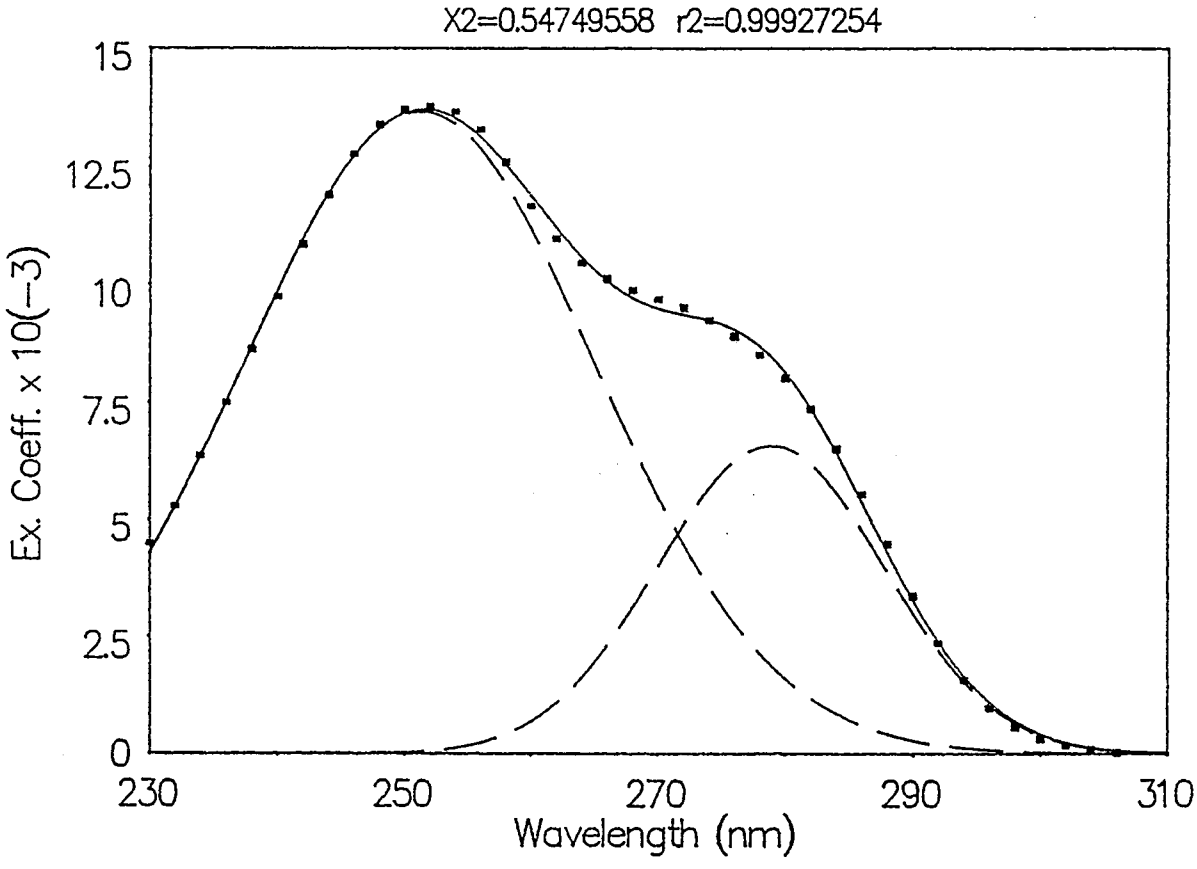

Figure 4.1a Gaussian fitting of absorption spectrum of guanosine (pH 7), digitized from P.L. Inc, (1976). The points are experimental data, the dashed line is gaussian component, the solid line is sum of the gaussians. These labels are applied to all gaussian fitting graphs.

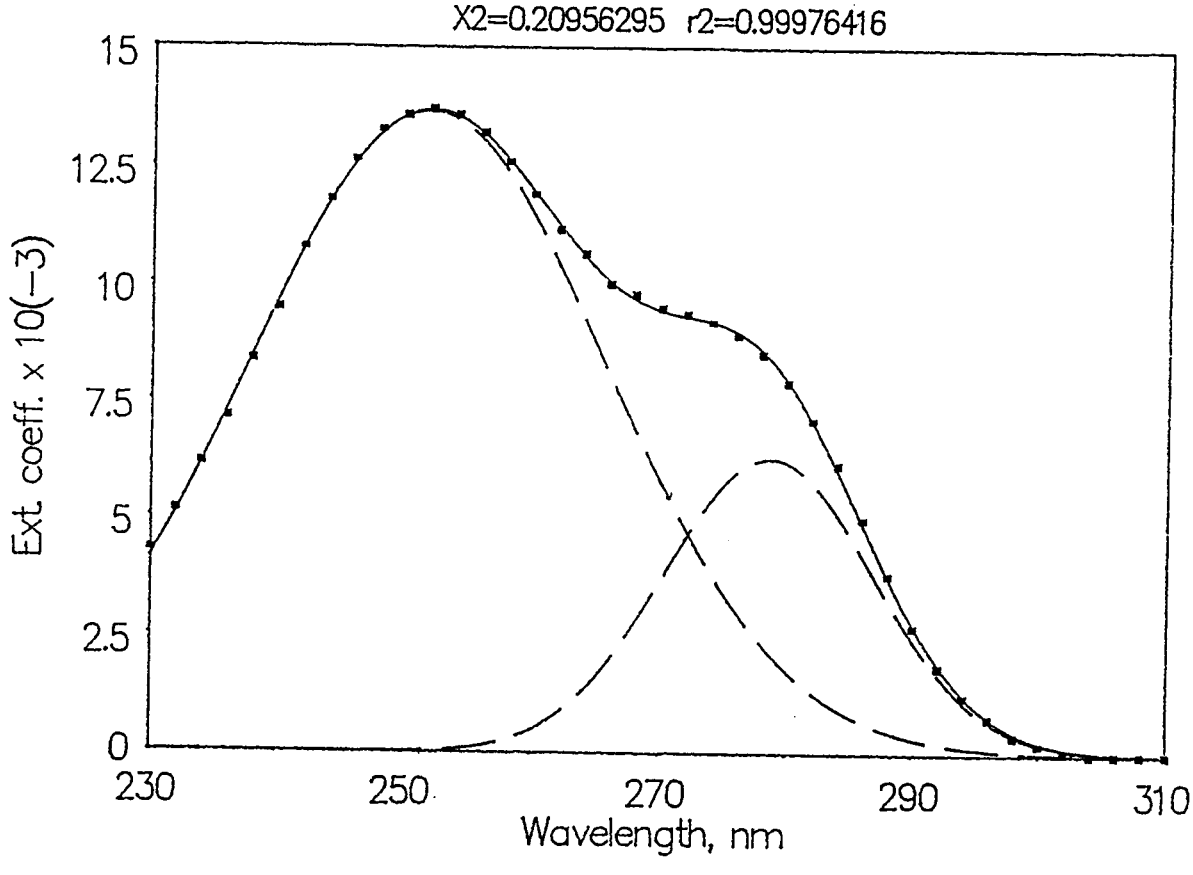

Figure 4.1b Gaussian fitting of absorption spectrum of guanosine (pH 5.5), digitized from Voet et al (1963).

amplitude of 6.6 x 10^3 M^{-1} cm^{-1} and width of 8.9 nm; the second stronger transition is at λ_{max} 251.2 nm with amplitude of 13.7 x 10^3 and width of 13.9 nm. Similar to this, in Figure 4.1b, the first transition is at λ_{max} 278.6 nm, amplitude of 6.3 x 10^3 and width of 8.2 nm, and the second transition is at λ_{max} 251.7 nm, amplitude of 13.7 x 10^3 and width of 14.0 nm. The differences between the fitting parameters of these spectra are very small. Because the pK_a value of guanosine anion is 9.2, to avoid a small fraction of anion involved in the spectra, the resolved spectrum of guanosine from Voet at al (pH 5.5) was chosen to fit d(CG) and polyd(GC) later.

The Step-fit process (section II) was used for fitting the absorption spectrum of deoxycytidine in neutral aqueous solution because the Curve-fit process in this case could not give reasonable widths of gaussians, i.e. one of the gaussians ended by being unreasonably wide (as wide as the entire spectrum). The fitting with four gaussians was used based on the known peak positions and the widths from literature (Callis, 1983; František et al, 1984), and the result is shown in Figure 4.2. It can be seen that the fitting with four gaussians is reasonably good although χ^2 is larger compared to guanine. The gaussian parameters (center wavelength, amplitude, width) for each transition are as follows. I. 272.5, 8.7 x 10^3, 11.05; II. 244.5, 5.3 x 10^3,12.10; III. 219.9, 7.5 x 10^3, 11.87; IV. 196.2, 20.96 x 10^3, 8.875.

Above gaussian fittings of absorption spectra of G and C have been carried out using the wavelength (nm) representation of spectra. Spectral

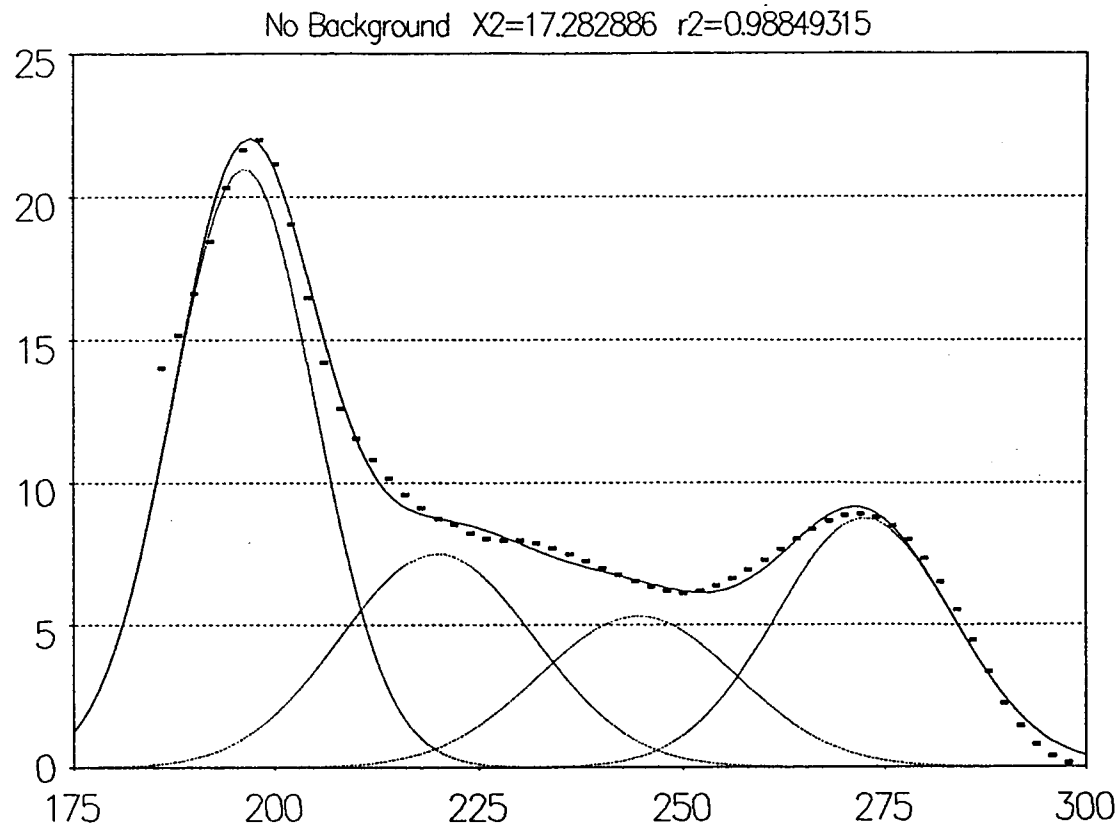

Figure 4.2 Four-gaussian fitting of absorption spectrum of deoxycytidine (pH 7.8), digitized from Voet et al (1963).

theory usually develops bandshapes in wavenumber (cm^{-1}) representation and according to the harmonic oscillator model (Inagaki, 1974; Levin, 19 ; Marcus, 1989) the fundamental bands should be gaussian and symmetric in cm^{-1}. This is found not to be the case here. The fittings of absorption spectra of guanosine and several cytidyl chromophore (see later) in cm^{-1} representation have been tried and compared with those in nm representation. It turns out that the fittings in nm representation are better, which can indicate that the fundamental bands are asymmetric. This has been noticed by several researchers (Morozov et al., 1986; Kang and Johnson, 1993). They chose to add a skewness factor to gaussian parameters and fit the spectra using log-normal fitting (four gaussian parameters for each fitted transition). To minimize the number of adjustable parameters in the present work, the nm representation of the spectra was chosen for the fitting.

A comparison has been made between the absorption spectra of d(CG), polyd(GC)·polyd(GC) and the average absorption spectrum of equimolar mixtures of G and C which would be expected if there were no interaction between the bases (Figures 4.3 and 4.4, respectively). The distinct shapes of differences between the two figures imply that there are interactions between G-C pair in d(GC) and that this interaction differs in polyd(GC)·polyd(GC). Hypochromism in d(CG) seems to occur only in the first absorption band, while in polyd(GC)·polyd(GC), hypochromism is also involved in the second. To attempt to account for this the gaussian components of G and C have been

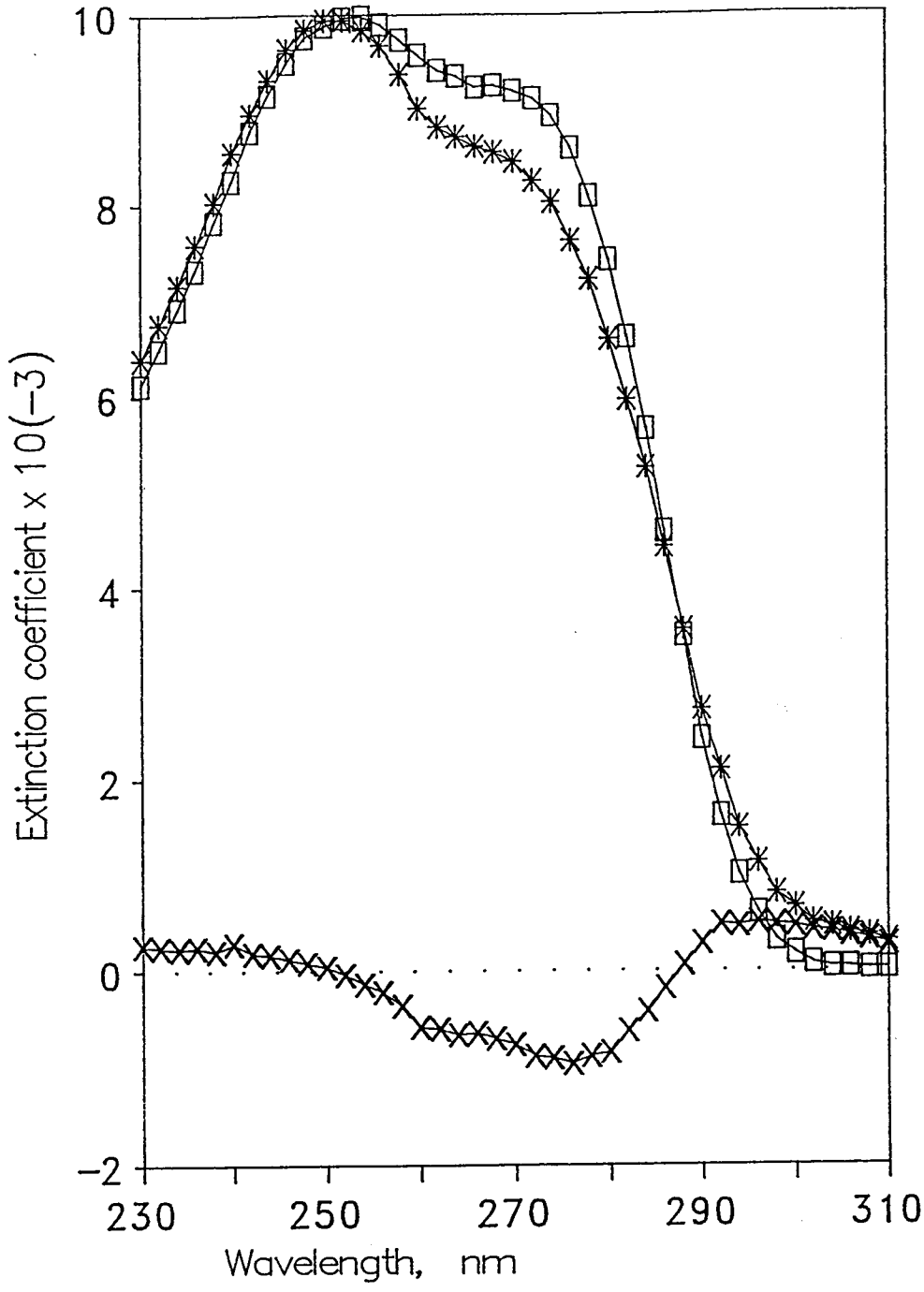

Figure 4.3 Absorption spectrum of d(GC) and average absorption spectrum of equimolar mixtures of G and C. d(CG) (***), (G+C)/2 (□□□), difference between d(CG) and (G+C)/2 (xxx).

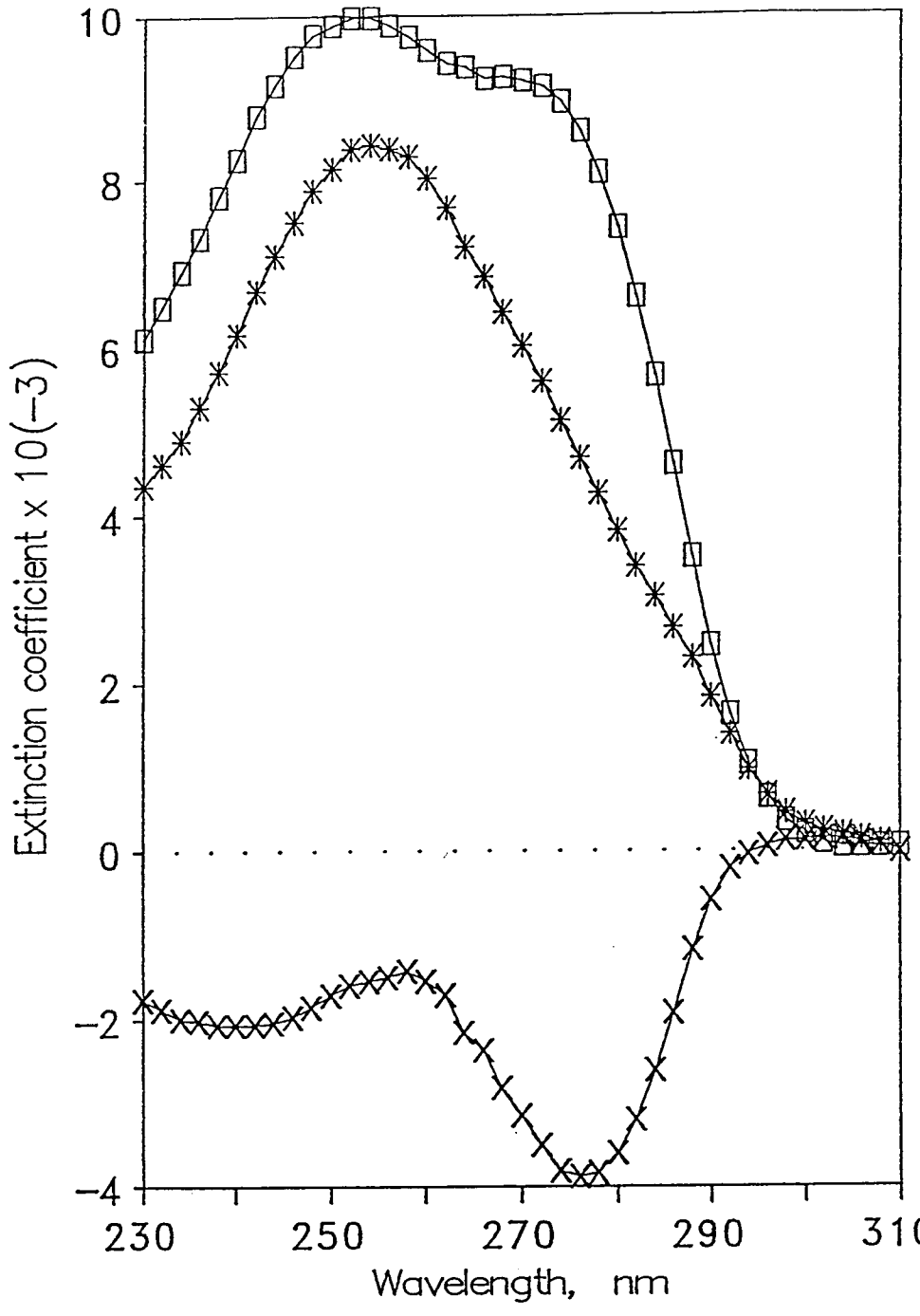

Figure 4.4 Absorption spectrum of polyd(GC)·polyd(GC) and average absorption spectrum of equimolar mixtures of G and C. polyd(GC)·polyd(GC) (***), (G+C)/2 (□□□), difference between polyd(GC)·polyd(GC) and (G+C)/2 (xxx).

weighted empirically and summed to fit the absorption spectra of d(CG) and polyd(GC)·polyd(GC) respectively.

The fitting function can be expressed as:

$$\hat{y} = (g1 * G1 + g2 * G2 + c1 * C1 + c2 * C2 + c3 * C3) / 2$$

where the coefficients g1, g2, and c1, c2, c3 are the weighting factors of gaussian components of G1, G2 (for guanosine) and C1, C2, C3 (for deoxycytidine) in the range of 230-310 nm, a range of the experimental absorption spectra of d(CG) and polyd(GC)·polyd(GC). Since the higher energy gaussian component C4 of deoxycytidine is beyond this range, it is not included in the fitting.

The coefficients of the individual gaussians G and C were adjusted during the fitting until the minimum sum of squares of residuals χ^2 and the best coefficient of determination r^2 were reached. The best fits then obtained to the experimental spectra are shown in Figure 4.5 and 4.6 and their statistic analysis are listed in Table 4.3.

Figures 4.5 and 4.6 show that the fittings of the absorption spectra of d(CG) and polyd(GC)·polyd(GC) using modified sum of the gaussian G and C components are reasonably good. The residuals are very close to zero except for those in the tail, which are still small. The positive residuals in this region imply that there may exist some other interactions (hyperchromism ?) between GC pair. Table 4.3 tells us that for d(CG) the hypochromism in the range of 255-285 nm only arises from the first transitions G1 and C1 because their weighting factors g1 and c1 are smaller than one, and the other transitions

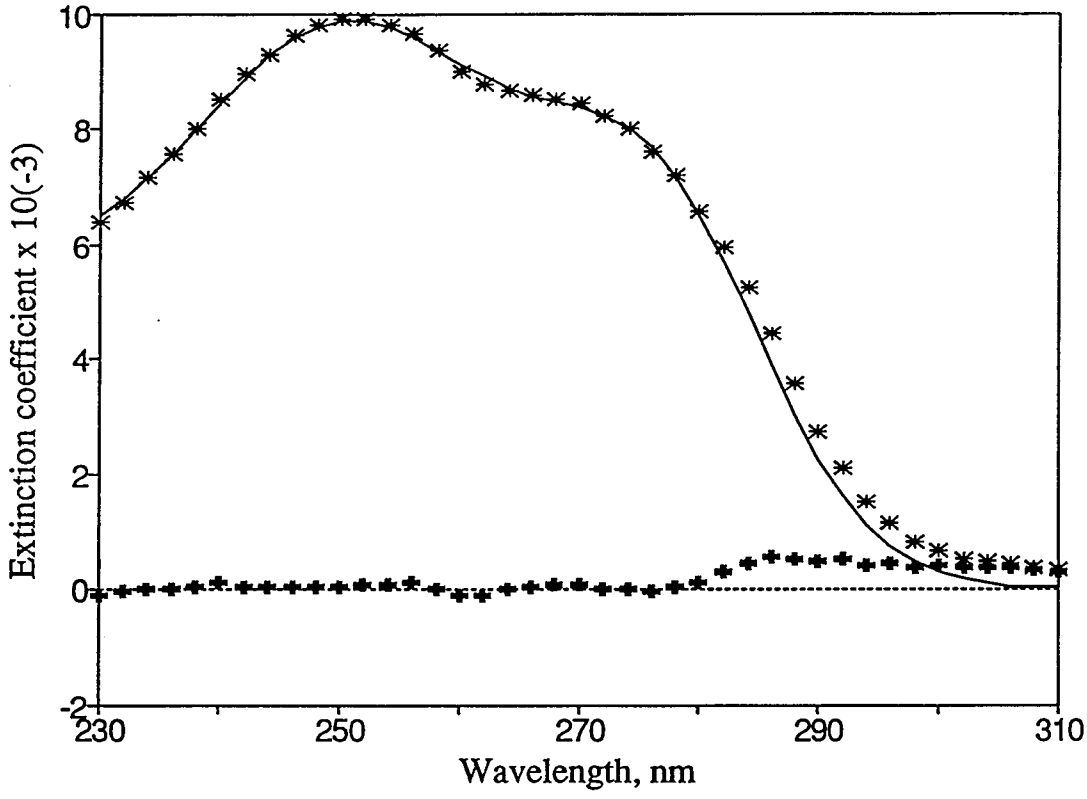

Figure 4.5 Fitting of absorption spectrum of d(CG) using C and G gaussian components. Absorption spectrum of d(CG) (***), fitting line (---), and residuals (+++).

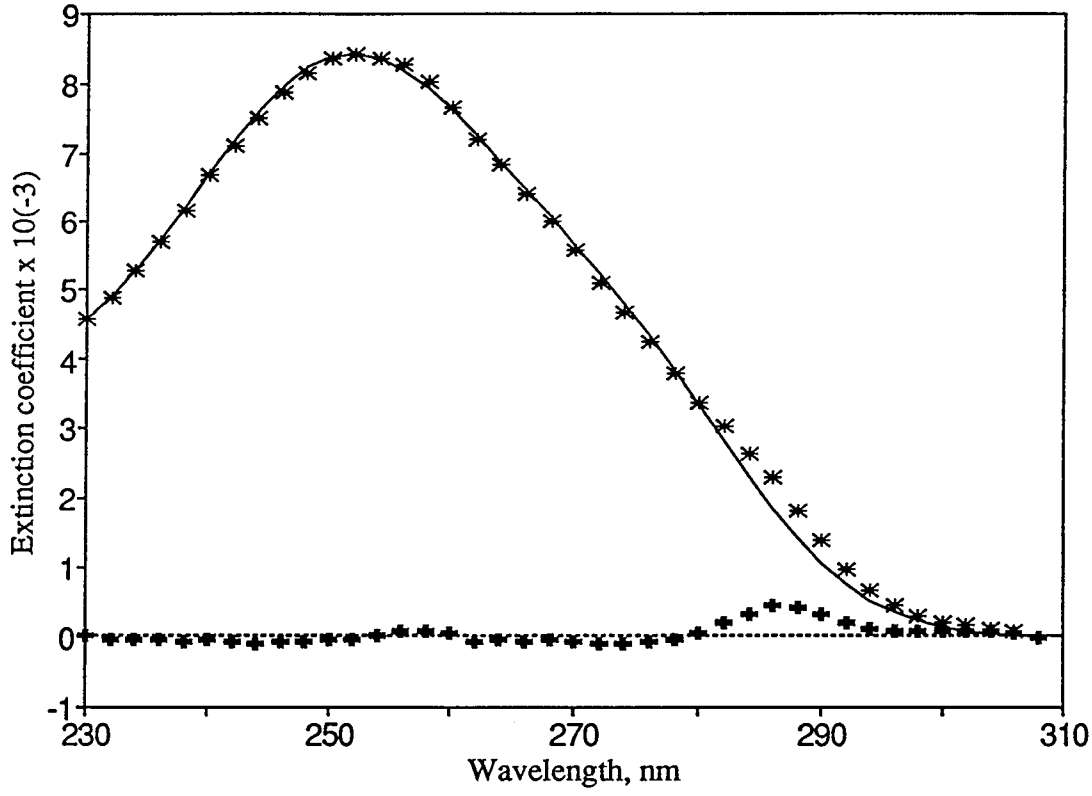

Figure 4.6 Fitting of absorption spectrum of polyd(GC)·polyd(GC) using C and G gaussian components. Absorption spectrum of polyd(GC)·polyd(GC) (***), fitting line (---), and residuals (+++).

Table 4.3 Fitting of absorption spectra of d(CG) and polyd(GC)·polyd(GC) with sum of G and C gaussian components in the range of 230-310 nm (four gaussian fitting to C)

Fitting compound	Precoefficient of gaussians g1	g2	c1	c2	c3	statistical analysis χ^2	r^2	s_e[a]
d(GC)	0.85	1.01	0.85	1.00	1.20	2.629	0.9945	0.2702
polyd(GC)·polyd(GC)[b]	0.2	1.02	0.52	0.45	0.73	0.842	0.9975	0.1530

[a]stansdard error of the curve fit ($s_e = [\chi^2/v]^{1/2}$), where v is the number of degrees of freedom.
[b]gaussians are shifted to +2 nm in the fitting.

Table 4.4 Oscillator strengths of G, C, d(CG) and polyd(GC)·polyd(GC) (four-gaussian fitting to C)

Compound	fitted transitions G1	G2[a]	C1	C2[a]	C3[a]	Σ gaussians	from experiment[b]
G	0.072	0.304				0.346	0.376
dC			0.143	0.101	0.034	0.278	0.277
d(CG)[c]	0.031	0.154	0.061	0.050	0.020	0.316	0.321
polyd(GC)·polyd(GC)[c]	0.007	0.155	0.037	0.023	0.012	0.234	0.239

[a]from integration of absorption spectrum, truncated at 230 nm.
[b]from integration of transformed gaussian, truncated at 230 nm.
[c]calculated on a per nucleotide basis.

G2 and C2 being unchanged. [The small hyperchromism below 250 nm may be due to higher transitions in d(CG). This has been accommodated by some increase in the tail of C3.]

The same procedure has been employed to polyd(GC)·polyd(GC) (Table 4.3). The transitions G1, C1, C2 and C3 contribute to the large hyperchromism, and the transition G2 is unchanged. In the fitting, the weighted sum of gaussians was shifted to +2 nm to improve χ^2 (2.817 before shift, and 0.842 after shift). The possible reason for the shift is due to two different data collections protocol for monomer and polymer.

Since oscillator strengths are defined on a $\bar{\nu}$ cm^{-1} basis, both experimental and fitted data were converted to cm^{-1} representation, and the experimental absorption and fitted areas were estimated. The resulting oscillator strengths of G, C, d(CG), polyd(GC)·polyd(GC) and fitted transitions are given in Table 4.4.

4.2.2 Resolved UV absorption spectra of cytidyl chromophore in different solvent solutions

In the previous section four gaussians were used to fit the spectrum of deoxycytidine (Figure 4.2). The detailed inspection shows that this fitting is not as satisfactory as guanosine (Figure 4.1), in particular, this produces oscillating residuals, which means that the fitting is not sufficiently adequate. In addition, it is found that the spectrum of the N, dimethyl substituted cytidine (Johnson et al, 1971) differs from deoxycytidine (Table 4.5). The two

Table 4.5 Experimental conditions and properties of absorption spectra of cytidyl chromophore in different solvent solutions

Compound	authors	pH	solvent	range, nm	f[a]	λ_1[b]	ε_1	λ_2[b]	ε_2
dCyd	Voet et al, 1963	7.8	aq.	190-310	0.837	272	8865	197	22450
dCyd	Voet et al, 1963	2.2	aq.	190-310	0.586	280	13160	212	18520
dCyd	Charnay & Gellet, 1964		MeCN	220-310	0.323	274	6610	238	7410
DmCyd	Johnson et al, 1971	7	aq.	196-310	0.881	280	14000	203	20500
DmCyd	Johnson et al, 1971		dioxane	212-310	0.549	280	11800		
Cyt	Voet et al, 1963	8.8	aq.	190-310	0.724	270	5840	197	22780
Cyt	Morita et al, 1968		MeCN	190-310	0.680	272	3880	200	20470
1-mCyt	Clark, 1986	6	aq.	190-310	0.707	272	7448	196	20110
dCMP	Voet et al, 1963	7.8	aq.	190-310	0.834	271	9230	197	22090

[a]oscillator strength for the whole spectrum.
[b]maximum in spectrum.

peak positions shift to red and the ratio of the first to second peak intensities is increased. Accordingly, to attempt to account for this difference, the UV absorption spectra of deoxycytidine (dCyd), N^4, N^4 dimethylcytidine (DmCyd), cytosine (Cyt), 1-methylcytosine (1-mCyt), dCMP in neutral aqueous solutions, dCyd in acid solution, and Cyd, Cyt and DmCyd in aprotic solvent solutions were digitized from different sources. The absorption properties and experimental conditions from the sources are summarized in Table 4.5.

Some characteristics of these absorption spectra are:

1. Comparing deoxycytidine with 1-methylcytosine and deoxyribose (Voet et al, 1963) in neutral solution, it can be seen that the sugar ring does not contribute to absorption to the spectra in the range of 220-300 nm. Accordingly, the differences between dCyd and 1-mCyt indicate some interactions between Cyt and the sugar group.

2. Phosphate group in dCMP does not contribute any absorption based on the fact that the absorption spectra of dCyd and dCMP are basically identical and phosphoric acid does not absorb above 200 nm.

3. The dimethyl group in DmCyd does not cause the long wavelength band to shift but its intensity almost doubles.

4. In acidic solution, the first band for dCyd intensifies,and the number of peaks are diminished.

5. In aprotic solvents such as acetonitrile and dioxane, the number of bands of Cyd and Cyt decrease.

6. The peak position for the highest energy transition in a series of cytidyl chromophore is almost the same (~ 200 nm) or only has a little change. Solvents do not affect this transition.

i). Resolved absorption spectra of cytidyl chromophore in neutral solutions

For fitting a series of the cytidyl chromophore in neutral aqueous solution the presettings of the gaussian parameters were based on number, positions and widths of the transitions found in the literatures (Raksányi and Földváry, 1978; Zaloudek et al, 1984). When these were not available, the automatic presettings by the PeakFit program were carried out and modified visually to approach the best fit. At first, the four-gaussian fitting of the five cytidyl chromophore (dCyd, DmCyd, Cyt, 1-mCyt, dCMP) was tried, and the results are shown in Figures 4.7a - 4.11a (the fitting of dCyd spectra are repeated here for a complete set). As in the case of dCyd, the results did not give satisfactory values of χ^2 and r^2. In order to improve the fitting, based on the four gaussian fitting, the fifth gaussian was added between the original third and fourth, and rest of the gaussians were modified manually to approach the best fit, and then the Curve-fit process were carried out to obtain the final fitting results. The results from five-gaussian fitting are shown in Figures 4.7b - 4.11b for comparison with those from four-gaussian fitting. The parameters for both four- and five-gaussian fitting are listed in Table 4.6. The significant improvement in both χ^2 (Table 4.7) and residuals

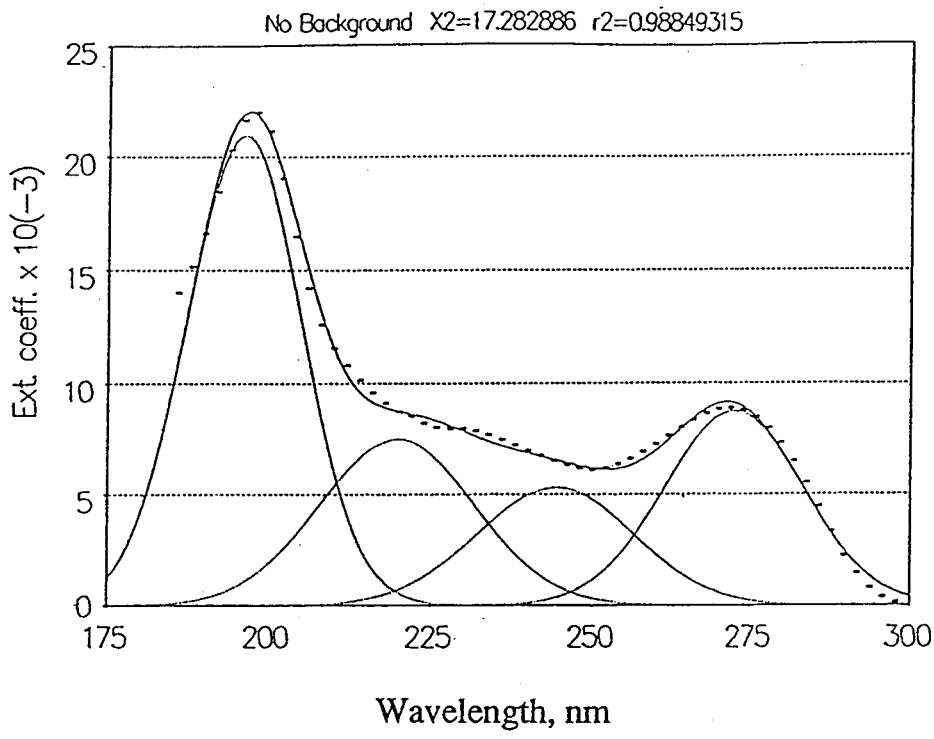

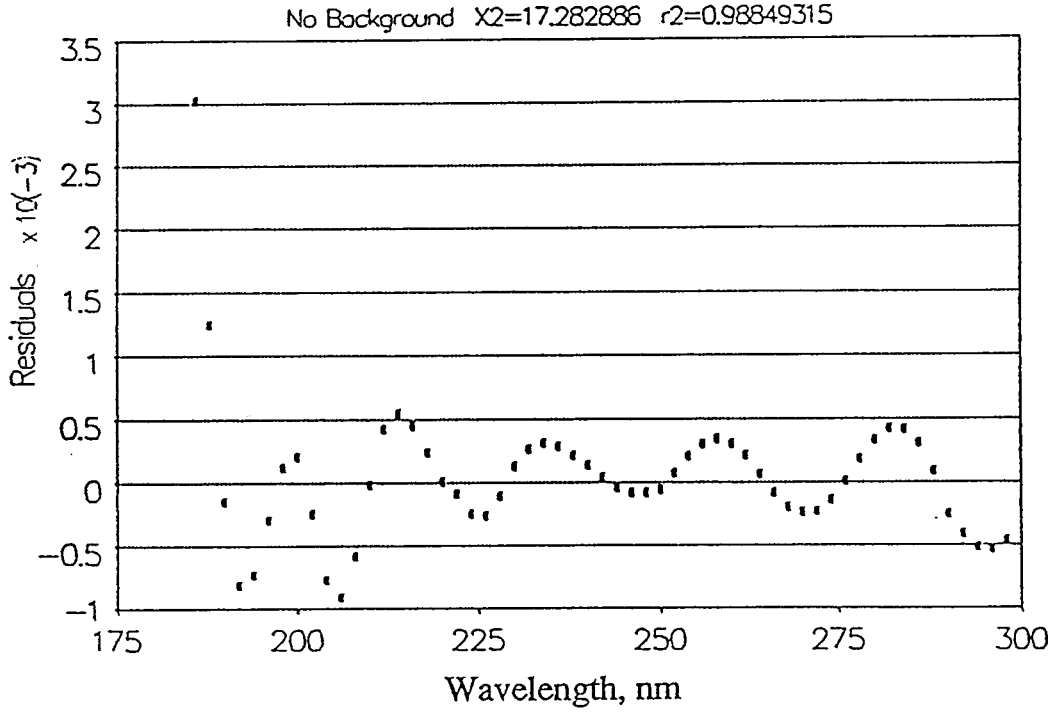

Figure 4.7a Four-gaussian fitting of absorption spectrum of deoxycytidine (pH 7.8, digitized from Voet et al (1963).

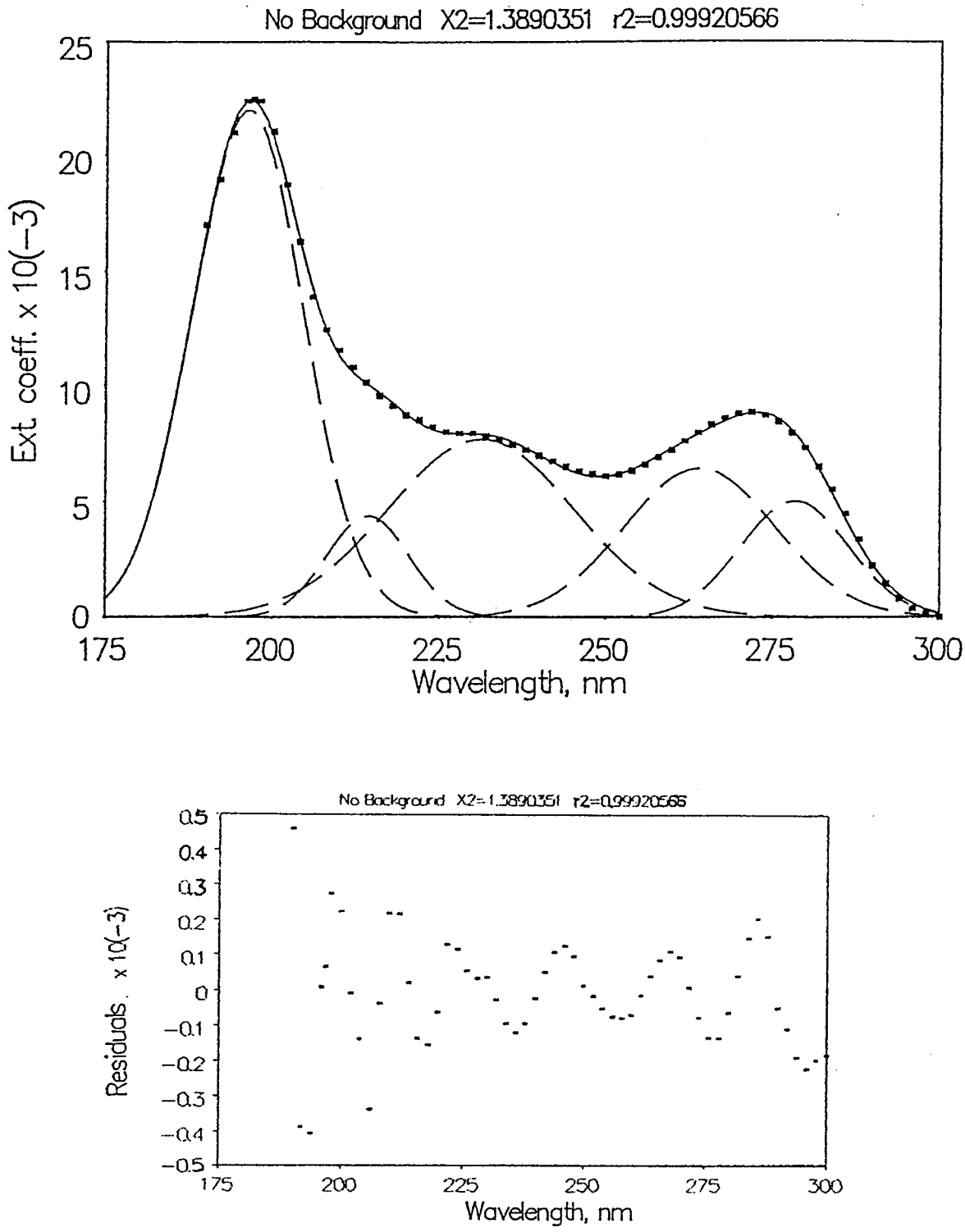

Figure 4.7b Five-gaussian fitting of absorption spectrum of deoxycytidine (pH 7.8), digitized from Voet et al (1963).

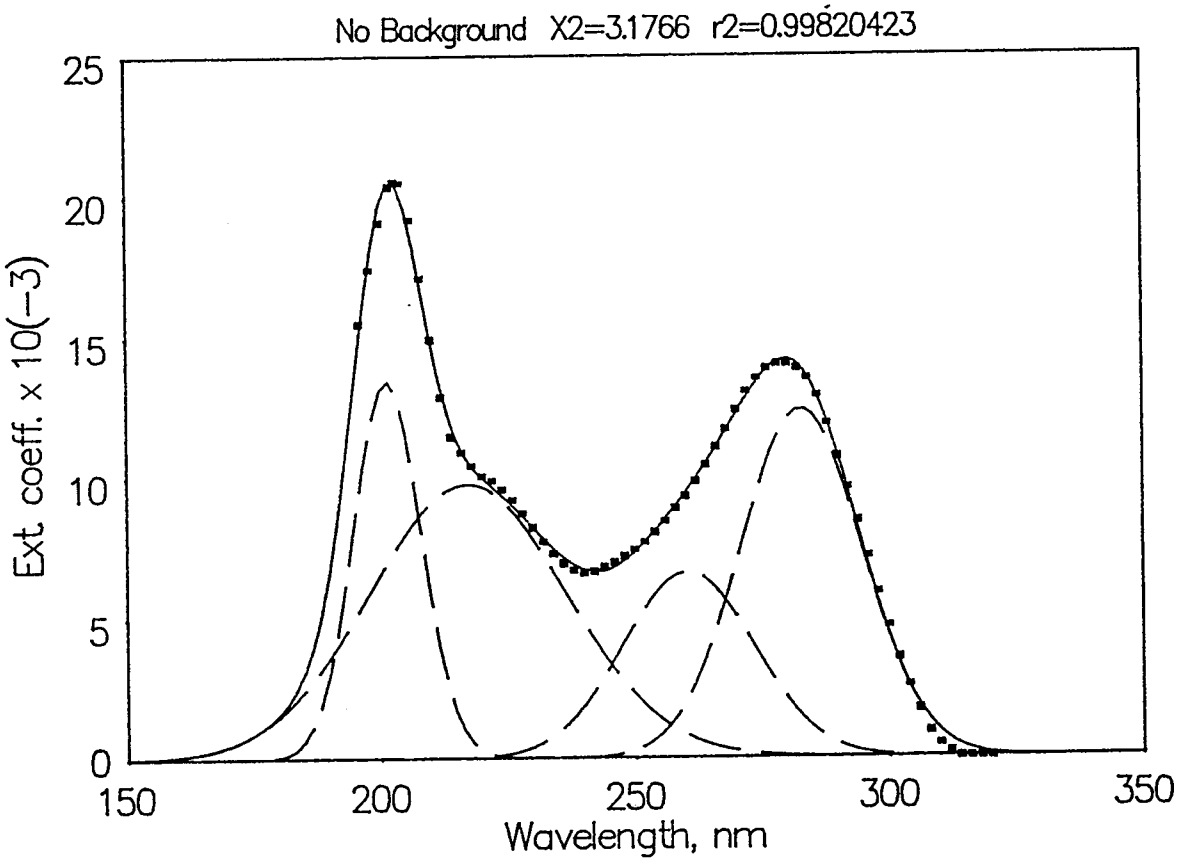

Figure 4.8a Four-gaussian fitting of absorption spectrum of N^4, N^4 dimethylcytidine (pH 7), digitized from Johnson et al (1971).

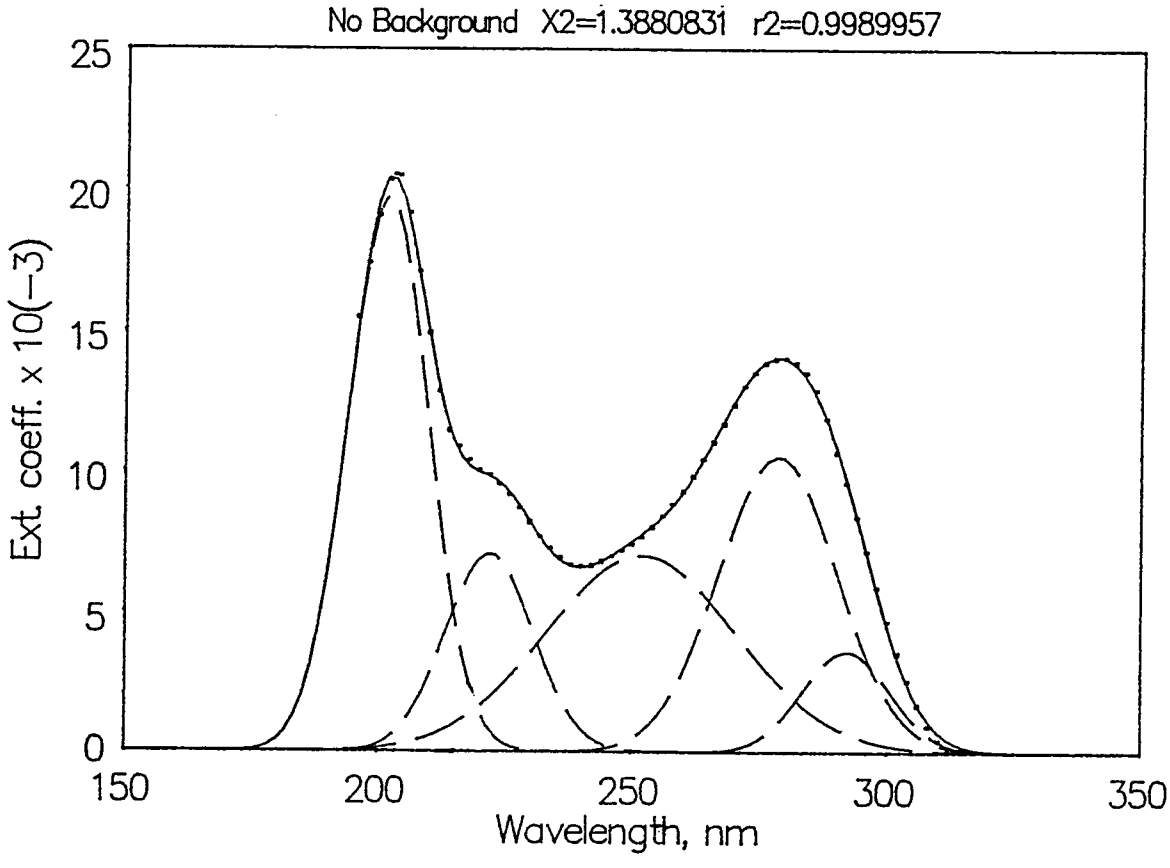

Figure 4.8b Five-gaussian fitting of absorption spectrum of N^4, N^4 dimethylcytidine (pH 7), digitized from Johnson et al (1971).

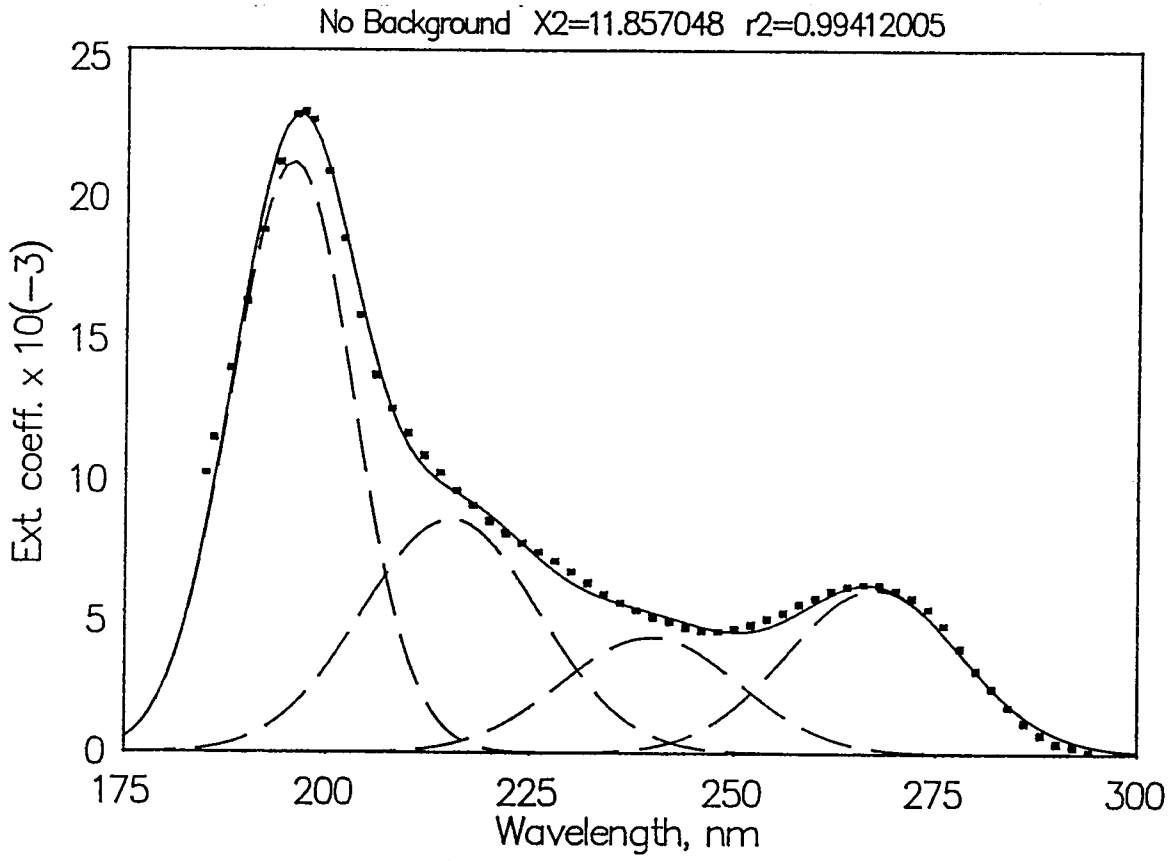

Figure 4.9a Four-gaussian fitting of absorption spectrum of cytosine (pH 8.8), digitized from Voet et al (1963).

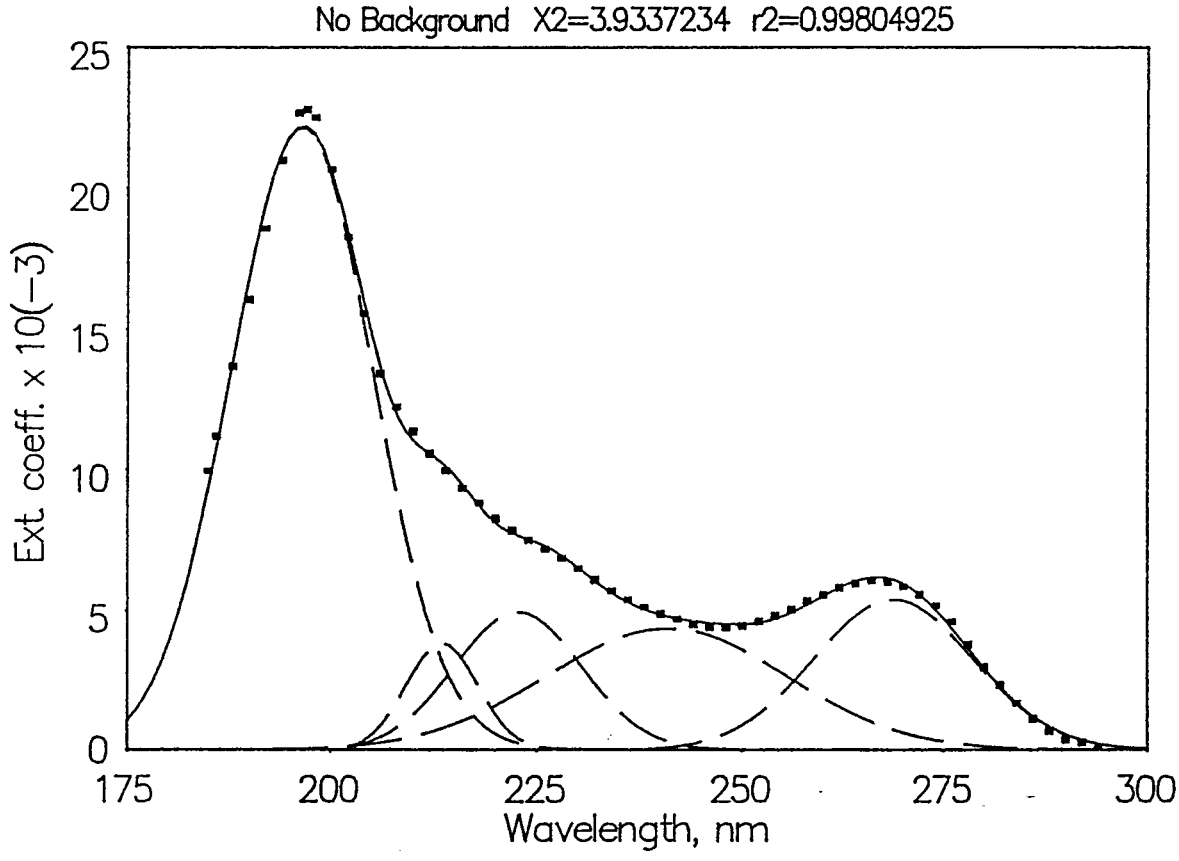

Figure 4.9b Five-gaussian fitting of absorption spectrum of cytosine (pH 8.8), digitized from Voet et al (1963).

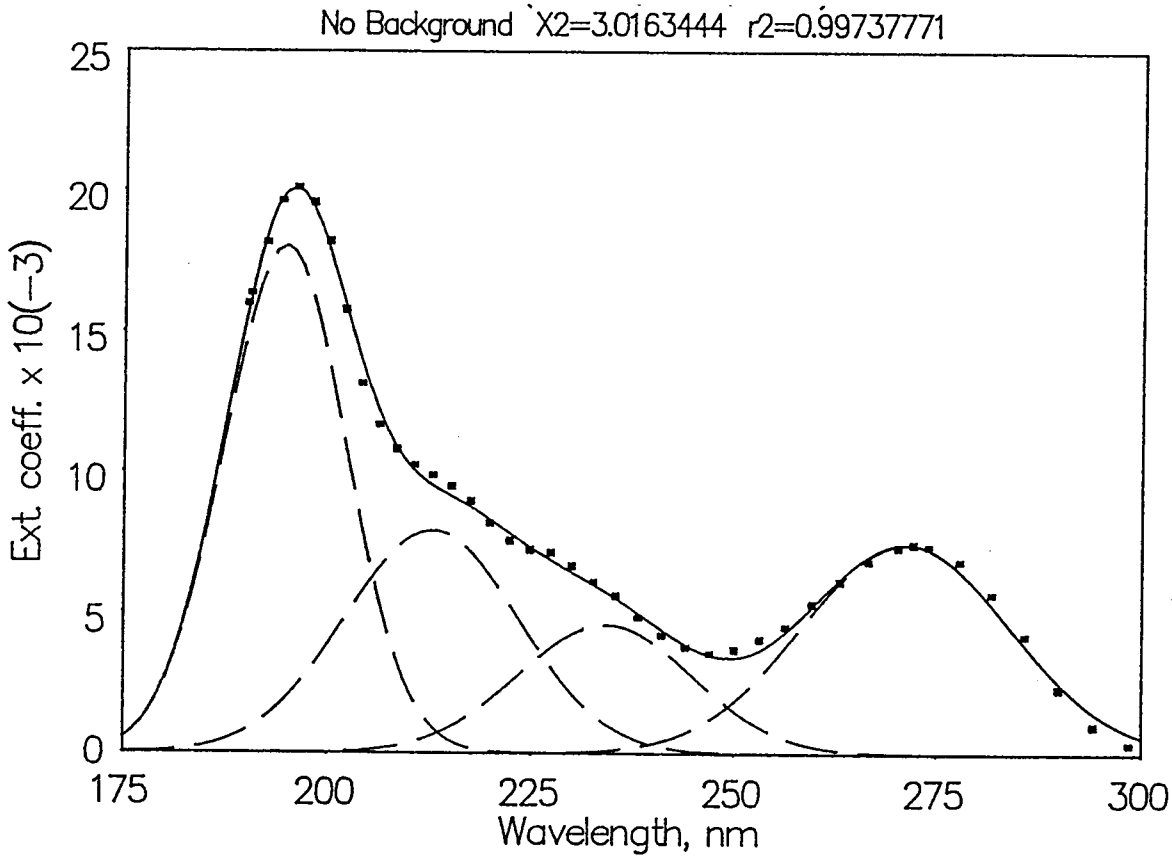

Figure 4.10a Four-gaussian fitting of absorption spectrum of 1-methylcytosine (pH 6), digitized from Clark (1986).

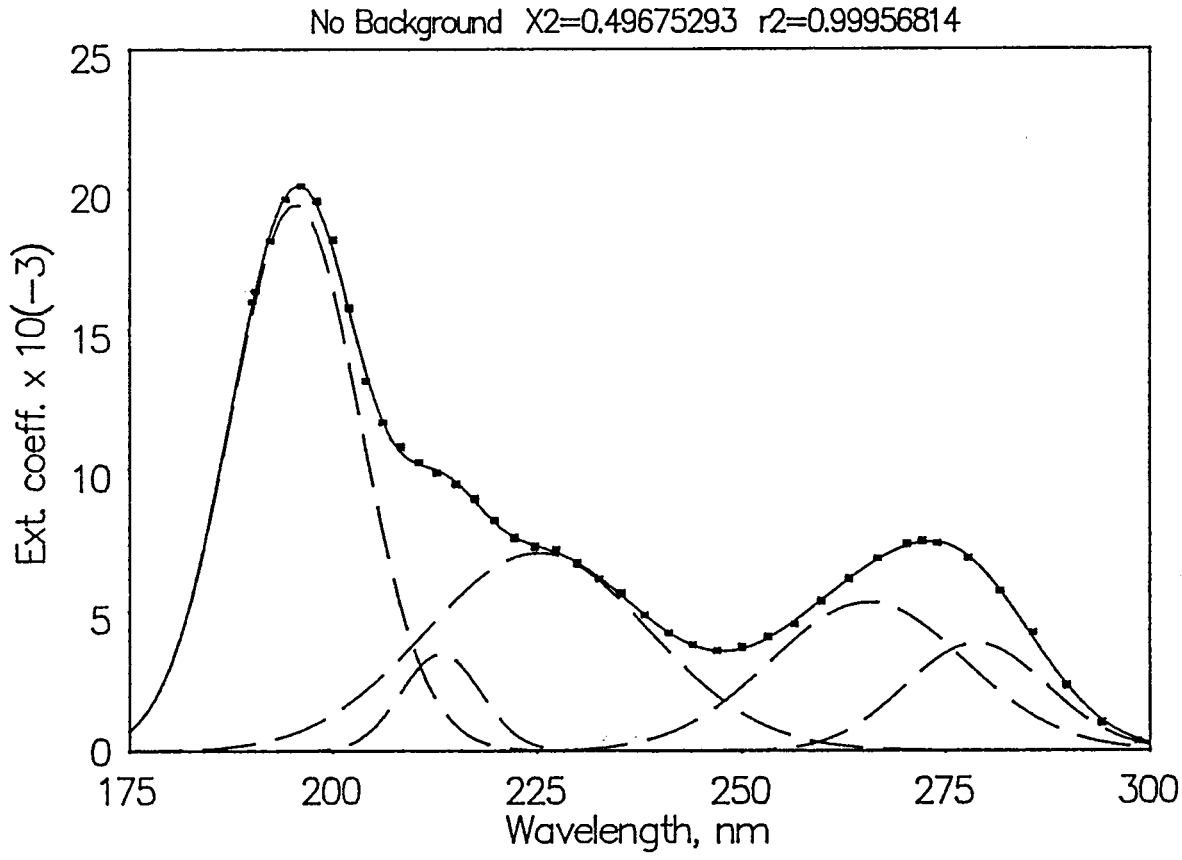

Figure 4.10b Five-gaussian fitting of absorption spectrum of 1-methylcytosine (pH 6), digitized from Clark (1986).

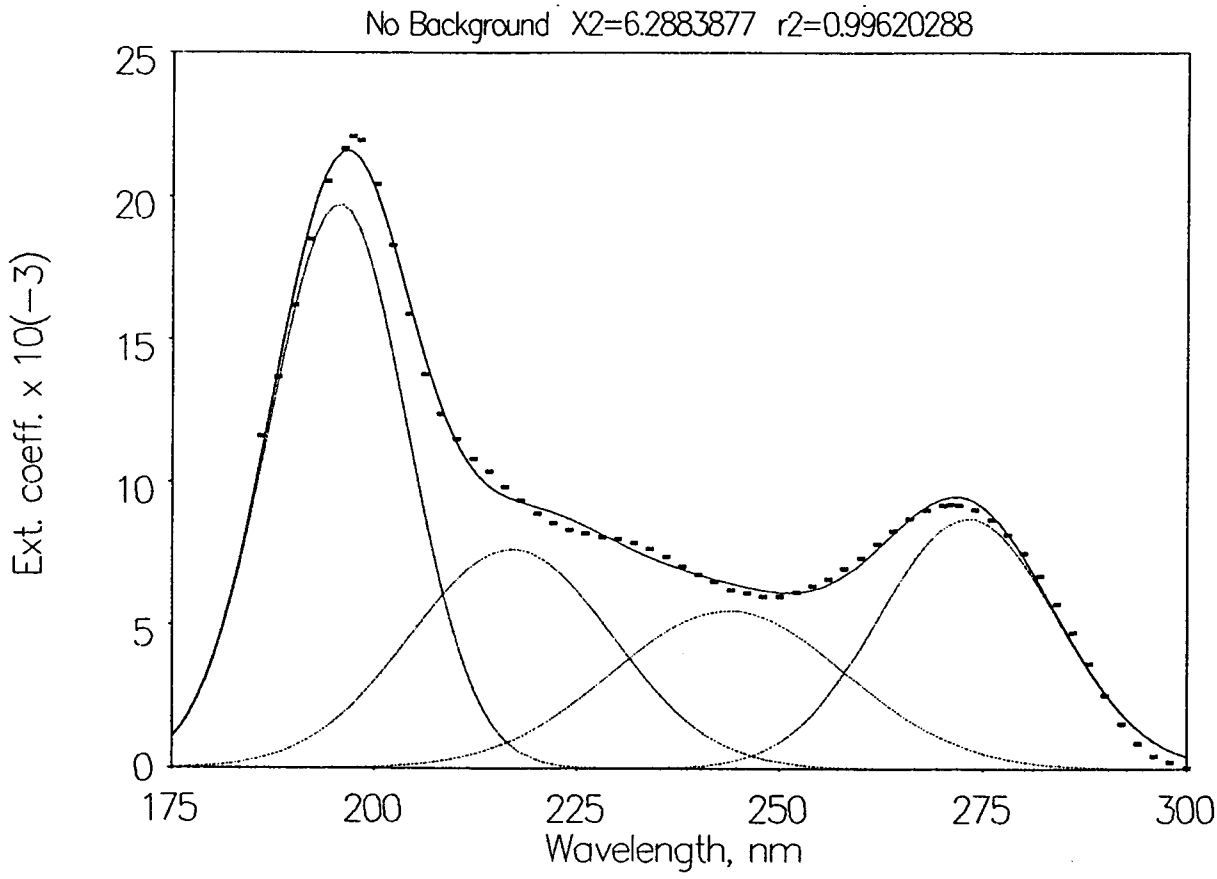

Figure 4.11a Four-gaussian fitting of absorption spectrum of dCMP (pH 7.8), digitized from Voet et al (1963)

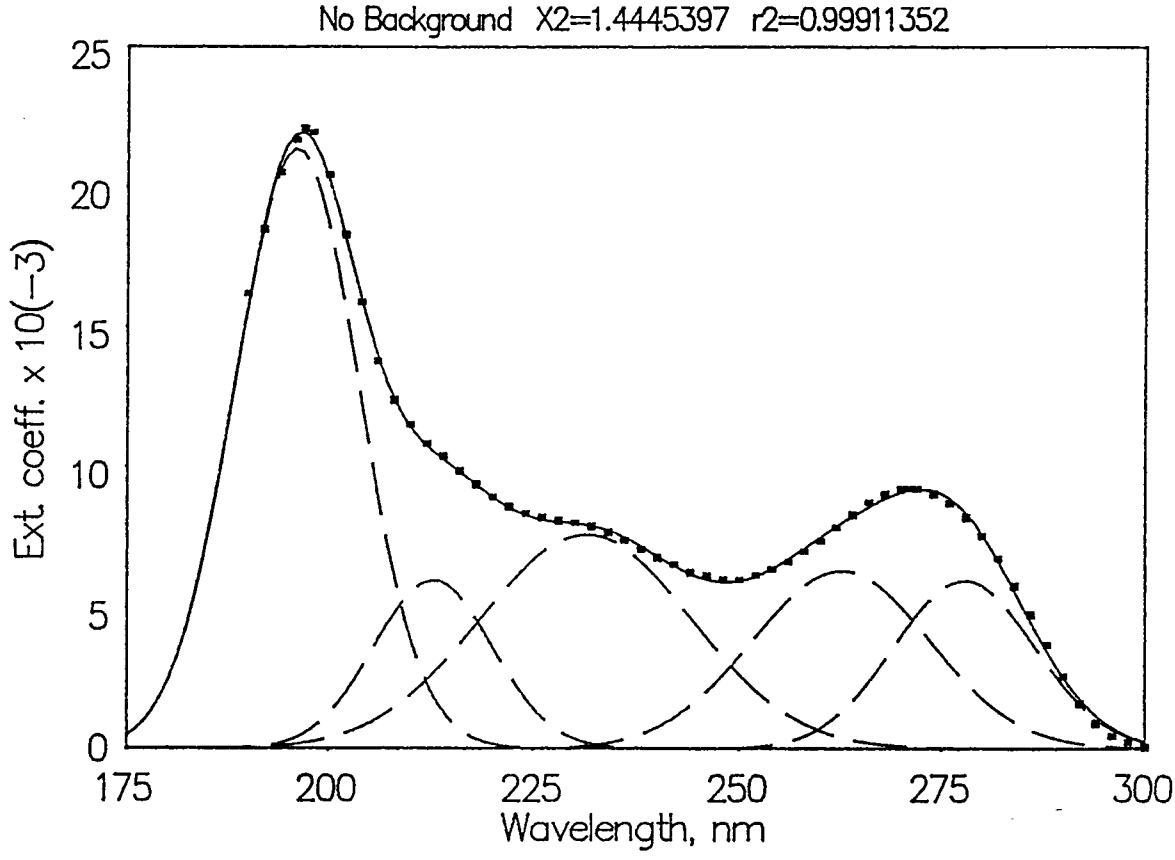

Figure 4.11b Five-gaussian fitting of absorption spectrum of dCMP (pH 7.8), digitized from Voet et al (1963)

Table 4.6 Gaussian parameters for fitting the absorption spectra of cytidyl chromophore in neutral aqueous solutions

Compound	pH	transition	four-gaussian fitting λ_0	$A_0 \times 10^{-3}$	δ (nm)	five-gaussian fitting λ_0	$A_0 \times 10^{-3}$	δ (nm)
dCyd	7.8	I	272.5	8.716	11.05	278.4	5.030	8.057
		II	244.5	5.289	12.10	264.2	6.451	11.32
		III	219.9	7.469	11.87	231.3	7.700	13.96
		IV	196.2	20.96	8.875	214.3	4.374	6.153
		V				196.3	22.01	8.241
DmCyd	7	I	282.8			292.1	3.624	8.495
		II	260.4			278.7	10.53	11.56
		III	271.2			251.9	7.014	18.58
		IV	201.4			222.2	7.077	8.642
		V				202.0	19.76	7.920
Cyt	8.8	I	267.3	5.854	10.81	268.7	5.379	9.898
		II	239.8	4.153	10.81	240.8	4.354	14.71
		III	215.3	8.324	10.81	222.8	4.932	7.682
		IV	195.7	20.99	7.585	213.6	3.821	4.347
		V				196.5	22.15	8.701
1-mCyt	6	I	271.2	7.448	12.75	278.7	3.830	8.708
		II	234.1	4.574	10.75	265.5	5.292	11.93
		III	212.7	7.916	10.64	225.1	7.037	13.66
		IV	194.7	18.03	7.417	213.3	3.476	4.835
		V				195.4	19.45	7.946
dCMP	7.8	I	273.1	8.725	10.89	277.8	5.970	8.701
		II	243.8	5.493	14.42	262.6	6.313	11.00
		III	216.9	7.628	12.46	231.4	7.589	12.81
		IV	195.5	19.73	8.447	212.8	5.976	7.191
		V				196.1	21.37	7.613

Table 4.7 Comparison of four- and five-gaussian fittings for absorption spectra of cytidyl chromophore in neutral aqueous solution (in wavelength presentation)

compound	four-gaussian fit		five-gaussian fit	
	χ^2	r^2	χ^2	r^2
deoxycytidine	17.28	0.9885	1.389	0.9992
dimethylcytidine	3.18	0.9982	1.388	0.9990
Cytosine	11.86	0.9941	3.933	0.9980
1-methylcytosine	3.02	0.9974	0.497	0.9996
dCMP	6.29	0.9960	1.445	0.9991

(as an example, see Figure 4.7a and b) suggest that it may be possible to have five electronic transitions in cytidyl chromophore in neutral solution in the range of 175-300 nm.

ii). Resolved absorption spectra of cytidyl chromophore in acidic and aprotic solutions

To examine the effect of proton on the spectral characteristics of cytidyl chromophore, the absorption spectra in acidic or aprotic solvents were fitted by the use of Step-fit process. Since the reported absorption spectra of cytidine in acetonitrile and N^4, N^4 dimethylcytidine in dioxane only covered a limited range, 220-310 nm for the former, and 210-310 nm for the latter, this could result in some arbitrary fittings in short wavelength range. To diminish this uncertainty, simulated data calculated from a gaussian function fixed at the highest energy peak position of C (~200 nm) were used to extend the data to 190 nm. The fitting results of absorption spectra of cytidyl chromophor in aprotic and acid solutions are shown in Figures 4.12-4.15, and the corresponding gaussian parameters are listed in Table 4.8.

The fitting spectra of cytidine and cytosine in acetonitrile solution (Figure 4.12 and 4.13, respectively) indicate that the solvents affect the resolution of the spectra of cytidyl chromophore significantly. Only three transitions (in terms of gaussians) are needed to account for cytidine and cytosine in aprotic solutions, in contrast to the situation in aqueous (protic) solution.

Table 4.8 Gaussian parameters for fitting the absorption spectra of cytidyl chromophore in aprotic and acid solutions

Compound	solvent or pH	transition	λ_0	$A_0 \times 10^{-3}$	δ (nm)
Cyd	MeCN	I	278	5.782	11.64
		II	238	7.404	19.13
		III	198	23.50	11.20
Cyt	MeCN	I	274.0	3.777	12.33
		II	236.0	5.597	14.74
		III	202.1	19.67	10.02
dCyd	2.2	I	285.4	7.859	9.283
		II	270.8	8.482	12.79
		III	211.5	10.16	13.83
DmCyd	dioxane	I	293.3	4.845	7.773
		II	279.3	7.758	11.26
		III	257.4	6.769	17.18
		IV	226.4	2.794	5.956
		V	205.4	25.20	10.26

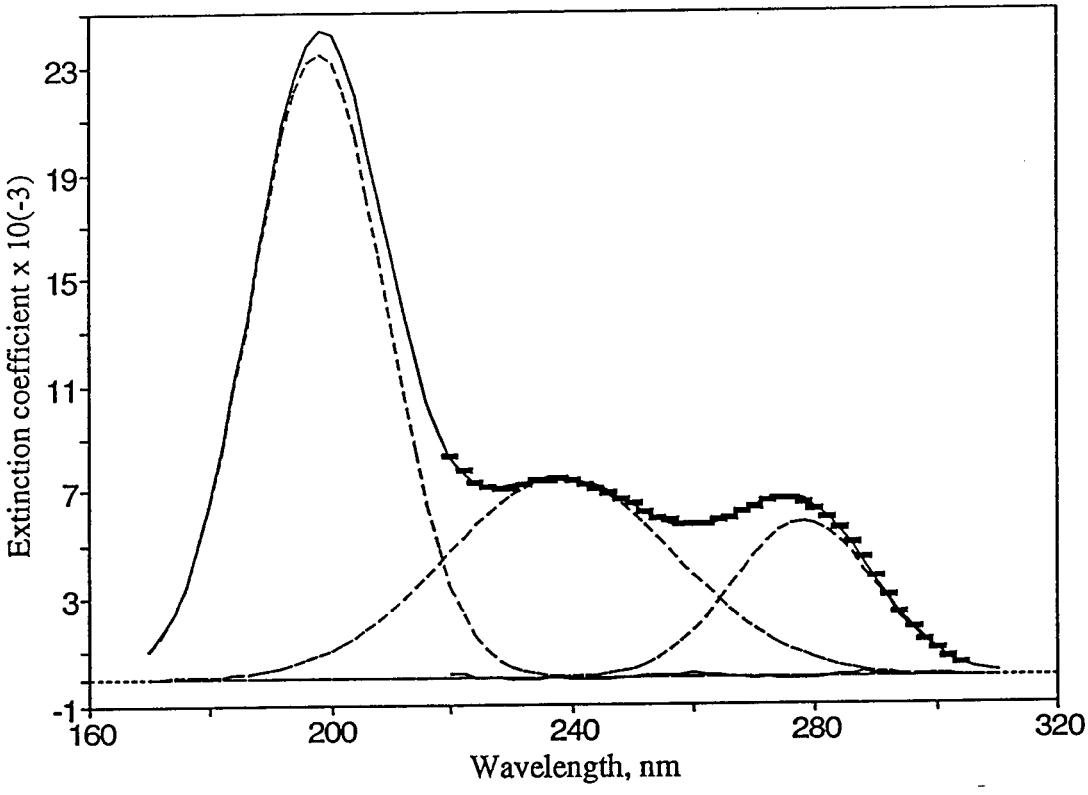

Figure 4.12 Gaussian fitting of absorption spectrum of cytidine in acetonitrile (MeCN), digitized from Charney and Gellert (1964).

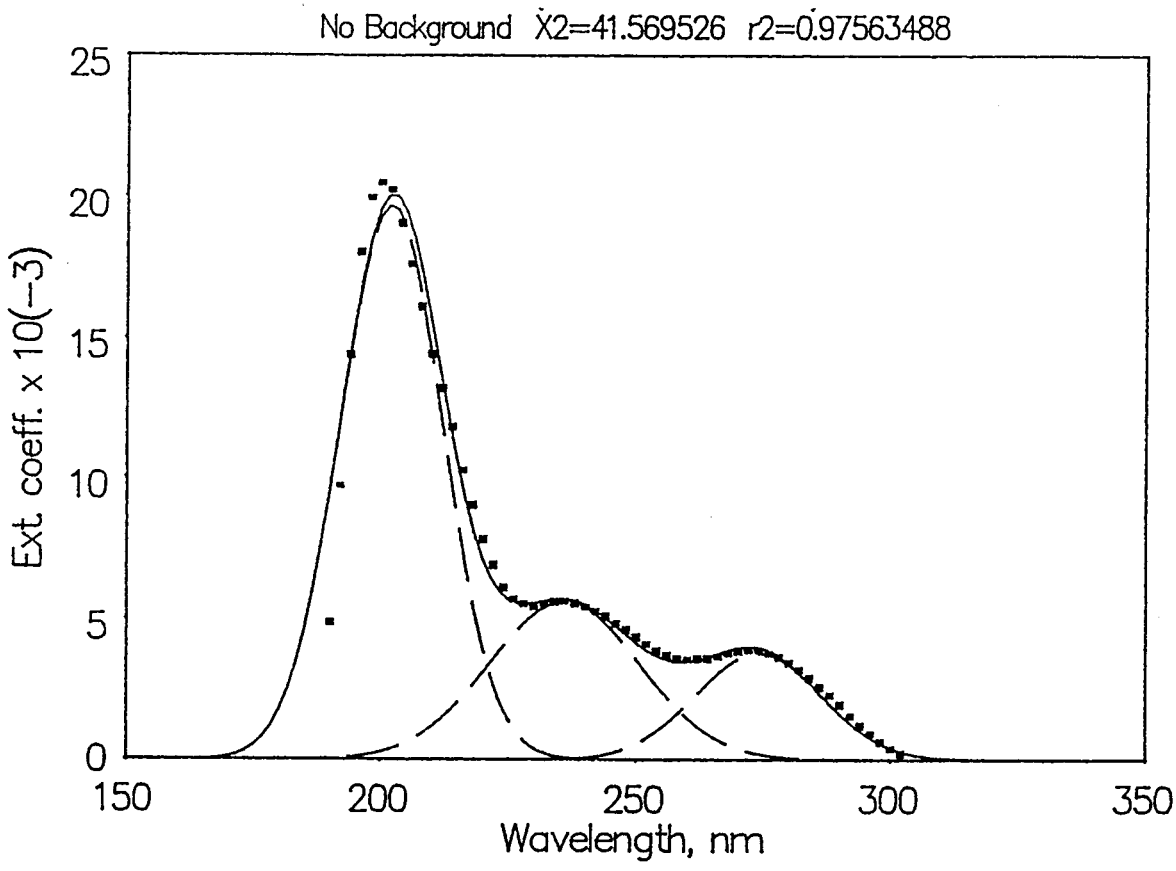

Figure 4.13 Gaussian fitting of absorption spectrum of cytidine in acetonitrile (MeCN), digitized from Morita Nagukura (1968).

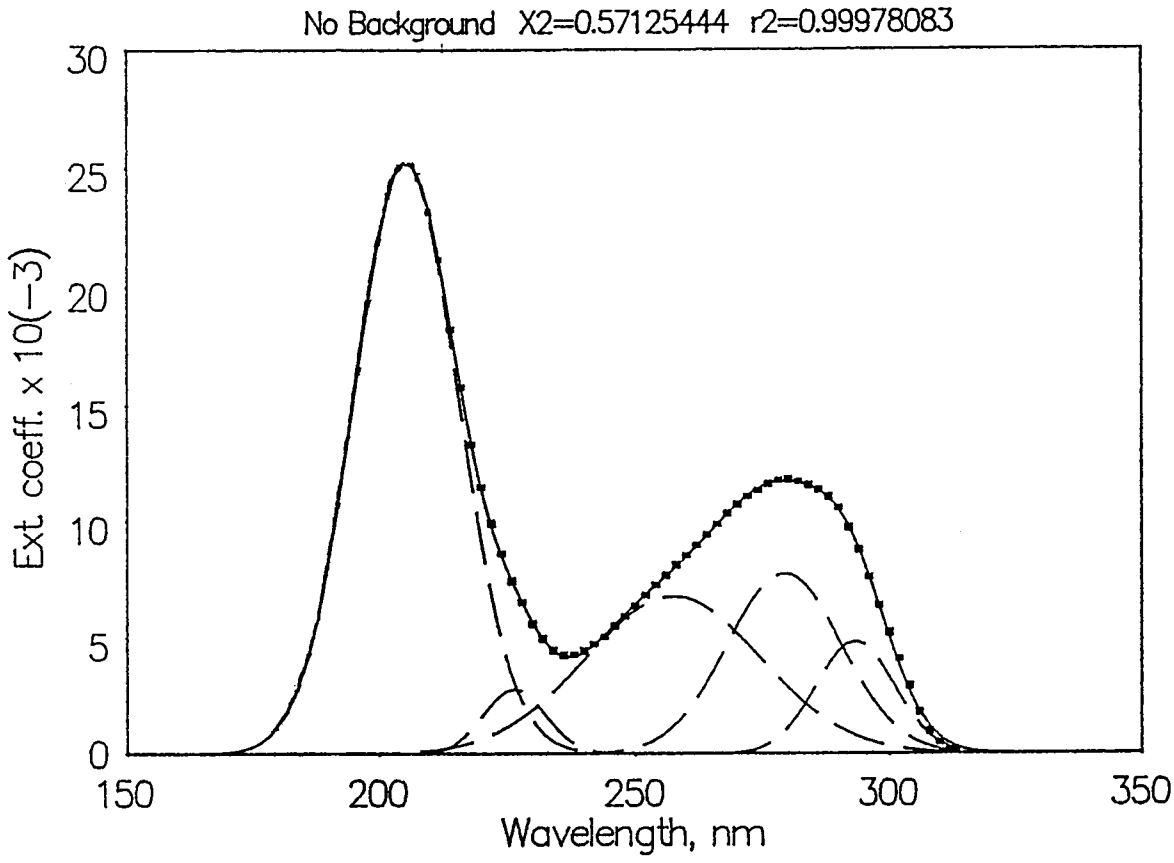

Figure 4.14 Gaussian fitting of absorption spectrum of deoxycytidine in acidic aqueous solution, digitized from Voet et al (1963).

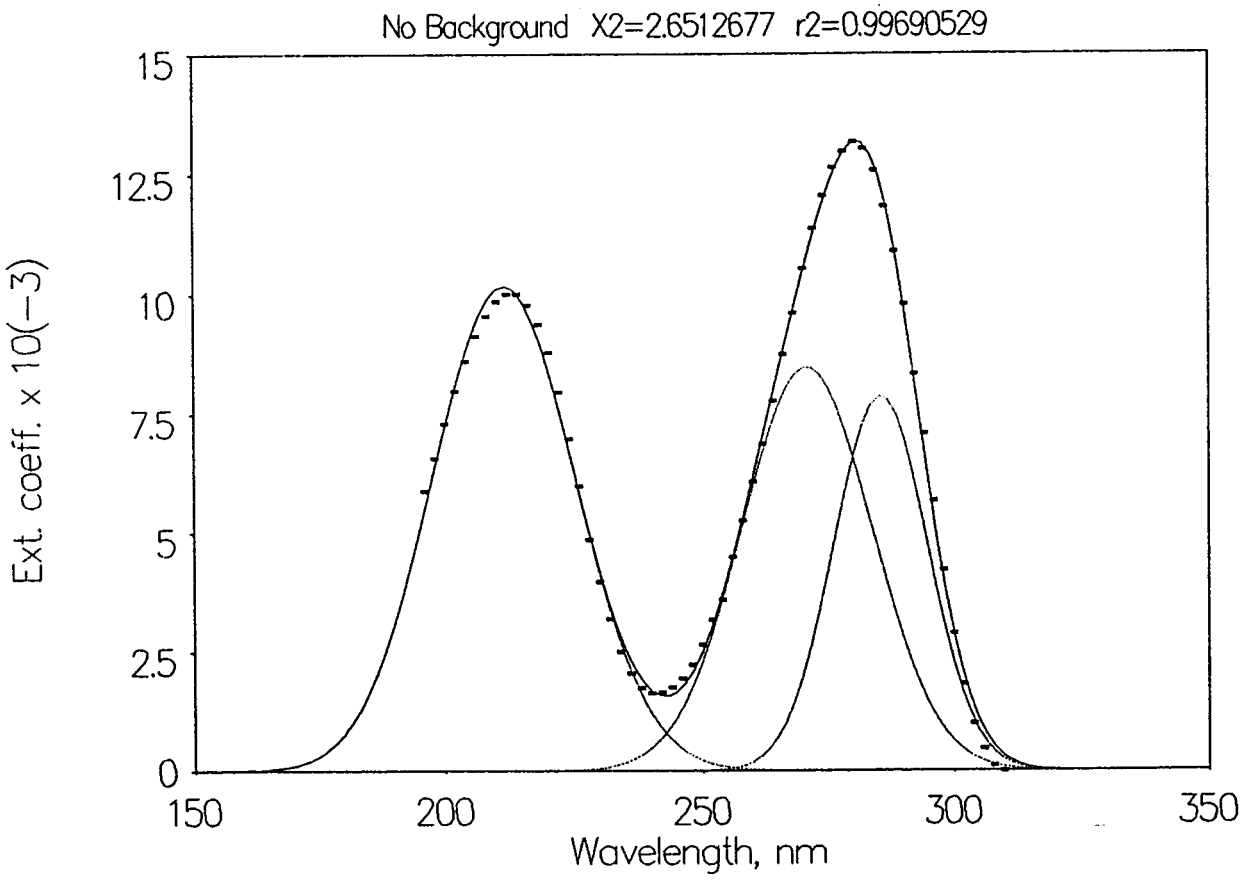

Figure 4.15 Gaussian fitting of absorption spectrum of N^4, N^4 dimethylcytidine in dioxane, digitized from Johnson et al (1971).

In acid solution, deoxycytidine has two observed bands but can not be fitted with two gaussians. As it is shown in Figure 4.14, two gaussians are needed to fit the first band. The peak positions are very different from the corresponding peaks in dCyd and Cyt in MeCN. These two lowest transitions are much narrower.

In the case of dimethylcytidine in dioxane solution (Figure 4.15), none of fitting characteristics are similar to above three. Although there are two absorption bands (including the simulated data), five gaussians are needed to give a satisfactory fitting.

The fitted spectral properties and the oscillator strengths of guanosine and several cytidyl chromophore in different solvent conditions are summarized in Table 4.9.

Table 4.9 Spectral properties and oscillator strengths of gaussian components for cytidyl chromophore

Fitted transition	S1				S2				S3				S4				S5				Σf	f(exp)
Compound	λ_0,nm	$\delta_{1/e}$	$\bar{\nu}$,cm^{-1}	f	λ_0,nm	$\delta_{1/e}$	$\bar{\nu}$,cm^{-1}	f	λ_0,nm	$\delta_{1/e}$	$\bar{\nu}$,cm^{-1}	f	λ_0,nm	$\delta_{1/e}$	$\bar{\nu}$,cm^{-1}	f	λ_0,nm	$\delta_{1/e}$	$\bar{\nu}$,cm^{-1}	f		
dCyd(4,pH7.8)	272.5	15.6	36699	0.14					244.5	17.1	40907	0.12	219.9	16.8	45468	0.20	196.2	12.6	50977	0.38	0.84	0.84
dCyd(5,pH7.8)	278.4	11.4	35916	0.06	264.2	16.0	37850	0.11	231.3	19.7	43233	0.22	214.4	8.7	46644	0.06	196.3	11.6	50944	0.38	0.83	0.84
dCyd(3,pH2.2)	285.4	13.1	35034	0.10	270.8	18.1	36929	0.16					211.5	19.6	47288	0.32						
Cyd(3,MeCN)	278.0	16.5	35971	0.10					238.0	27.1	42017	0.27					198.0	15.9	50505	0.53	0.90	
																				(220-310 nm)	0.32	0.32
Cyt(3,MeCN)	274.0	17.4	36496	0.07					236.8	20.8	42373	0.16					202.1	14.2	48489	0.46	0.69	0.68
DmCyd(4,pH7)	282.8	16.9	35360	0.20	260.4	18.2	38397	0.14					217.2	27.2	46048	0.39	201.4	9.35	49642	0.23	0.96	
DmCyd(5,pH7)	292.1	12.0	34235	0.04	278.7	16.3	35882	0.17	251.9	26.3	39699	0.23	222.2	12.2	45013	0.14	202.0	11.2	49513	0.38	0.96	
																				(196-310 nm)		0.88
DmCyd(4,dioxane)	293.3	10.7	34099	0.04	279.7	17.2	35748	0.13	256.9	26.1	38918	0.20					202.5	18.8	49383	0.73	1.10	
DmCyd(5,dioxane)	293.3	11.0	34100	0.05	279.3	15.9	35803	0.12	257.4	24.3	38848	0.19	226.4	8.42	44160	0.04	205.5	14.5	48673	0.61	1.01	
																				(212-310 nm)	0.55	0.55
1-mCyt(4,pH6)	271.2	18.0	36870	0.14	234.1	15.2	42717	0.10	212.7	15.0	47009	0.20					194.7	10.5	51349	0.27	0.71	0.71
1-mCyt(5,pH6)	278.7	12.3	35877	0.05	265.5	16.9	37672	0.10	225.1	19.3	44429	0.21	213.3	6.84	46889	0.04	195.4	11.2	51166	0.32	0.72	0.71
Cyt(4,pH8.8)	267.3	14.4	37406	0.09	239.8	15.3	41705	0.08					215.3	14.4	46443	0.20	195.7	10.7	51109	0.34	0.71	0.72
Cyt(5,pH8.8)	268.7	14.0	37212	0.08	240.8	20.8	41525	0.12	222.8	10.9	44890	0.08	213.6	6.2	46816	0.04	196.5	12.3	50895	0.40	0.72	0.72
Cyt(4,pH7.8)	273.1	15.4	36611	0.13	243.8	20.4	41020	0.15					216.9	17.6	46105	0.22	195.5	11.9	51160	0.34	0.84	0.83
Cyt(5,pH7.8)	277.8	12.3	35993	0.07	262.6	15.6	38079	0.11	231.4	18.1	43220	0.20	212.8	10.2	46986	0.10	196.1	10.8	51005	0.35	0.83	0.83

Note: The number in parenthesis is the number of gaussians.

4.2.3 Time-resolved emission spectroscopy of G and C

4.2.3.1 GMP

i) Lifetime analysis

The decay profiles of GMP in pH aqueous solutions of different pH were measured at several emission wavelength following excitation at 265 nm. The results of the lifetime analysis are listed in Table 4.10a, b a nd c.

In acidic solution (Table 4.10a), clearly, there is only one component with lifetime of 0.18 ns at all emission wavelengths. In buffered pH 7.0 aqueous solutions,there exist two possibilities. Table 4.10b lists two model analysis for comparison. The single exponential model gives a very fast component with lifetime ~ 0.06 ns. Increasing the number of exponential model to two, the standard fit is improved to some extent (< 10%), but the fast component with τ_1 ~ 0.06 ns is still the predominant, and only a very small fraction of slow component ($f(\alpha_2)$ = 0.1%) with τ_2 of 4.3 is obtained. On increasing the wavelength from 330 to 400 nm, there are no significant changes in individual emission fractions. Thus, the single exponential model may be the best, but two exponential model is possible.

As mentioned earlier, Rigler et al (1985) measured the decay of GDP, a similar compound to GMP, in unbuffered aqueous solution. For comparison with their result, GMP solution in the present work was also made in the

Table 4.10 Lifetime analysis of GMP in different pH aqueous solutions.

a. GMP (1 x 10^{-5}M) in $HClO_4$ solution (pH 1.1)

λ_{em}, nm	τ, ns	f(α)	f(ατ)
330	0.18 ± 0.001	100%	100%
380	0.18 ± 0.001	100%	100%
420	0.18 ± 0.001	100%	100%

b. GMP (2 x 10^{-5} M) in phosphate buffered solution (pH 7.0)

λ_{em}, nm	stdfit	τ, ns	f(α)	f(ατ)
350	2.62 x 10^{-3}	0.07	100%	100%
	2.38 x 10^{-3}	0.06	99.9%	92%
		4.31 ± 0.78	0.1%	8%
390	7.13 x 10^{-3}	0.06	100%	100%
	6.85 x 10^{-3}	0.05	99.9%	92%
		4.30 ± 1.13	0.1%	8%

c. GMP (1 x 10^{-5} M) in unbuffered solution (pH ~6)

λ_{em}, nm	τ, ns	f(α)	f(ατ)
330	0.06	98%	85%
	0.53 ± 0.14	2%	15%
400	0.05	99%	87%
	0.72 ± 0.13	1%	13%

same condition (pH of the solution can not be measured accurately due to the absorption of CO_2), and the lifetime results are shown in Table 4.10c.

In this unbuffered aqueous solution, the predominant component is the one with τ_1 ~ 0.06 ns ($f(\alpha_1 \geq 98\%$ and $f(\alpha_1\tau_1) \geq 85\%$) and the minor with τ_2 of 0.6 ns ± 0.14, which is not in agreement with Rigler's result on GDP (τ_1 = 0.2 ns and τ_2 = 1.4 ns).

Comparing the Tables 4.10a, b and c, it can be seen that the lifetimes of the emitting components are strongly dependent of pH. The component with lifetime of 0.18 ns in acid solution is not observed in either neutral and unbuffered solutions. In neutral buffer solution, the fast component with τ_1 ~ 0.06 ns, similar to that in unbuffered solution, is the predominant component, however the minor one with τ_2 of 4.3 ns ± 1.1 is very distinct from that in unbuffered solutions (τ_2 = 0.6 ns) although there is only one pH unit difference in these two cases.

ii) TRS analysis

To examine the spectral characteristics of guanyl chromophore, the time-windowed emission spectra of GMP in different pH aqueous solutions were measured at 0 and 1.0 ns delay times with 100 ps width for each window. Because there is only one component in GMP acidic solution, TRS was not carried out, the time-windowed spectra with delays of 0 ns and 1.0 ns were corrected for the spectral sensitivity and smoothed by 9-linear smoothing factors (Figure 4.16). The TRS program was applied to both GMP

in neutral buffered and unbuffered solutions and their corrected and smoothed time-resolved spectra are shown in Figure 4.17a, b and 4.18a, b respectively.

It can be observed from Figure 4.16 that the emitting component of GMP with τ of 0.18 ns in acidic solution has a clear peak at 370 nm, and the shapes of the spectra at different delay times are basically identical although the one with delay 1.0 ns seems a few nm (< 4 nm) wider on the long wavelength side, which may arise from a residual solvation effect.

In neutral buffer solution (Figure 4.17a), the fast component with τ_1 ~ 0.06 ns and peak at 340 nm is predominant, and the slow component with τ_2 of 4.3 ns is barely observed because the integrated α_2 is two orders lower than α_1. The normalized spectrum of the slow component is shown in Figure 4.17b. The large noise for this component is due to the enlargement of the very weak fluorescence signal. Consequently, this poorly separated component spectrum may be meaningless.

In unbuffered solution (Figure 4.18a and b), the convoluted spectra have been well separated into two distinct spectra. Similar to buffered pH 7 solution, the fast component (C1) with τ_1 ~ 0.06 ns and peak at 340 nm is predominant, and the slower component with τ_2 of 0.6 ns and peak ~ 370 nm is one order of magnitude lower than the first one. The shapes, peak positions and lifetimes of the fast component in buffered and unbuffered solutions imply that they may be the same emitting species.

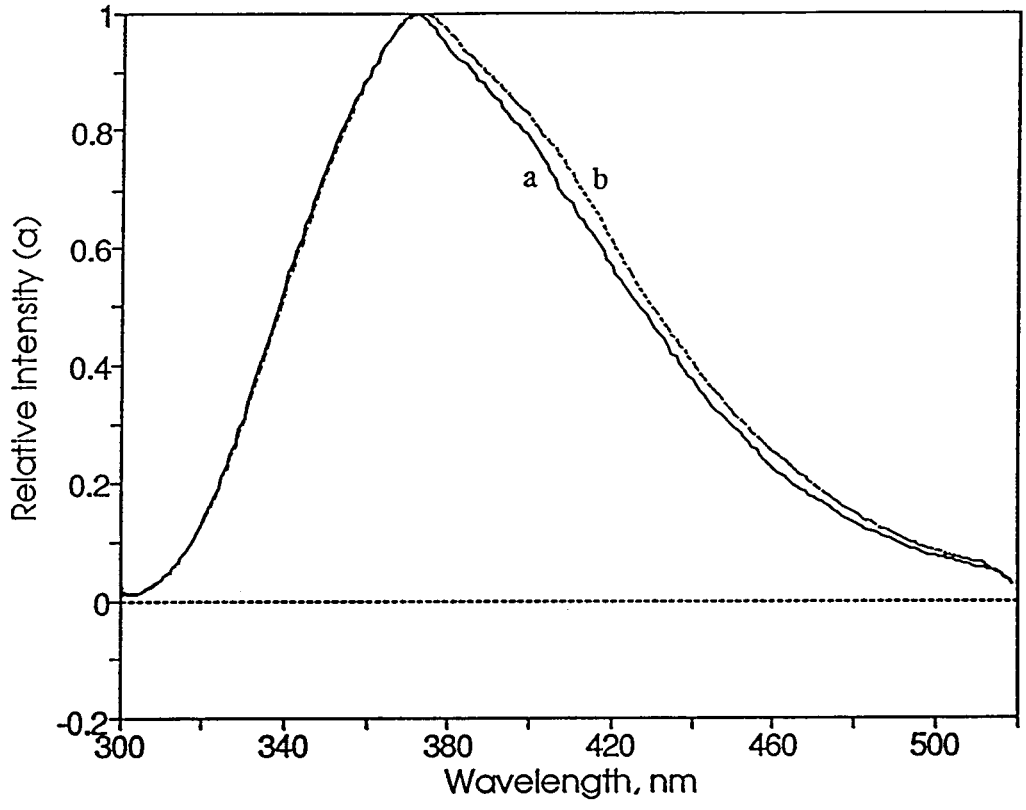

Figure 4.16 Corrected time-windowed emission spectra of GMP (1 x 10^{-5} M) in $HClO_4$ solution (pH 1.1). τ_1 = 0.18 ns. (a) 0 ns delay, (b) 1.0 ns delay.

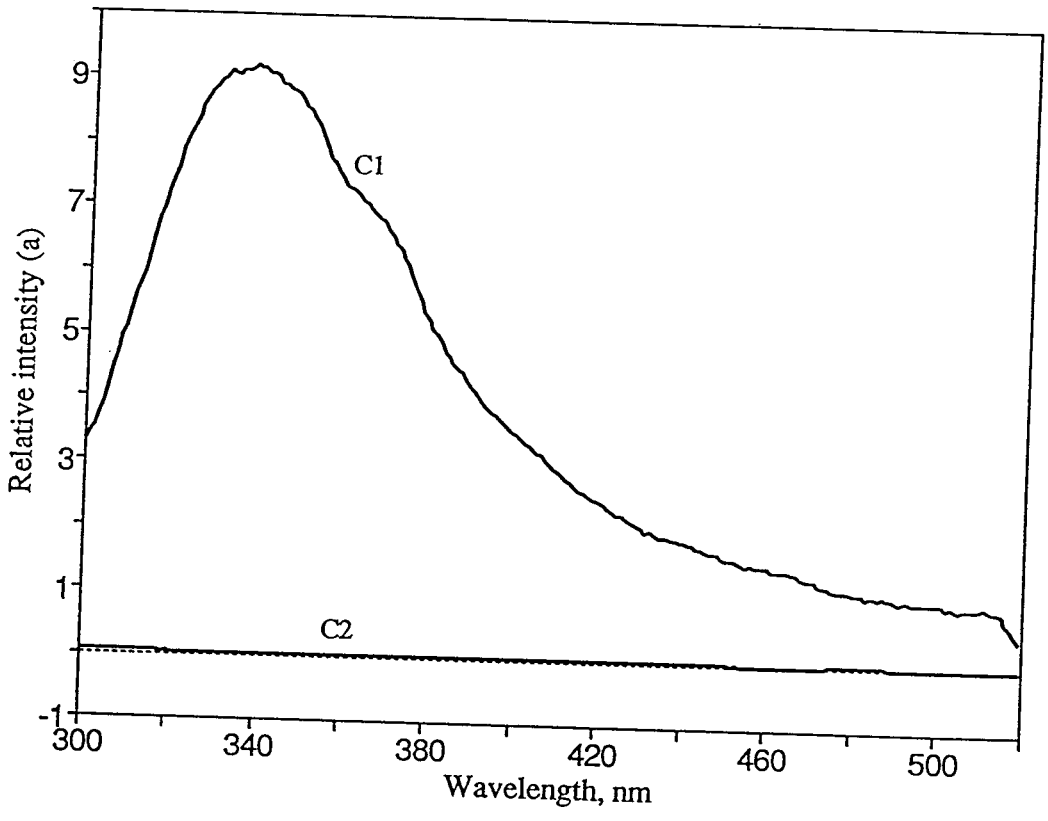

Figure 4.17a Corrected time-resolved emission spectra of GMP (1×10^{-5} M) in neutral buffer solution (pH 7). Using $\tau_1 = 0.06$ ns, $\tau_2 = 4.3$ ns, (C1) fast component, (C2) slow component. The ratio of integrated α_1 to α_2 is 234.

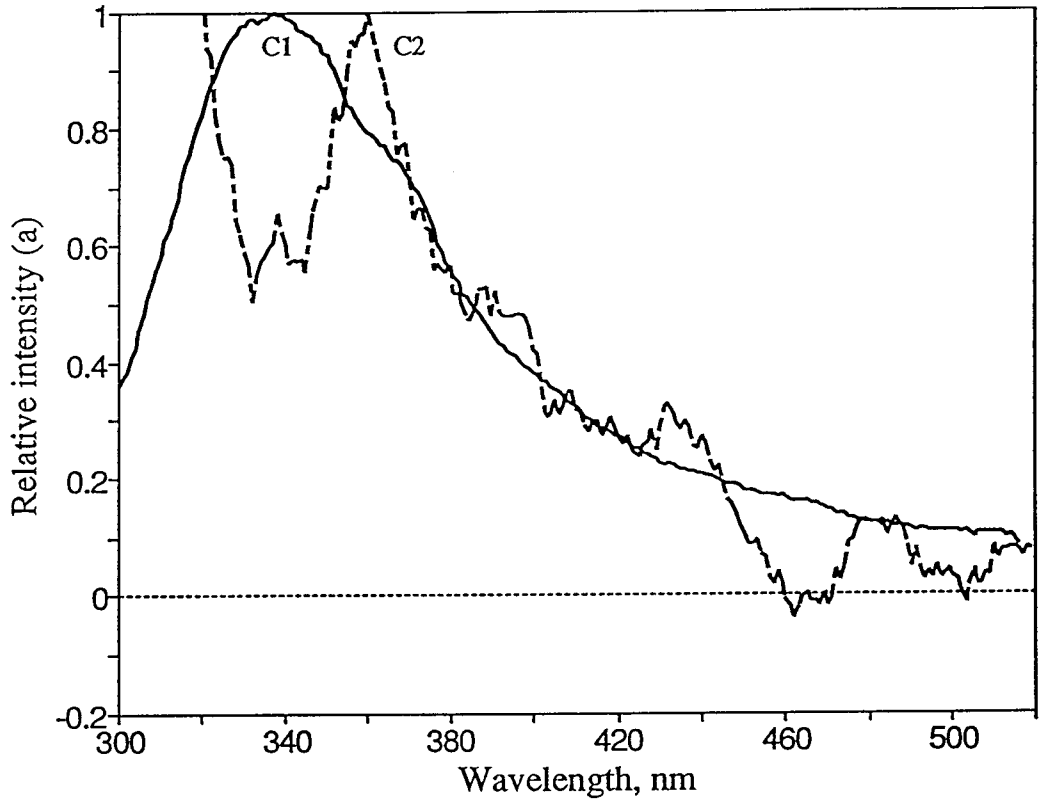

Figure 4.17b Corrected and normalized time-resolved emission spectra of GMP (1 x 10^{-5} M) in neutral buffer solution (pH 7). Using τ_1 = 0.06 ns, τ_2 = 4.3 ns, (C1) fast component, (C2) slow component. The ratio of integrated α_1 to α_2 is 234.

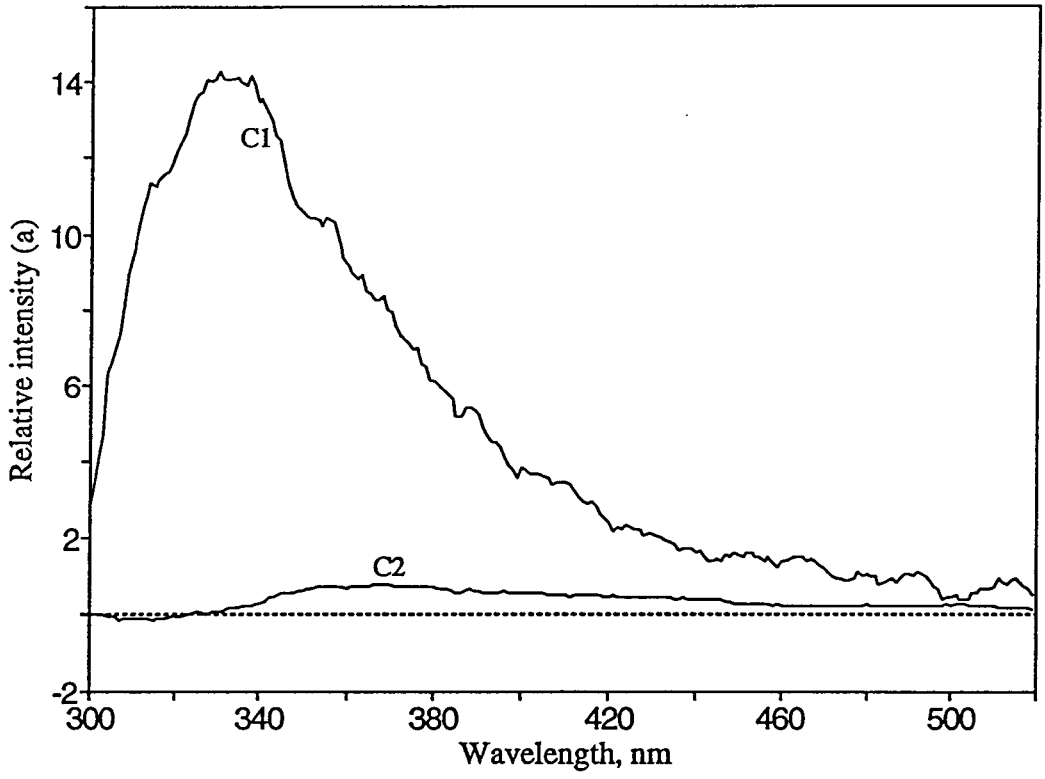

Figure 4.18a Corrected time-resolved emission spectra of GMP (1 x 10^{-5} M) in unbuffered aqueous solution (pH 6). Using τ_1 = 0.06 ns, τ_2 = 0.6 ns, (C1) fast component, (C2) slower component. The ratio of integrated α_1 to α_2 is 13.5.

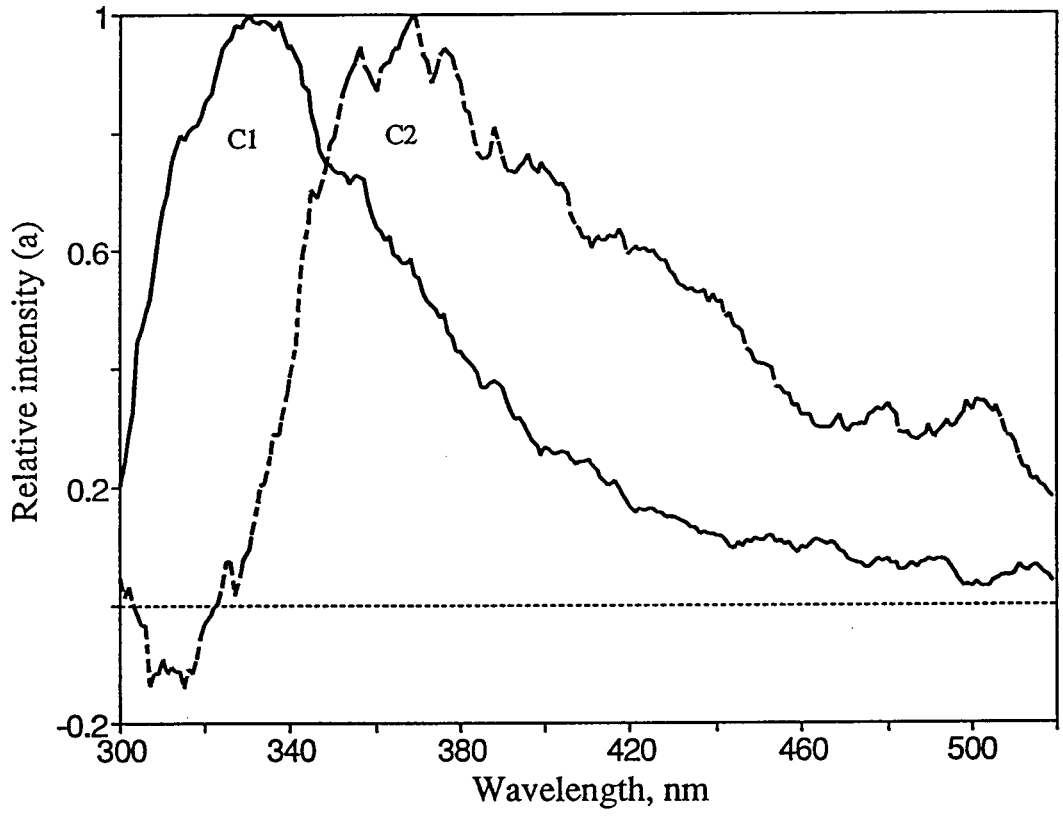

Figure 4.18b Corrected and normalized time-resolved emission spectra of GMP (1 x 10^{-5} M) in unbuffered aqueous solution (pH 6). Using τ_1 = 0.06 ns, τ_2 = 0.6 ns, (C1) fast component, (C2) slower component. The ratio of integrated α_1 to α_2 is 13.5.

4.2.3.2 dCMP and m^5dCMP

i) Lifetime analysis

The decay profiles of dCMP and m^5dCMP aqueous solutions at different pH were measured at different emission wavelengths following the excitation at 265 nm. Their lifetime analysis are listed in Table 4.11a, b, and c.

It turns out that only one fast component with $\tau \leq 100$ ps is present in all unmethylated and methylated dCMP solutions. Contrary to GMP solution, the lifetimes are independent of pH.

ii) Time-windowed spectra analysis

The time-windowed emission spectra of dCMP and m^5dCMP solutions were measured at delay time of 0 and 1.0 ns with width of 100 ps for each window. Because there is only one emitting component in each system, the time-windowed spectra were simply corrected by spectral sensitivities and smoothed by 9-linear smoothing factors. These resultant spectra are compared in Figure 4.19.

The emitting component of dCMP in acidic solution has a peak at 327 nm, essentially unchanged from pH 6. With a methyl group at 5-carbon position, the peak is red shifted to 340 nm again is unchanged from pH 7. This behavior is strikingly different from the absorption spectra of dCMP and

Table 4.11 Lifetime analysis of dCMP and m^5dCMP in different pH aqueous solutions.

a. dCMP in $HClO_4$ solution (pH 1.1)

Conc., M	λ_{em}, nm	τ, ns	$f(\alpha)$	$f(\alpha\tau)$
2×10^{-5}	330	0.08	100%	100%
	380	0.06	100%	100%

b. m^5dCMP in $HClO_4$ solution (pH 1.1)

Conc., M	λ_{em}, nm	τ, ns	$f(\alpha)$	$f(\alpha\tau)$
4×10^{-5}	350	0.05	100%	100%
	390	0.05	100%	100%

c. m^5dCMP in neutral buffered solution (pH 7)

Conc., M	λ_{em}, nm	τ, ns	$f(\alpha)$	$f(\alpha\tau)$
4×10^{-5}	350	0.06	100%	100%
	390	0.06	100%	100%

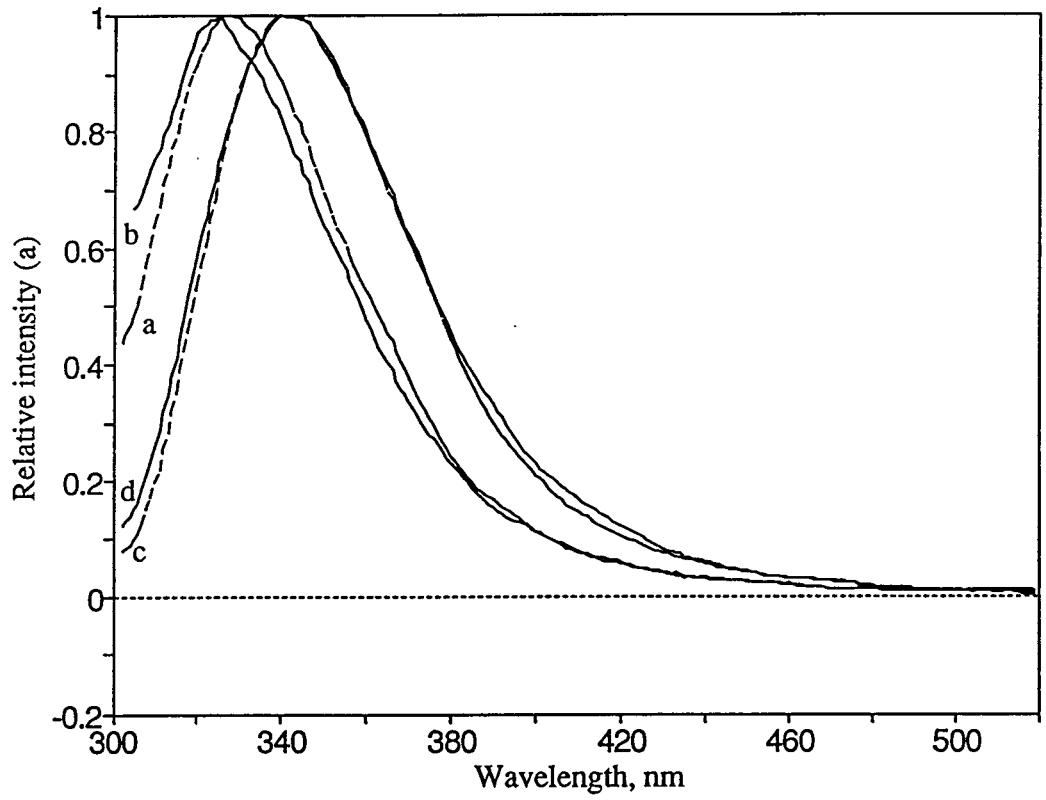

Figure 4.19 Corrected time-windowed emission spectra of dCMP and m^5dCMP in different pH aqueous solutions. Delay time: zero ns, $\tau_1 < 100$ ps. (a) and (b) dCMP in acidic (pH 1.1) and unbuffered solutions (pH ~ 6), (c) and (d) m^5dCMP in acidic (pH 1.1) neutral buffer solution (7.0).

m^5dCMP which do change with acidity. [dCyd absorption in acid and neutral solutions has been presented earlier in this chapter].

The emission spectroscopic characteristics of GMP, dCMP and m^5dCMP in different pH aqueous solutions are summarized in Table 4.12.

Table 4.12 Emission spectroscopic characteristics of GMP, dCMP and m^5dCMP in aqueous solutions

compounds	pH	Conc. (mM)	τ_1 (ns)	$\lambda_{1,max}$	τ_2 (ns)	$\lambda_{2,max}$	$[\alpha_1]/[\alpha_2]^*$
GMP	1.0	0.01	~0.18	372			
	7.0	0.02	~0.06	340	4.3	~360	234
	6	0.01	~0.06	330	0.6	370	13
dCMP	1.1	0.02	~0.06	327			
dCMP	~ 6	0.02		330			
m^5dCMP	1.1	0.04	~0.06	340			
	7.0	0.04	~0.06	340			

*From integrated time-resolved emission spectra, i. e. $\int\alpha(\lambda)d\lambda$.

4.3 Discussion

The resolved absorption spectra show that the solvents affect the spectral characteristics of cytidyl chromophore. In neutral aqueous solution, there are four or five possible transitions; in protic and aprotic solutions, there are three but the peak positions, intensities and widths differ from each other. The results of time-resolved fluorescence spectroscopy G and C in aqueous solutions (Table 4.12) indicate that pH largely affects the lifetimes and emission spectra of GMP although there is no essential change in its absorption spectrum. In acid solution, only single component emission exists with τ of 180 ps and λ_{max} 372 nm. On increasing pH to 7, the single-exponential model is the best. Although the two-exponential model is possible, the very fast component with $\tau \sim 60$ ps, λ_{max} 340 nm is predominant. Contrary to GMP, the emission characteristics of dCMP and m^5dCMP are independent of pH from 1 to 7 and they both show a single fast emission behavior although their absorption spectra are considerably changed with pH.

4.3.1 The number of the possible transitions in cytidyl chromophore in aqueous solutions

The resolved absorption spectrum of cytidine in acetonitrile (Figure 4.12) shows there are two possible transitions below the benchmark (6.3 eV, 50,000 cm^{-1}) and their peak positions are very close to those of cytidine in solid state (Raksanyi et al., 1978). However, most of the crystal reflection data and fitting results of absorption spectra of C in neutral aqueous

solutions (Johnson, 1971; Zaloudek et al., 1985, Morozov, 1987) gave three transitions. This indicate the solvent effects of the spectral characteristics of cytidyl chromophore. It should be kept in mind that the number of the transitions has not been settled yet. The theoretical calculations (Hug and Tinoco, 1973; Srivastava and Mishra, 1980; Matos and Roos, 19) do not agree with the experiment results, predicting the existence of two transitions. It is noticed that for wathever reasons, none of the fitting results in literature present statistical analysis. To improve this situation, the present work resolved several cytidyl chromophore in neutral aqueous solutions into three and four gaussians respectively, and carried out a series of statistical analysis, such as χ^2, r^2 and the test for random distribution of residuals. The results show that the four-gaussian fitting for all of C is considerably better than three-gaussian fitting. Take a example of deoxycytidine, the χ^2 is decreased more than one order and residuals are reduced two or three times (Figures 4.7a and b). Rest of the C's (cytosine, 1-methylcytosine, dimethylcytidine and dCMP) show the same tendency (Figures 8 - 11). All of this indicates that the four-gaussian fit (in λ)provides a good description of the observed data and raises the probablility that there may be four possible electronic transitions in cytidyl chromophore in neutral aqueous solution below the benchmark.

4.3.2 Assignment of the major components of GMP in aqueous solution

It is easy to see that the general emission characteristics of GMP are quite similar to those of ATP (Part III). In neutral solution the major component is a very fast one which may arise from the unprotonated form. In acid, the lifetime of the major component is increased and the spectrum shifted to the red, and it may originate from the protonated form. Based on this, a possible dynamic mechanism can be described as follows (Figure 4.20).

In acid solution (pH 1.0):

$$GMPH^+ \xrightarrow{h\upsilon} (GMPH^+)^*$$

$$(GMPH^+)^* \longrightarrow GMPH^+ + \text{fluo. at } \lambda_{max} \text{ 370 nm}$$

In neutral solution:

$$GMP \xrightarrow{h\upsilon} GMP^*$$

$$GMP^* \longrightarrow GMP + \text{fluo. at } \lambda_{max} \text{ 340 nm}$$

The red shift in peak position from neutral to acid solution (340 nm to 370 nm) is possibly due to a solvation process. Since the protonated excited form has a higher polarity than the unprotonated one, it is easier to be solvated completely by H_2O before emission. Consequently, it has a longer lifetime and longer wavelength emission. Whilethe unprotonated form may fluoresce before completing solvation.

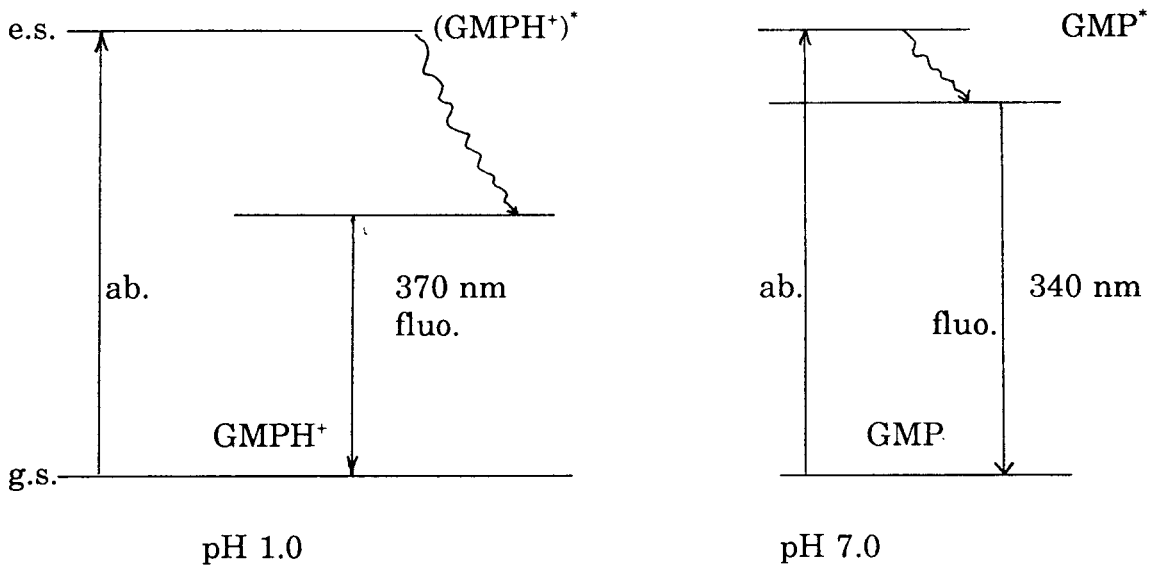

Figure 4.20 A possible scheme for the excitation and emission of GMP.

4.3.3 Assignment of emission components of dCMP and m^5dCMP in aqueous solution

In view of the distinctive absorption behavior (Figures 4.2 and 4.14) and the identical emission behavior (Figure 4.19) of cytidyl chromophore (C) at various pH aqueous solutions, and comparing these with its anion emission spectrum, a possiblechanism can be proposed.

In neutral solution, the fast emission species may arise from the unprotonated C:

$$C \xrightarrow{h\nu} C^*$$

$$C^* \longrightarrow C + h\upsilon \text{ (fluorescence)}$$

In acid solution, the identical fast emission may originate indirectly from a indirect unprotonated C arise via the following processes:

$$CH^+ \xrightarrow{h\nu} (CH^+)^*$$

If $pK_a(CH^+)^* < pK_a(CH^+)$, i.e. the excited protonated C is a stronger acid than the ground one, then it is possible to have

$$(CH^+)^* \longrightarrow H^+ + C^*$$

$$C^* \longrightarrow C + h\upsilon \text{ (fluorescence)}$$

The scheme of this mechanism is illustrated in Figure 4.21.

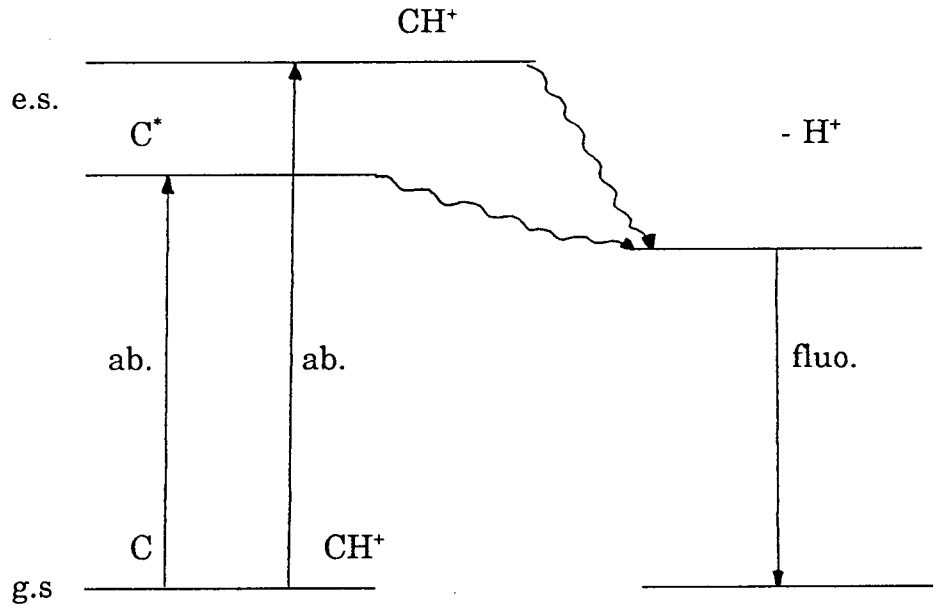

Figure 4.21 A possible scheme of the excitation and emission of cytidyl chromophore.

4.4 Conclusions

The results of resolved absorption spectra of G, C's, d(GC) and polyd(GC)·polyd(GC), and time-resolved emission spectra of G and C can be summarized as follows:

1. The results of gaussian fittings of Guo and dCyd in neutral aqueous solutions show there are two possible electronic transitions in Guo in the range of 230-310 nm and four or five (fitting is better) possible transitions in dCyd in the range of 190-310 nm.

2. The fittings of absorption spectra of d(CG) and polyd(GC)·polyd(GC) with gaussian components of Guo and dCyd in the range of 230-310 nm indicate that the hypochromism in the range of 255-285 nm for d(CG) only arises from the first transitions G1 and C1; the large hypochromism in the range of 230-295 nm for polyd(GC)·polyd(GC) is attributed to the transitions G1, C1, C2 and C3. The second transition G2 does not contribute to the hypochromism for either d(CG) or polyd(GC)·polyd(GC).

3. The five-gaussian fitting is better than the four gaussian fitting for several absorption spectra of C's in neutral aqueous solutions.

4. There are three possible transitions for C in protic and aprotic solutions in the UV range, but their gaussian characteristics are very different from each other.

5. pH affects the lifetimes and spectral characteristics of GMP. In acid solutions, there is only a fast component with τ of 180 ps and λ_{max} of 372 nm.

In neutral solution, there are two, but the fast one with τ_1 ~ 60 ps and λ_{max} of 340 nm is predominant. pH does not affect the lifetimes and emission spectral characteristics of CMP. Only a single fast component with lifetime ~ 60 ps exists.

BIBLIOGRAPHY

Ballini, J. P., Daniels, M. and Vigny, P. (1988), Synchrotron-excited time-resolved fluorescence spectroscopy of adenosine, protonated adenosine and ^{6}N, ^{6}N-dimethyladenosine in aqueous solution at room temperature. Eur. Biophys. J., **16**, 131-142.

Ballini, J. P., Daniels, M. and Vigny, P.(1991), Time-resolved fluorescence emission and excitation spectroscopy of d(TA) and d(AT) using synchrotron radiation. Biophy. Chem., **39**, 253-265.

Ballini, J. P. , Vigny, P. and Daniels, M. (1984a) at LURE, France, Yellow Book, p. 100 with a file named "CDG20.dat", (unpublished).

Ballini, J. P. Vigny, P. and Daniels, M. (1984b) at LURE, France, Yellow Book, p. 98 with a file named "DGC20.dat", (unpublished)

Blumberg, W. E., Eisinger, J. and Navon G. (1968), Lifetimes of excited states of some biological molecules. Biophys. J., **8**, A-106

Bobruskin, I. D., Gottikh, B. P., Kritsyn, A. M., Lysov, Yu. P., Pokrovaskaya, M. U. , Tychinskaya L. Yu and Florent'ev, V. L., (1980), Study of the conformational situation in aqueous solution of dinucleoside phosphates by the method of nuclear magnetic resonance. Biophys., **25**, 761-778.

Börresen, H. C. (1963), On the luminescence properties of the some purines and pyrimidines. Acta Chem. Scan. **17**, 921-929.

Börresen, H. C. (1967), Fluorescence and tautomerism of protonated and methylated adenine derivatives. Acta. Chem. Scan, **21**, 2463-2473.

Cadet, J. and Vigny. P. (1990), Photochemistry of nucleic acids. In Bioorganic Chemistry, Vol. 1 (H. Morrison, Ed.), Wiley, New York, pp. 1-272.

Callis, P. R. (1979), Polarized fluorescence and estimated lifetimes of the DNA bases at room temperature. Chem. Phys. Lett., **61**, 563-567.

Callis, P. R. (1983), Electronic states and luminescence of nucleic acids system. Ann. Rev. Phys. Chem., **34**, 329-357.

Callis, P. R. (1986), An extended semi-empirical molecular orbital study of the $\pi\pi^{*}$ excited states of nucleic acid bases. Photochem. Photobiol., **44**(3), 315-332.

Cantor, C. R. and Schimmel, P. R. (1980), Biophysical Chemistry, Part II, W. H. Freeman and Company, San Francisco, pp. 399-404.

Cantor, C. R. and Schimmel, P. R.(1980), Biophysical Chemistry, Part II, (W. H. Freeman and Company), p. 39

Charney, E. and Gellert, M. (1963), Quantum aspects of polypeptides and polynucleotides. Biopolymers, Symposium No 1, 469-477.

Clark, L. B. (1977), Electronic spectra of crystalline 9-ethylguanine and guanine hydrochloride. J. Am. Chem. Soc., **99**, 3934-3938.

Clark, L. B. (1986), Transition-moment directions of protonated 1-methylcytosine. J. Chem. Soc., **108**, 5109-5113.

Clark, L. B. (1989), Polarization assignments in the 270 nm band of the adenine chromophore. J. Phys. Chem., **93**, 5345-5347.

Clark, L. B. (1990), Electronic spectrum of the adenine chromophore. J. Phys. Chem. **94**, 2873-2879.

Daniels, M. (1976), Excited states of the nucleic acids: bases, mononucleosides, and mononucleotides. In Photochemistry and Photobiology of Nucleic Acids, Vol. 1 (S. Y. Wang, Ed.), Academic press, New York, pp. 23-108.

Daniels, M. and Hauswirth, W. (1971), Fluorescence of the purine and pyrimidine bases of the nucleic acid in neutral aqueous solution at 300K. Science, **171**, 675-677.

Daniels, M., Hart, L. P., Ho, P. S. and Vigny, B. (1990), Time-resolved spectroscopy of intrinsic fluorescence of nucleic acids species. In Time-Resolved Laser Spectroscopy in Biochemistry II, SPIE proceedings, Vol. 1204 (J. R. Lakowicz, Ed.), pp. 304-313.

Daniels, M. Shaar, C. S. and Morgan, J. P. (1988), Sequence dependence emission from stacked forms of ApC and CpA evidence for stacked base ('dimer') absorption and lift-handed stacked conformation. Biophys. Chem., **32**, 229-237.

Doornbas, J., Leeuw, H. P. M. de, Olsthoorm, C. S. M., Wille-Hazeleger, G., Westerink, H. P., Boom, J. H. van. and Altona, C. (1983), Conformational analysis of m_2^4C-m_2^4C- m_2^6A: a chemically modified 3'-acceptor end of tRNA, studied by NMR and CD methods. Nucleic Acids Res., **11**, 7517-7536.

Eastman, J. (1969), The fluorescence and tautomerism of adenine. Ber. Bunsenges. Phys. Chem. **73**, 407-412.

Einstein, A. (1917), On the quanta theory of radiation. Physik Z. **18**, 121-128.

Eisinger, J. and Lamola A. A. (1971), The excited state of nucleic acids. In Excited State of Proteins and Nucleic Acids (R. F. Steiner and I. Weinryb, Eds.) Plenum Press, New york-London, p. 151.

Fornasiero, D., Roos, I. A. G., Rye Kerry-Anne and Kurucsev. T. (1981), Near-ultraviolet vibrational transitions of adenosine 5'-phosphate, adenosine, and its complexes with cis- and trans-diamminedichloroplatinum(II): Spectral study of isotropic absorption, linear dichroism, and circular dichroism. J. Am. Chem. Soc., **103**, 1908-1913.

Fu, Y. (1987), Spectral sensitivity measurement, Lab-notebook I, pp. 1-20 (unpublished).

Fucaloro A. F. and Forster, L. S. (1971), Streched-film spectra and transition moments of nucleic acid bases. J. Am. Chem. Soc. **93**, 6443-6448.

Gill, J. E. (1970), Transfer energy from reaction center to light harvesting chlorophyll in a photosynthetic bacterium, Photochem. Photobiol., **11**, 259-269.

Gratzer, W. B., (1967), Ultraviolet absorption spectra of polypeptides. In Poly-L-amino Acids, (G. D. Fasman, Ed.) New York: Marcel Dekker, p. 177.

Hart, L. P. and Daniels, M. (1989), Lifetime evidence for a weak lowest electronic transition in adenosine. Biochem. Biophy. Res. Com., **162**(2), 781-787.

Hart, L. P. and Daniels, M. (1992), Lifetime analysis of weak emissions and time-resolved spectral measurements with a subnanosecond dye laser and gated analog detection. Applied Spectroscopy, **46** (2), 191-205.

Hauswirth, W. and Daniels, M. (1971), Fluorescence of thymine in aqueous solution at 300K. Photochem. Photobiol. **13**, 157-163.

Herzberg, G. (1945), Molecular Spectra and Molecular Structure, Van Nostrand Renhold Company, Vol. 2, p. 244, 254.

Hosur, R. V., Govil, G., Hosur, M. V. and Viswamitra, M. A. (1981), Sequence effects in structures of the dinucleotides d-pApT and d-pTpA. J. Mol. Struct. **72**, 261-267.

Hug, W.and Tinoco, I.(1973), Electronic spectra of nucleic acid bases. I. Interpretation of the in-plane spectra with the aid of all valence electron MO-CI calculations. J. Am. Chem. Soc., **95**, 2803-2813.

Ito, H. I'Haya, Y. J. (1976), The approximate self-consistent renormalized RPA: the electronic excited states of DNA bases in the CNDO/S method. Bull. Chem. Soc. Jpn., **49**, 3466-3471.

Inagaki, F., Tasumi, M. and Miyazawa, T. (1974), Excitation profile of the resonance Raman effect of β-carotene. J. Mol. Spec., **50**, 286-303.

Izett, R. M., Chestensen, J. J. and Rytting, J. H. (1971), Site and thermodynamic quantities associated with proton and metal ion interaction with ribonucleic acid, deoxyribonucleic acid, and their constituent bases, nucleosides and nucleotides. Chem. Rev., **7**(5), 439-481.

Jandel Corporation (1990), PeakFit, Computer software, Version 2.

Johnson, W. C. Vipond, P. M. and Girod, J. C. (1971), Tautomerism in cytidine. Biopolymers, **10**, 922-933.

Knighton, W. B. (1980), Excited lifetimes of pyrimidines and purines in room temperature solution from fluorescence quantum yields and anisotropies. MS thesis, Montana State University., Bozeman, Montana. 108 pp.

Knighton, W. B. Giskaas, G. O. and Callis, P. R. (1982), Fluorescence from adenine cations. J. Phys. Chem., **86**, 49-55.

Knutson, J. R. Beechem, J. M. and L. Brand (1982), Simultaneous analysis of multiple fluorescence decay curves: a global approach. Chem. Phys. Lett. **102**, 501-507.

Kripke, M. L. and Sass E. R. (1978), International conference on carcinogenesis, Maryland, National Cancer Institute Monograph, No. 50, pp. 1-248.

Lakowicz, J. (1988), Time-resolved laser spectroscopy in biochemistry I, Proc. SPIE, Vol 909.

Lakowicz, J. (1990), Time-resolved laser spectroscopy in biochemistry II, Proc. SPIE, Vol. 1204.

LeBreton, P. R., Yang, X., Urano, S., Fetzer, S., Yu, M., Leonard, N. J. and Kumar, S. (1989), Photoemission properties of methyl-substituted guanines: photoelectron and fluorescence investigations of 1,9-dimethylguanine, O^6,9-dimethylguanine, and 9-methylguanine. J. Am. Chem. Soc., **112**(6), 2138-2147.

Levin, I. N. (1983), Quantum Chemistry, third edition. The Allyn and Bacon, Inc., Boston, pp 58-65.

Longworth, J. W. Rahn, R. O. and Shulman, R. G. (1966), Luminescence of pyrimidines, purine, nucleosides, and nucleotides at 77K, The effect of ionization and tautomerization. J. Chem. Phys., **45**(8), 2930-2939.

Matos, J. M. and Roos, B. O. (1988), Ab Initio quantum chemical study of the π-electron spectrum of the cytosine molecule. J. Am. Chem. Soc. **110**, 7664-7671.

Matsuoka, Y. and Norden, B.(1982), Linear dichroism studies of nucleic acid bases in stretched poly-vinyl alcohol) film. Molecular orientations and electronic transition moment directions. J. Phys. Chem. **86**, 1378-1386.

Marcus, R. A. (1989), Relation between charge transfer absorption and fluorescence spectra and the inverted region. J. Phys. Chem., **93**, 3078-3086.

Morgan, J. P. and Daniels , M. (1980), Excited states of DNA and its components at room temperature-IV. Spectra, polarization and quantum yield studies of emissions from CpC and poly rC. Photochem. Photobiol. **31**, 207-213.

Morita, H. and Nagukura, S. (1968), The electronic absorption spectra and the electronic structures of cytosine, isocytosine and their anions and cations. Theoret. Chim. Acta. (Berlin), **11**, 279-295.

Morozov, Yu. V., Bazhulin, N. P., Bokovoi, V. A. and Chkhov, V. O. (1987), Principles of reconvolution of complex spectra of biologically-active compounds into bands corresponding to individual electronic transitions. Biofizika, **32**,(4), 699-715.

Mulliken, R. S. (1939), Intensities of electronic transitions in molecular spectra. J. Chem. Phys. **7**, 14-34.

Nikogosyan, D. N. (1990), Two-quantum UV photochemistry of nucleic acids: comparison with conventional low-intensity UV photochemistry and radiation chemistry. Int. J. Radiat. Biol., **57** (2), 233-299.

Norden, B. and Kubista M. and Kurucsev, T. (1992), Linear dichroism spectroscopy of nucleic acids. Quart. Rev. Biophys., **25** (1), 51-170.

Novros, J. S. and Clark, L. B. (1986), On the electronic spectrum of 1-methyluracil. J. Phy. Chem., **90**, 5666-5668.

P. L. Biochemicals, inc. (1976), Ultraviolet absorption spectra of 5'ribonucleotides, Pabst Brewing Company, Milwoukee, Wisconsin, 21 pp.

Parkanyi, C. Bouin, D., Shieh, D. C., Tunbrant, S., Aaron, J. J. and Tine, A. (1983), The effect of pH on the electronic absorption, fluorescence and phosphorescence spectra of purines and pyrimidines. Determination of the lowest excited singlet and triplet state ionization constants. Journal de Chimie Physique, **81**(1), 3099.

Provencher, S. W. and Vogel, R. H. (1983), Regularization Techniques for Inverse Problems in Molecular Biology in Progress in Scientific Computing, Vol. 2 (P. Deuflhard and E. Hairer, Eds.). Birkhaüser, Boston, pp. 304-319.

Raksányi, K. and Földváry, I. (1978), The electronic structure of cytosine,5-azacytosine, and 6-azacytosine. Biopolymers, **17**, 887-896.

Rigler, R., Claesens, F. and Kristenen, O. (1985), Picosecond Fluorescence spectroscopy in the analysis of structure and motion of biopolymers. Anal. Instr., **14**, 525-546.

Sprecher, C. A. and Johnson, W. C. (1977), Circular dichroism of the nucleic acid monomers. Biopolymers, **16**, 2243-2264.

Srivastava, S. K. and Mishra, P. C. (1979), Elctronic structure, spectra, and mechanism of photodimerization of pyrimidine bases. Int. J. Quantum Chem., **16**, 1051-1068.

Stewart, R. F. and Davidson, J. (1963), Polarized absorption and purines and pyrimidines. J. Chem. Phys., **39**, 255-266.

Stewart, R. F. and Jensen, L. H. (1964), Crystal structure of 9-methyladenine. J. Chem. Phys., **40**, 2071-2075.

Strickler, S. J. and Berg, R. A. (1962), Relationship between absorption intensity and fluorescence lifetime of molecules. J. Chem. Phys. **37** (4), 814-822.

Vigny, P. and Ballini, J. P. (1977), In Excited States in Organic Chemistry and Biochemistry (B. Pullman and N. Goldblum, Eds.), pp. 1-13.

Vigny, P and Duquesne M. (1976), On the fluorescence properties of nucleotides and polynucleotides at room temperature. In Excited States of Biological Molecules (J. B. Birks, Ed.), Wiley, New York, pp. 167-177.

Voelter, W., Records, R., Bunnenberg, E. and Djerassi, C. (1968), Magnetic circular dichroism studies. VI. Investigation of some purines, pyrimidines, and nucleosides. J. Am. Chem. Soc. **90**, 6163-6170.

Voet, D., Gratzer, W. B., Cox, R. A. and Paul Doty (1963), Absorption spectra of nucleotides, polynucleotides, and nucleic Acids in the far Ultraviolet. Biopolymer, **1**, 193-208.

Vogel, R. H. (1986), SPLMOD (Version 2) Users Manual, EMBL. Technical Report DAO6 (European Molecular Biology Laboratory, Heidelberg, Germany), 30 pp.

Volosov, A and Woody, R. W. (1992), Calculation of transition moments on isolated adenine and guanine and their methyl-substituted derivative. J. Phys. Chem., **96**, 4845-4851.

Ward, D. C. and Reich, E. (1969), Fluorescence studies of nucleotides and polynuleotides. J. Biol. Chem., **244**(5), 1228-1237.

Wells, R. D., Larson, J. E. and Grant, R. C.(1970), Physicochemical studies on polydeoxyribonucleotides containing defined repeating nucleotide sequences. J. Mol. Biol., **54**, 465-497.

Wilson, R. W. and Callis, P. R. (1980), Fluorescence tautomers and the apparent photophysics of adenine and quanine. Photochem. Photobiol., **31**, 323-327.

Yamashita, M., Koboyashi, S., Torizuka, K. and Sato, T.(1987), Observation of the diffussion-free intermolecular excimer of 9-methyladenine in aqueous solution by picosecond time-resolved spectroscopy. Chem. Phys. Let., **137**(6), 578-582.

Yamashita, M., Sibbett, W., Welford, D. and Bradley, D. J. (1980), Introcavity second-harmonic generation in a synchronously mode-locked cw dye laser. J. Appl. phys., **51**, 3559-3562.

Zaloudek, F., Novros, J. S. and Clark L. B. (1985), The electronic spectrum of cytosine. J. Chem. Soc., **107**, 7344-7351.

APPENDICES

APPENDICES

I. Lifetime and TRS analysis

In the present work, the lifetimes of nucleic acids component are determined by using a non-linear least square reiterative convolution program, and the time-windowed emission spectra are resolved by applying TRS (decay associated) program. Here, the two examples are selected, one with small fluorescence signals (ATP/buffer system) and the other with large fluorescence signals (ATP/acid system), respectively, to describe the whole processes of lifetime and TRS analysis and to show how these programs work in detail.

ATP (0.1 mM) in neutral buffered aqueous solution

i) Lifetime analysis

The decay profiles for ATP neutral aqueous solution (0.1 mM) fluorescence at 320, 350 and 390 nm following excitation at 265 nm are shown in Figure Ia, b, and c respectively, together with the Rayleigh scatter (instrument response function) at 267 nm. The residuals and their autocorrelation function (c(t)), for the best multi-exponential are shown in the figures as well.

[In all Figures the upper most plot shows the data points, the instrument response and the fitting line, the middle plot shows the minimized residuals, and the lowest plot is the autocorrelation functions.]

(1)

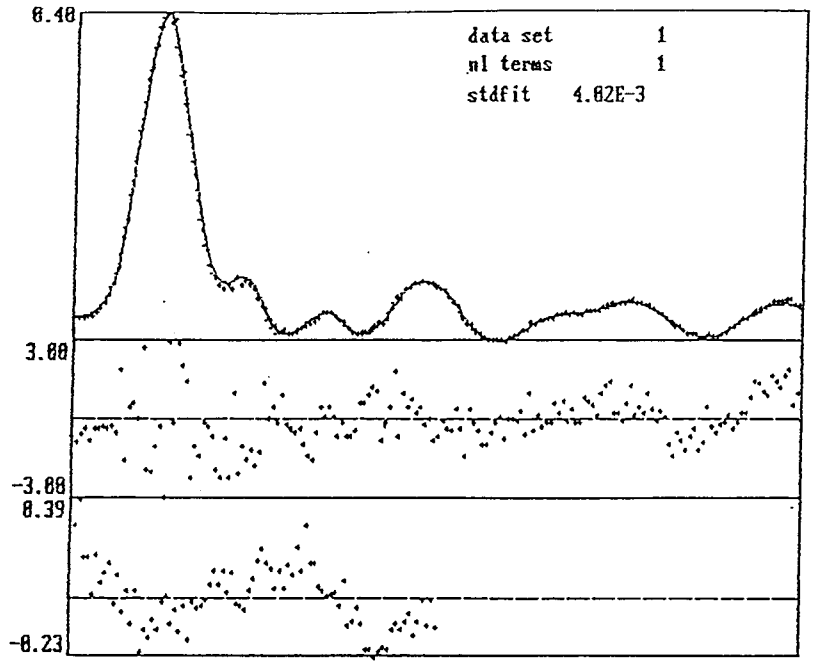

(2)

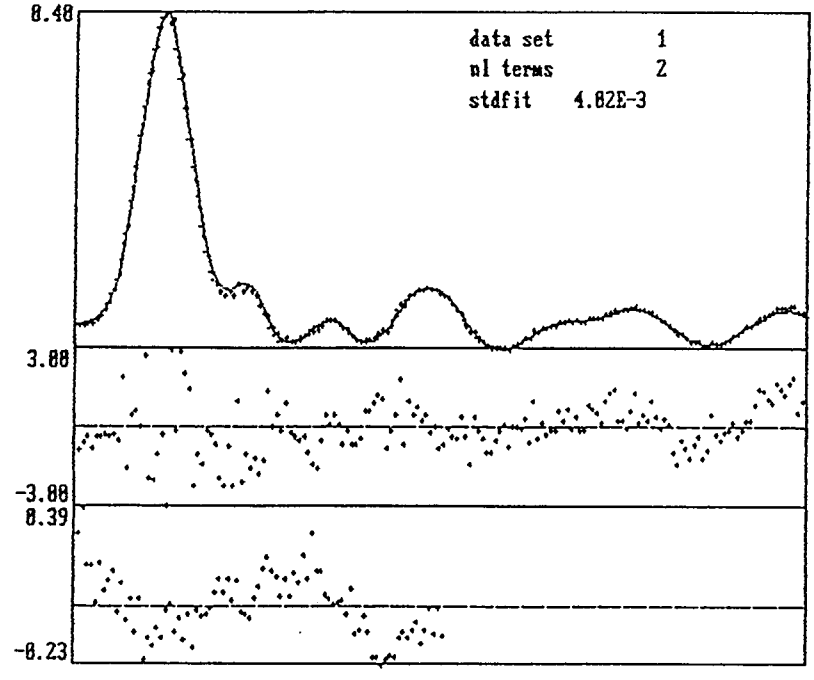

Figure Ia Decay profiles of ATP (0.1 mM) in phosphate buffer solution (pH 7.0) at λ_{em} 320 nm. Time delay range: 15-32 ns. (1) one-exponential, (2) two exponential. .... instrument response; ---- fitting line; ++++ data points (top plot), residuals (middle plot), and autocorrelation function (lowest plot). This representation is the same for all Figures and will not be repeated.

(1)

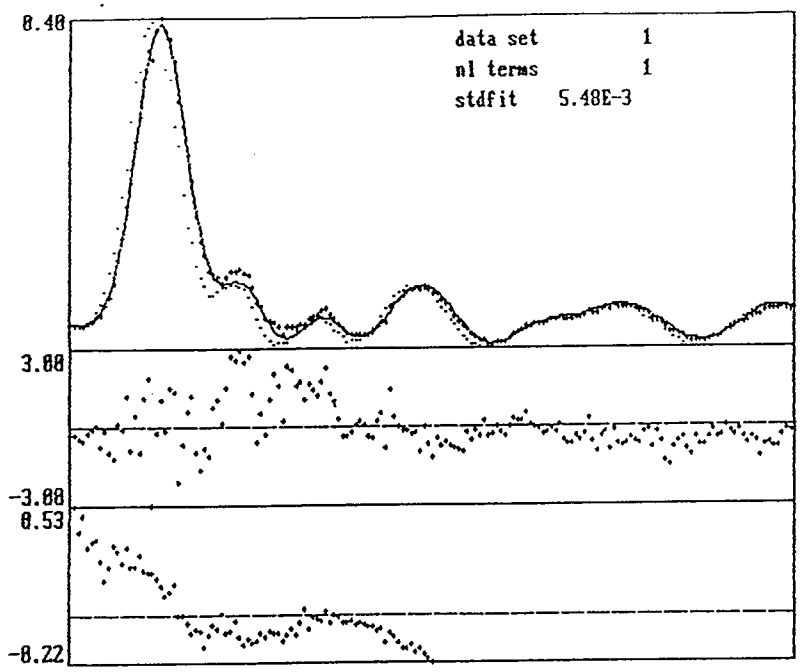

(2)

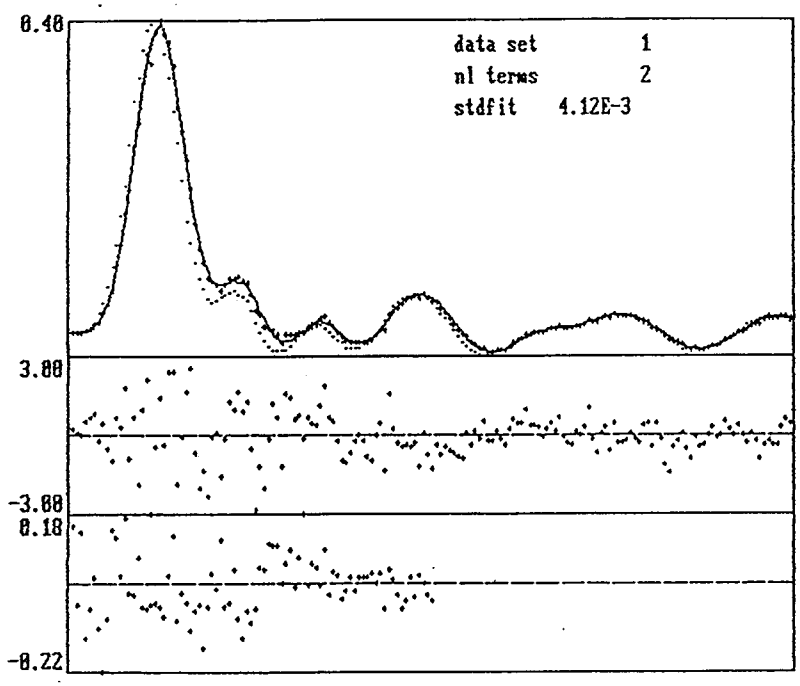

Figure Ib Decay profiles of ATP (0.1 mM) in phosphate buffer solution (pH 7.0) at λ_{em} 350 nm. Time delay range: 15-32 ns. (1) one-exponential, (2) two exponential.

(1)

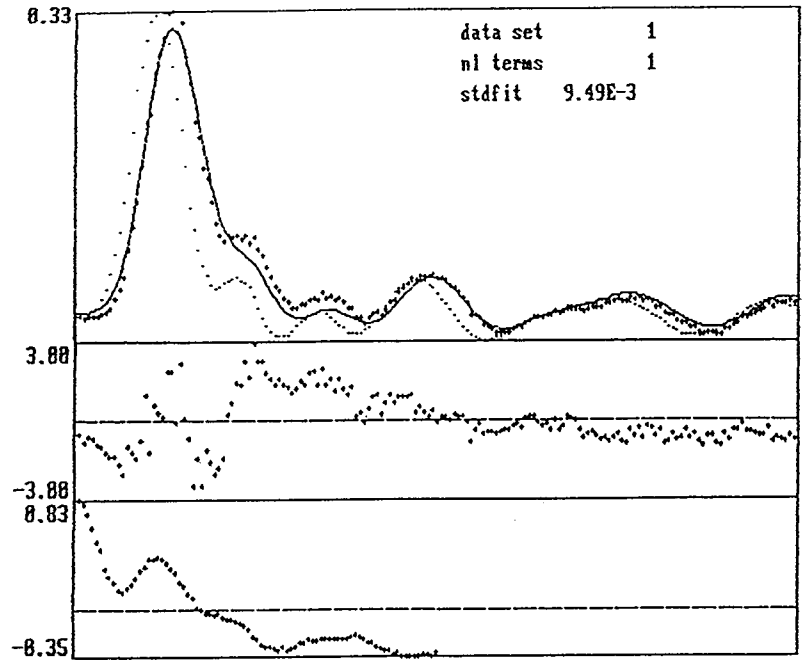

(2)

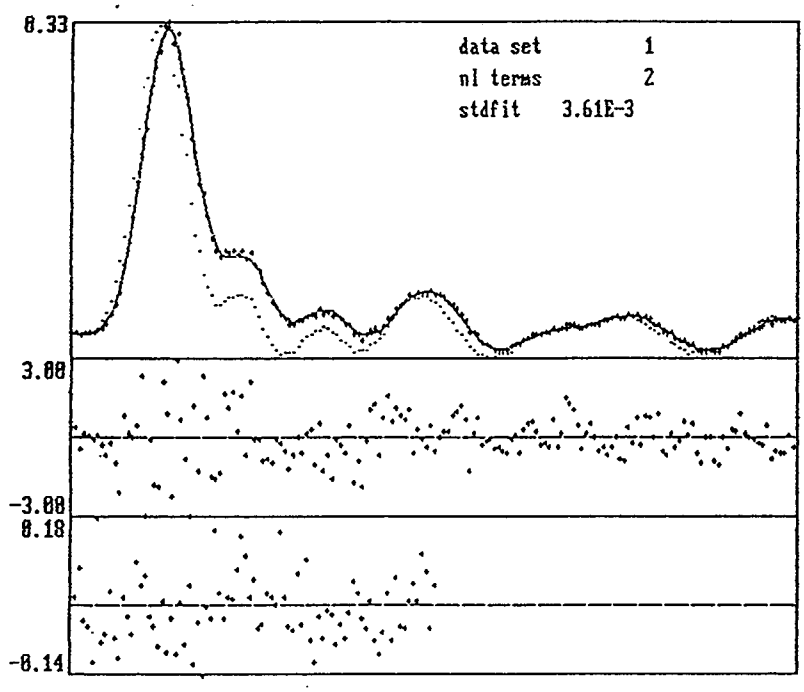

Figure Ic Decay profiles of ATP (0.1 mM) in phosphate buffer solution (pH 7.0) at λ_{em} 390 nm. Time delay range: 15-32 ns. (1) one-exponential, (2) two exponential. (3) three exponential.

Figure 1c, continued

(3)

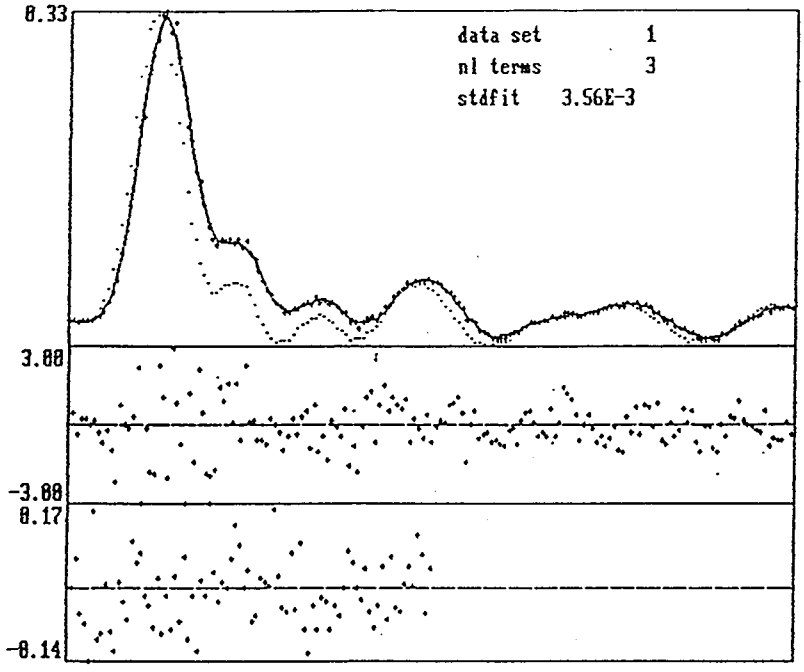

The corresponding detailed numerical results for various exponential models of analysis are given in Table I. In Tables I, the `stdfit' is a abbreviation for standard fit of the decay curve, $\alpha(\lambda)$ is a preexponential factor representing the fractional contribution to the time-resolved decay of the component with a lifetime τ_i at wavelength λ, $f(\alpha)$ denotes the fraction of initial emission magnitude, $\alpha(\lambda)\tau$ is an integral over whole time of exponential decay, $\alpha(\lambda)\tau = \int_0^\infty \alpha(\lambda)e^{-t/\tau}\, dt$, $f(\alpha\tau)$ represents the fraction of total emission intensity with respect to the steady state, and the value immediately following the lifetime is its standard error. The data are grouped in the order of increasing number of exponentials. For a successful fit the standard fit should be small, the residuals and their autocorrelation functions should be randomly distributed around zero.

Examining the decay profiles and their numerical analysis carefully, some characteristics can be found.

Analysis of the 320 nm delay profile for one and two exponential models is shown in Figure Ia. It can be noticed that at this emission wavelength, the fluorescence signal (crossed point) is almost the same as the excitation flash (dotted point, instrument response function) in width. This implies that a fast component with lifetime as short as or shorter than the instrument response time (~ 60 ps) may exist in the shorter wavelength range. It also can be seen that both residuals and autoccorelation functions are not improved by increasing the number of exponential from one to two. But the numerical analysis (Table Ia) shows a significant difference. The

Table I Lifetime analysis of ATP (0.1 mM) in phosphate buffer solution (pH 7.0)

$\lambda_{em}/\lambda_{exc}$: 320/265, file name: TA10acc

stdfit	α	τ	std err	f(α)	f(ατ)
4.0603e-3	1.010e+1	0.088	0.002		
4.0847e-3	4.959e-5	85.000	24042.560	0.000	0.005
	1.010e+1	0.088	0.003	1.000	0.995

b. $\lambda_{em}/\lambda_{exc}$: 350/265, file name: ta8cc1

stdfit	α	τ	std err	f(α)	f(ατ)
5.5340e-3	4.657e+0	0.198	0.004		
4.1831e-3	5.425e-2	2.380	0.404	0.008	0.132
	6.561e+0	0.129	0.004	0.992	0.868

c. $\lambda_{em}/\lambda_{exc}$: 390/265, file name: ta7acc

stdfit	α	τ	std err	f(α)	f(ατ)
9.5749e-3	1.851e+0	0.466	0.012		
3.6608e-3	1.548e-1	2.412	0.125	0.031	0.372
	4.766e+0	0.132	0.004	0.969	0.628
3.6365e-3	1.053e-1	2.953	0.894	0.021	0.307
	9.654e-2	1.015	0.944	0.019	0.097
	4.914e+0	0.123	0.009	0.961	0.596

single exponential model (first group of data) gives τ ~ 0.088 ns; two exponential model (second group of data) shows a deterioration of the standard fit and introduce an unrealistic second lifetime 85 ns with a standard error of ± 24 μs. Accordingly, it can be concluded that there exist single component with very fast decay (a discussion of the lower lifetime resolution capacity will be given later) at 320 nm.

On increasing the emission wavelength to 350 nm then to 390 nm, (Figure Ib and c) the width of the fluorescence signal increases gradually. This indicates that some slow components are probably present in the longer wavelength range. At λ_{em} of 350 nm, both residuals and autocorrelation function are considerably improved by increasing the number of exponential from one to two (Figure Ib), and this improvement can be see from the numerical analysis (table Ib). The standard fit is better for two-exponential fitting, and also it gives two reasonable lifetimes and standard errors (τ_1 ~ 0.129 ns, τ_2 = 2.4 ns ± 0.4). The fast component is still the major component since $f(\alpha_1) > 99\%$, $f(\alpha_2) < 1\%$, and $f(\alpha_1\tau_1) = 87\%$, $f(\alpha_2\tau_2) = 13\%$. Further increasing the number of exponential to three (data are not shown here), α_1 and α_2 remain the same and $\alpha_3 = 0$, which means that two exponential with a fast decay and slow decay (τ_2 = 2.4 ns) is the best model at this wavelength.

Similar to the situation at 350 nm, at emission 390 nm (Figure Ic, Table Ic) the standard fit, residuals and c(t) are significantly improved when changing the exponential from one to two. The two lifetimes are as same as those at 350 nm, but the contribution of emission from the slow component

is increased since $f(\alpha_1) = 97\%$, $f(\alpha_2) = 3\%$, and $f(\alpha_1\tau_1) = 63\%$, $f(\alpha_2\tau_2) = 37\%$. When the three-exponential model is used it only has a little improvement on standard fit (1%) and c(t) but the standard errors for the lifetimes are larger. Especially for the lifetime of 1.015 ns, its standard error is almost as large as the lifetime itself. Therefore, the two exponential are still the best model. However, three is possible. From the above analysis, the following points can be reached:

1. In the whole system, there were at least two emission components, the fast component with a lifetime $\tau_1 \approx 60$ ps (due to the instrument limit in lifetime resolution, see later), and the slow component with a lifetime τ_2 of 2.5 ns ± 0.2. The fast one is major component.

2. At the emission wavelength of 320 nm, only fast component exist since $f(\alpha)$ and $f(\alpha\tau)$ are around 100%.

3. Increasing the emission wavelength to 350 nm and then to 390 nm, more and more slow component is observed in addition to the fast one.

ii) TRS analysis

The time-windowed emission spectra (Figure II) were measured at delay time 0, and 2.0 ns relative to the time at the maximum of Rayleigh scatter as time zero, using a width of 100 ps for each window. The sharp peak at about 290 nm is Raman scatter, and a little bump in the range of 360-390 nm is due to monochromator grating holographic sensitivity. It can be seen that the shape of the fluorescence signal is different in two delay windows.

a.

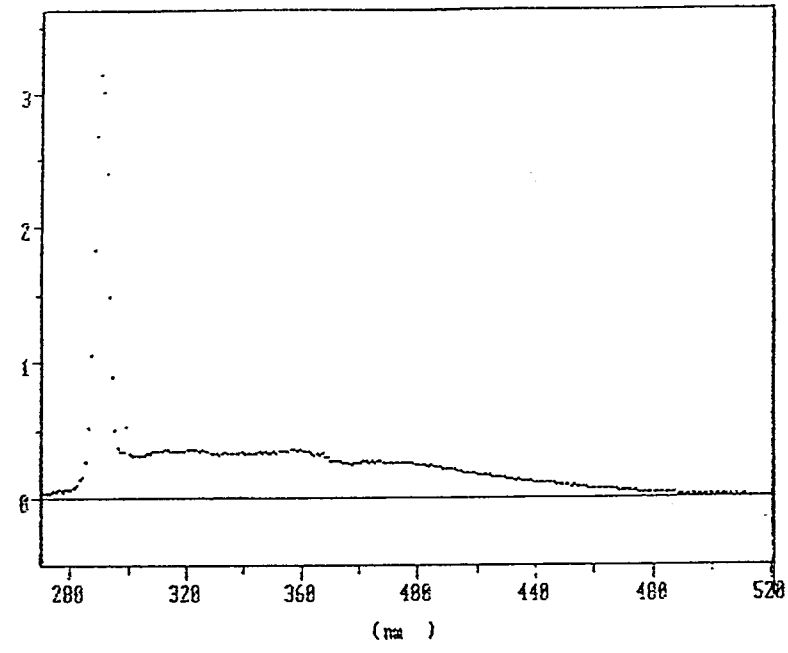

b.

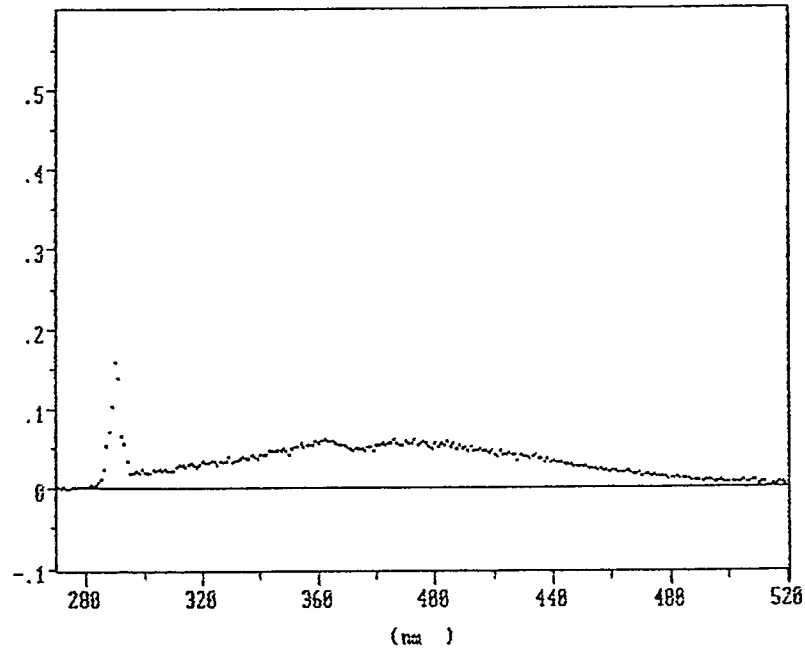

Figure II Time-windowed emission spectra of ATP (0.1mM) in phosphate buffer solution (pH 7.0). (a) 0 ns delay, (b) 2.0 ns delay.

In the early window (delay 0) the relative intensity of emitting signal in the short wavelength range is stronger than that in the longer wavelength range, while in the late window (delay 2.0 ns) the contribution of emitting signal in the short wavelength range is decreased. These imply that there exist at least two components (emitters) with different lifetimes, the fast component being at short wavelengths and the slow one at longer wavelengths.

In order to resolve the time-windowed emission spectra, the TRS program was applied, and then the resulted spectra (TRS) were corrected by dividing by the spectral sensitivities (Yingxian Fu, 1989). Finally, the corrected TRS were smoothed by linear regression smoothing factors, 9 points linear smoothing for fast emitting species and 15 for the slow. The normalized, smoothed and corrected time-resolved emission spectra (in terms of α) of ATP in neutral buffer solution with τ_1 = .060 ns, and τ_2 = 2.5 ns are shown in Figure III.

We can see clearly from Figure III that the convoluted spectra have been successfully separated into two individual spectra. The ratio of integrating α ($[\alpha] = \int^{\lambda}\alpha(\lambda)d\lambda$) of fast component (C1) to slow component (C2) is 101, which indicates that the fast component with the peak at 310 nm is predominant and the slow component with the peak at 385 nm is two orders of magnitude smaller than the fast one. It should be mentioned that for comparison with steady state spectra and quantum yields, account must be taken of lifetimes of the species. Three-component analysis was tried using

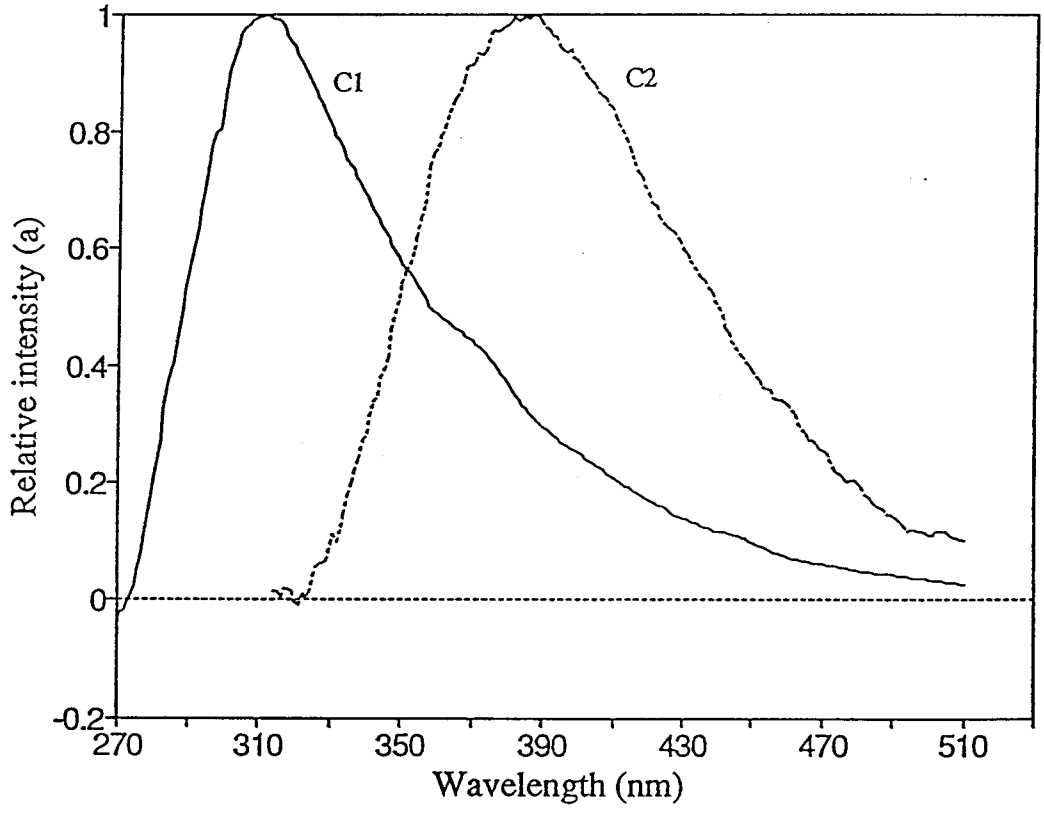

Figure III Corrected time-resolved emission spectra of ATP (0.1 mM) in phosphate buffer solution (pH 7.0). τ_1 = 0.06 ns, τ_2 = 2.5 ns are used. (C1) fast component, (C2) slow component. $[\alpha_1]/[\alpha_2]$ = 101.

three time-windowed spectra (delay 0, 1.0, and 2.0 ns) and three lifetimes of 0.06, 2.5 and 1.0 ns, but the results were not satisfactory because a large negative spectrum was always occurred in one of the three component spectra.

ATP (0.1mM) in acidic solution (pH1.1)

i) Lifetime analysis

The decay profiles of ATP in acidic solution ($HClO_4$, pH 1.1) as well as their residuals and autocorrelation functions (c(t)) at different emission wavelengths following the excitation at 265 nm are shown in Figure IVa, b and c. The detailed numerical results of lifetime analysis for various exponential models are listed in Table IIa, b and c.

From the decay profiles we can observe the following. In contrast to ATP in neutral buffer solution, the width of fluorescence signal in acidic solution is much greater in time scale than that of the excitation flash (dotted point) at all emission wavelengths, which immediately suggests that there exists a considerable amount of slow component with lifetime much longer than instrumental response time.

Figure IVa shows the analysis of the 320 nm decay profiles for one to three exponential models. It can be seen that both residues and autocorrelation functions are improved significantly by changing the exponential model from one to two. The corresponding numerical analysis

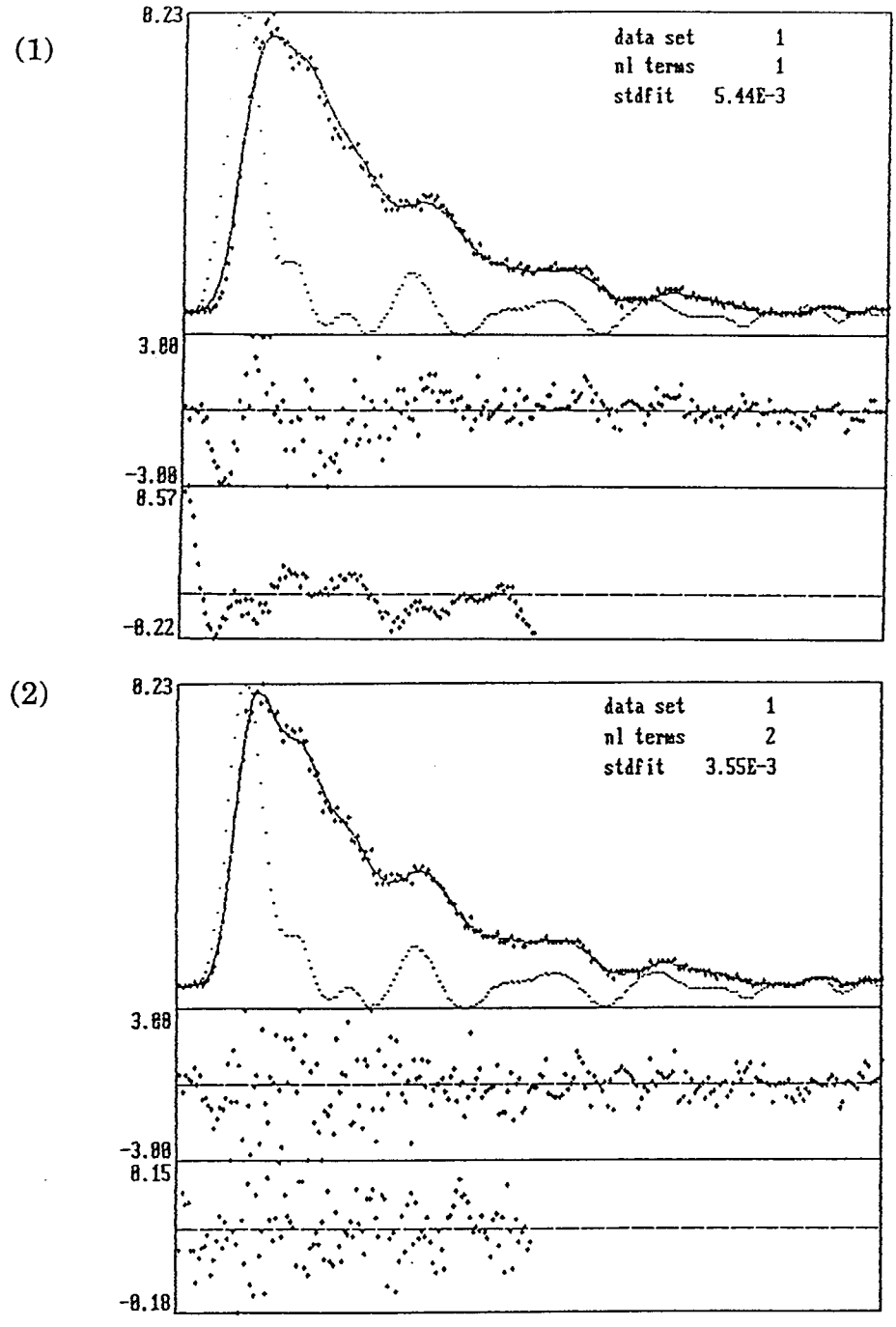

Figure IVa Decay profiles of ATP (0.1 mM) in $HClO_4$ aqueous solution (pH 1.1) at λ_{em} 320 nm. Time delay range: 15-40 ns. (1) one-exponential, (2) two exponential, (3) three exponential.

Figure IVa, continued

(3)

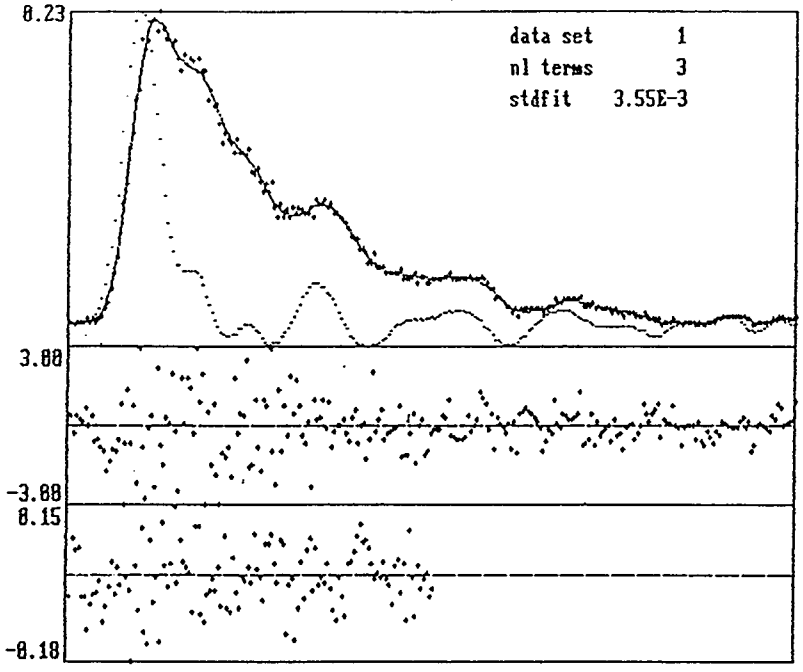

(1)

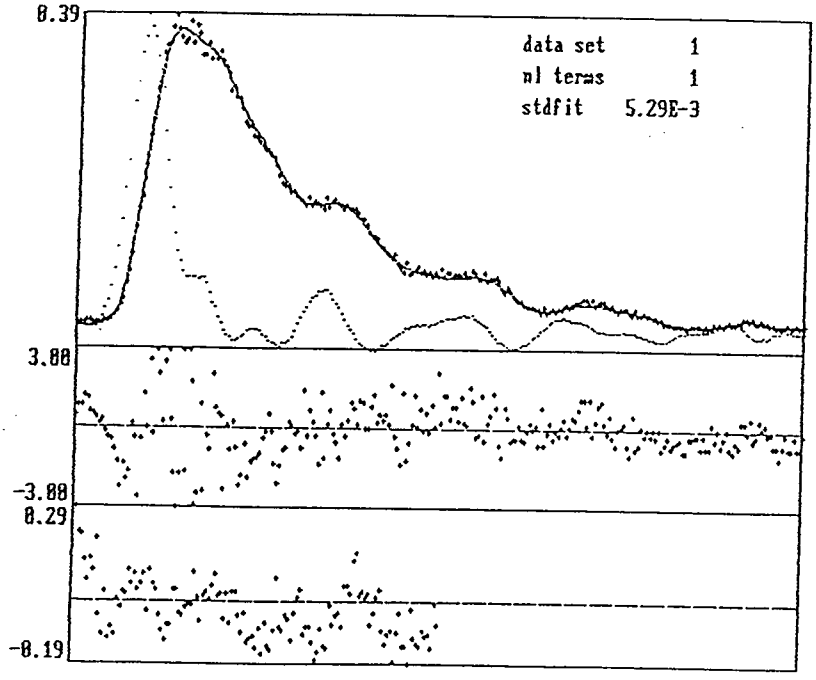

(2)

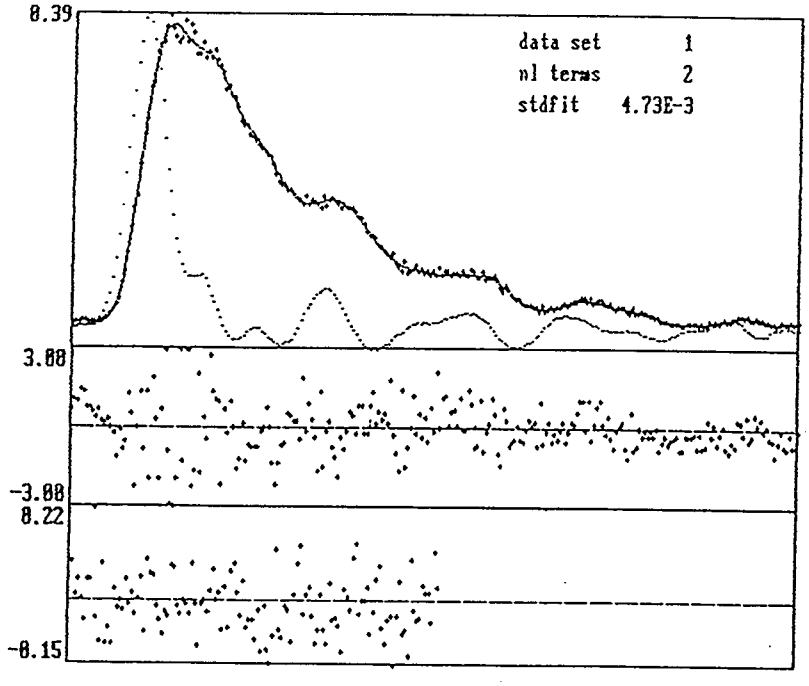

Figure IVb Decay profiles of ATP (0.1 mM) in $HClO_4$ aqueous solution (pH 1.1) at λ_{em} 350 nm. Time delay range: 15-40 ns. (1) one-exponential, (2) two exponential, (3) three exponential.

Figure IVb, continued

(3)

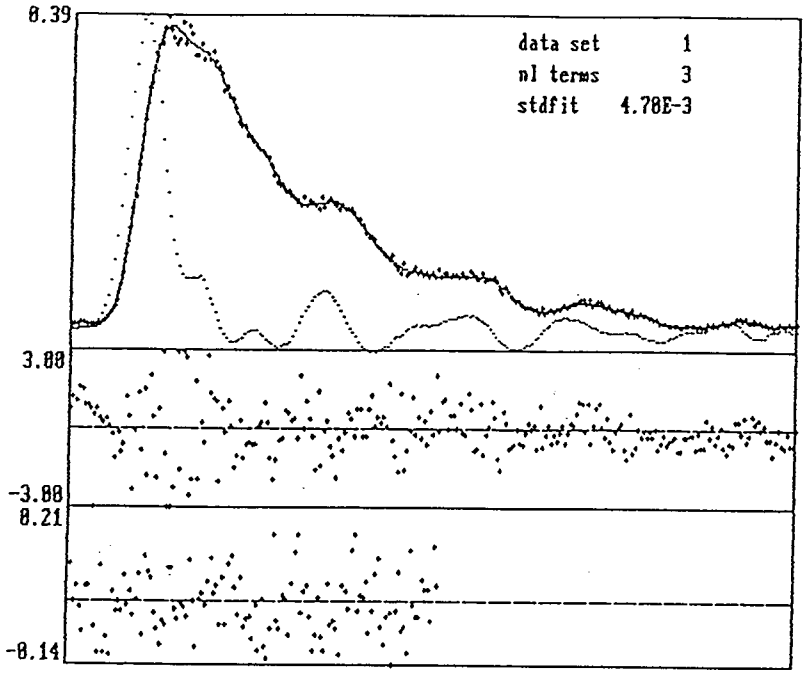

(1)

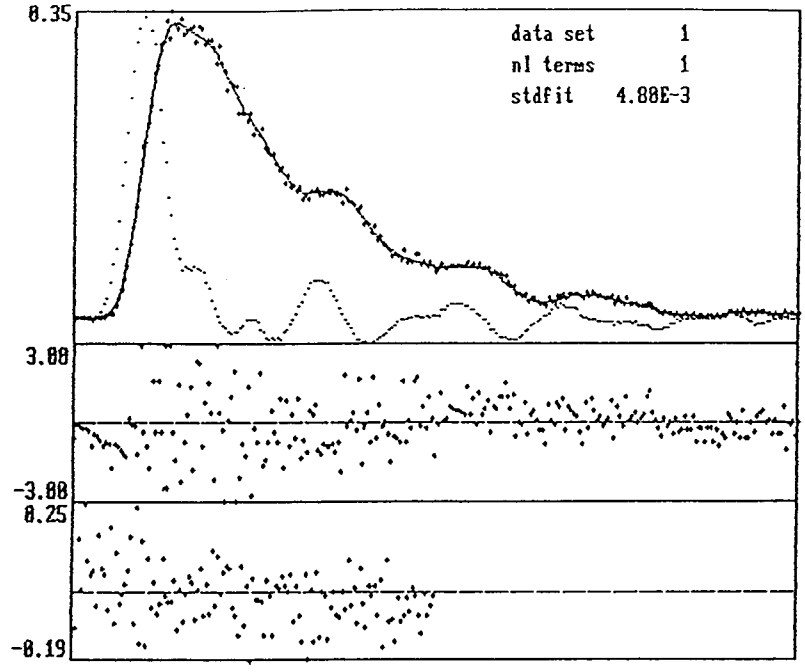

(2)

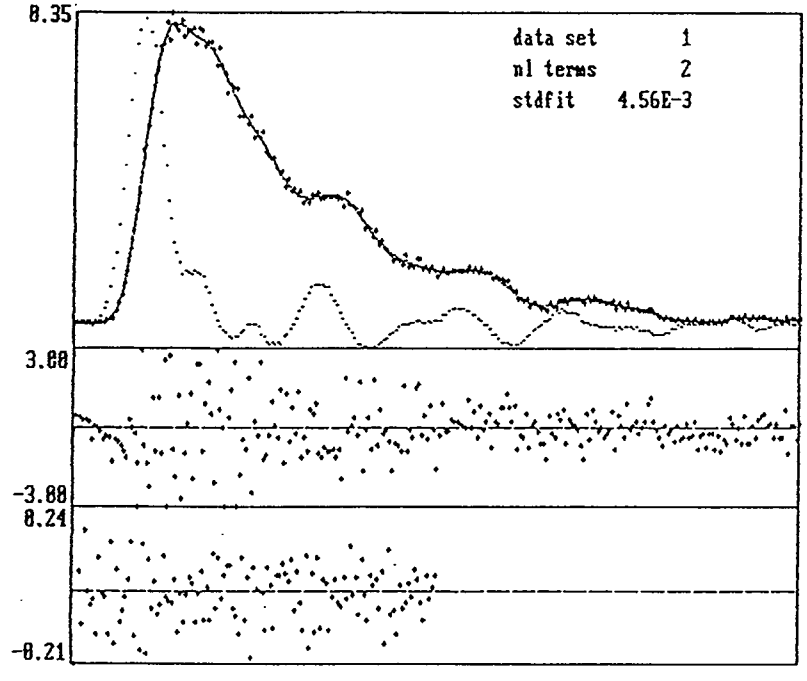

Figure IVc Decay profiles of ATP (0.1 mM) in $HClO_4$ aqueous solution (pH 1.1) at λ_{em} 390 nm. Time delay range: 15-40 ns. (1) one-exponential, (2) two exponential, (3) three exponential.

Figure IVc, continued

(3)

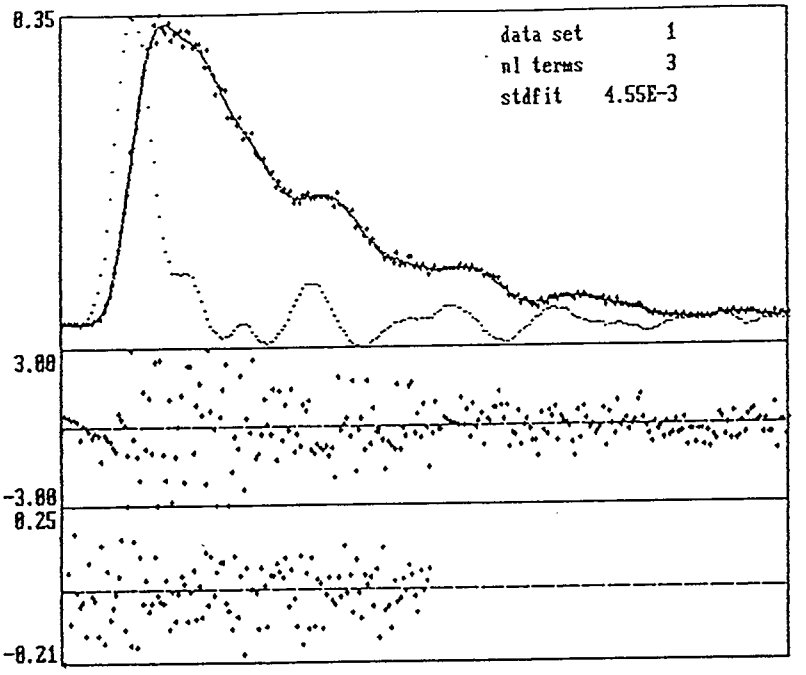

Table II Lifetime analysis of ATP (0.1 mM) in $HClO_4$ solution (pH 1.1)

a. $\lambda_{em}/\lambda_{exc}$: 320/265, file name: TAA1AC

sdtfit	α	τ	std err	f(α)	f(ατ)
5.4718e-3	4.634e-1	4.038	0.044		
3.5896e-3	3.880e-1	4.403	0.048	0.109	0.916
	3.179e+0	0.049	0.011	0.891	0.084
3.6038e-3	3.867e-1	4.412	0.130	0.108	0.915
	4.158e-3	0.959	10.093	0.001	0.002
	3.199e+0	0.048	0.020	0.891	0.083

b. $\lambda_{em}/\lambda_{exc}$: 340/265, file name: TAA2AC

std fit	α	τ	std err	f(α)	f(ατ)
5.3232e-3	7.289e-1	4.299	0.027		
4.7740e-3	6.813e-1	4.436	0.037	0.399	0.957
	1.028e+0	0.131	0.024	0.601	0.043
4.7658e-3	6.633e-1	4.531	0.119	0.335	0.947
	4.789e-2	1.172	1.335	0.024	0.018
	1.272e+0	0.089	0.044	0.641	0.036

c. $\lambda_{em}/\lambda_{exc}$: 390/265, file name: TAA4AC

std fit	α	τ	std err	f(α)	f(ατ)
4.8274e-3	6.929e-1	4.469	0.028		
4.6098e-3	4.226e-1	5.419	0.820	0.596	0.715
	2.870e+0	3.174	0.819	0.404	0.285
4.6163e-3	4.904e-1	5.237	0.683	0.584	0.804
	2.219e-1	2.800	1.063	0.264	0.194
	1.281e-1	0.048	0.435	0.152	0.002

(Table IIa) gives consistent result. It shows that the standard fit is improved considerably and the standard errors of the two lifetimes are reasonably small for two exponential fitting. The fast component has τ_1 ~ 100 ns (due to the limit of lifetime resolution), and the slow one has τ_2 of 4.4 ns ± 0.05. Contrary to ATP in neutral buffer solution, the major component in acidic solution is slow component since the fractions of total emission $f(\alpha_1\tau_1)$ = 8%, and $f(\alpha_2\tau_2)$ = 92%, although the fractions of initial emission go another way around. Further increasing the number of exponential to three (Figure Vb and Table IIb) there are no improvements on standard fit or in residuals and c(t), and also the standard error of the 0.96 ns lifetime for the third component is one order greater than the lifetime itself, which is not reasonable. Therefore, the two exponential is the best model at 320 nm.

At λ_{em} of 340 nm (Figure IVb), the situation are almost as same as that at 320 nm. There are considerable improvements in residuals and c(t) when changing the exponential model from one to two, the standard fit (Table IIb) is improved significantly for two exponential fitting, the two lifetimes are basically the same as those at 320 nm, and their standard errors are small. The fraction of the fast component $f(\alpha_1\tau_1)$ decreases to 4% and the slow $f(\alpha_2\tau_2)$ is 96%. Increasing the number of exponential to three, neither the standard fit, the residuals nor c(t) are improved significantly, and the standard errors of the lifetimes are larger, especially in the case of the third component, whose error is larger than the lifetime (1.172 ns). Thus, the two exponential model is still probably the best model although three exponential is possible.

At the longest emission wavelength 390 nm (Figure IVc and Table IIc), the situation is different. It can be noticed that the single exponential fitting is much better than that at 320 and 340 nm. When increasing the number of exponential to two and three, the improvement on standard fit, residuals and c(t) is not as larger as at above two wavelengths, and the errors of the lifetimes are larger. It is safe to say that the predominant component is the slow one (τ_2 = 4.5 ns) at this wavelength. Accordingly, the single exponential should be the proper model to describe this.

Based on above lifetime analysis, the following characteristics can be summarized:

1. There are at least two emitting components in the whole system, the fast one with τ_1 ~ 100 ps, and the slow one with τ_2 of 4.4 ns ± 0.5. The major component is the slow one.

2. At λ_{em} of 320 and 340 nm, two exponential model is the best model, but at 340 nm three exponential is possible. The fraction of fast component decreases with increasing the wavelength.

3. With increasing emission wavelength to 390 nm, only the slow component exists.

ii) TRS analysis

Two time-windowed spectra with delay time 0 and 1.0 ns and width of 100 ps for each window are shown respectively in Figure Va and b. Unlike ATP in neutral buffer solution, the intensity ratio of Raman to fluorescence

a.

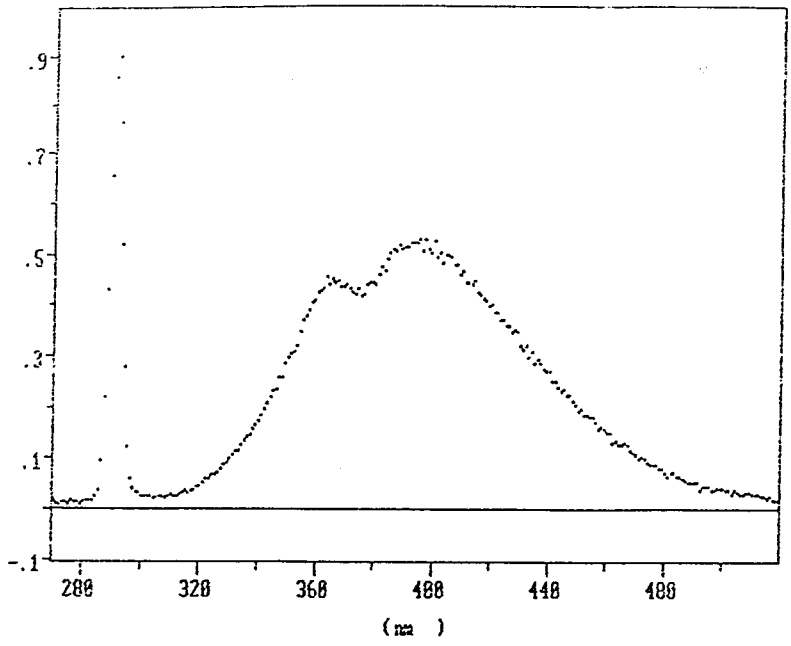

b.

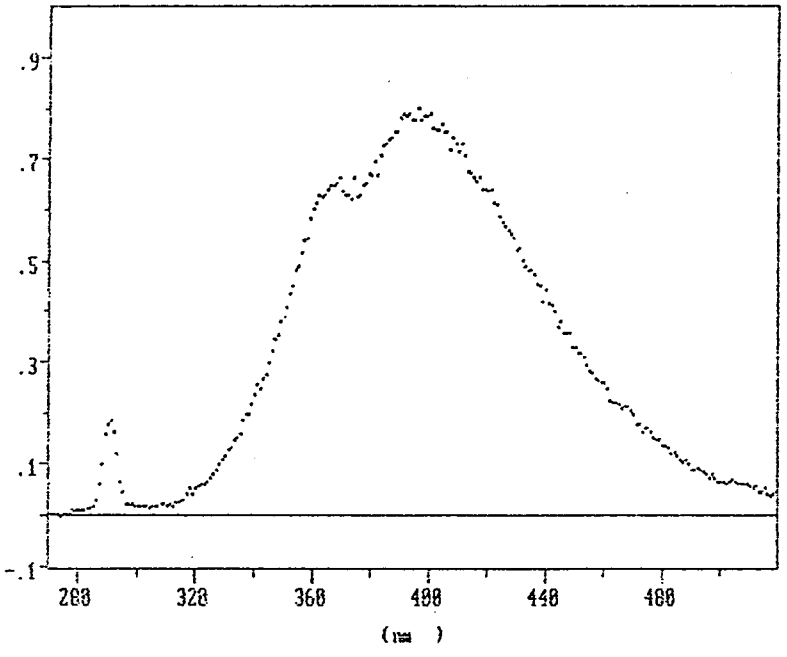

Figure V Time-windowed spectra of ATP (0.1mM) in $HClO_4$ solution (pH 1.1). (a) 0 ns delay, (b) 1.0 ns delay

signal of ATP in acidic solution is much smaller, which indicates that the quantum yield of fluorescence in acidic solution is much greater than that in buffer solution. Again the difference in the shape of emission can be observed by comparing the two delay windows, which means that more than one emitting component exists, the slow one lying at the longer wavelength. These time-windowed spectra were successfully resolved into two individual spectra by applying TRS program using τ_1 = 100 ps and τ_2 = 4.4 ns. And then the resolved spectra were corrected for the spectral sensitivity and smoothed with 9-point linear smoothing factor (Figure VI). It should be kept in mind that the ordinate in TRS is the relative intensity in terms of the pre-exponential $\alpha(\lambda)$. Figure VI represents this in the same way as Figure III, i.e. the wavelength integrated α value of slow component (C2) is 2.9 times smaller than that of fast component (C1). When account is taken of lifetimes of the species, i.e. integrating [α] with respect to time, then the slow component is by far predominant. A striking characteristic is that the time-resolved spectra of these two individual components are almost overlapped completely. Without TRS program it is hard to imagine that one could separate multicomponents from overlapped band. How charming the TRS program is!

Three component analysis was tried using three time-windowed spectra with delay 0, 1.0 and 2.0 ns respectively and lifetimes of 0.1, 1.0 and 4.4 ns, but the result is not satisfied because one of the resolved spectra is either zero or negative.

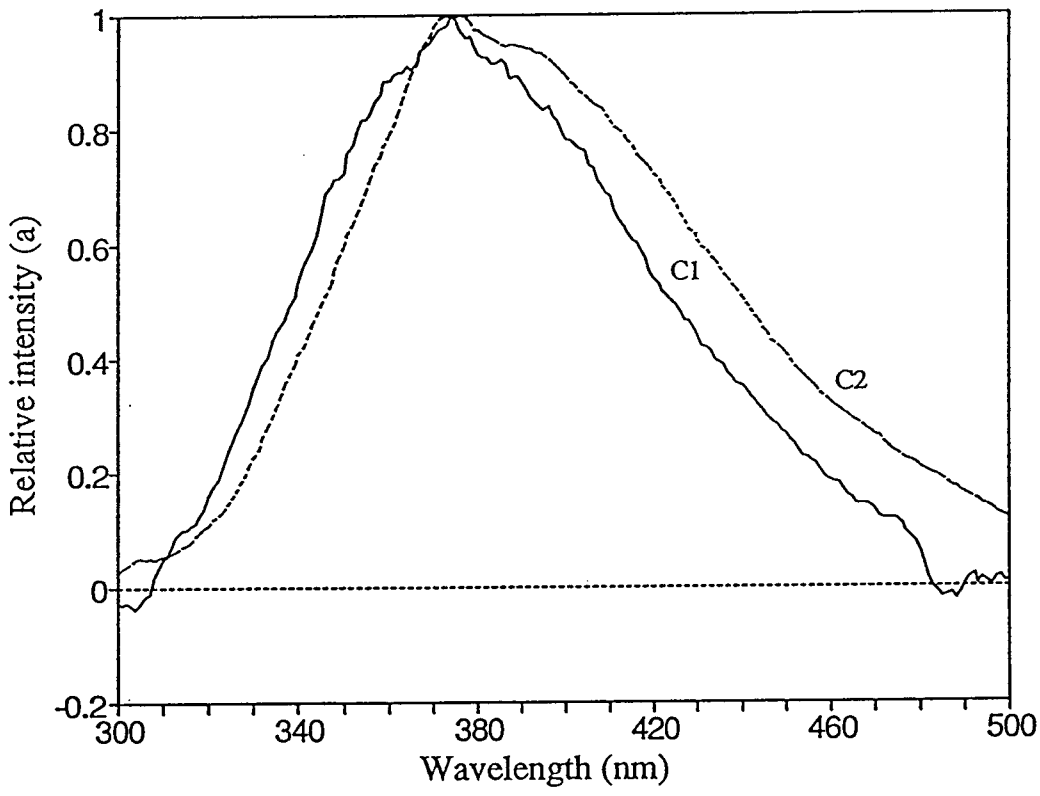

Figure VI Corrected time-resolved emission spectra of ATP (0.1 mM) in $HClO_4$ solution (pH 1.1). τ_1 = 0.1 ns, τ_2 = 4.4 ns are used. (C1) fast component, (C2) slow component. $[\alpha_1]/[\alpha_2]$ = 2.9.

II. Estimation of lifetime resolution limit

In order to estimate lifetime resolution limit under our experimental condition, and to check how well the NLLS reiterative convolution (SPLMOD) program works on the resolution of lifetimes from the decay data, simulated data were created by convoluting a flash (Raman scatter including instrumental noise) with the desired pure exponential terms as the input values. Then, the simulated data were deconvoluted using SPLMOD program to obtain the output values The comparison of the input and output values of lifetimes for one emission component system is shown in Figure VII, and their % errors are shown in Figure VIII.

It can be seen well that the lifetime above 200 ps can have a good resolution. When the input lifetime is 100 ps, 5% error occurs in the extracted lifetime, and when the input is 50 ps, 30% error results. These indicate that the lifetimes above 100 ps from SPLMOD program are relatively reliable, and the lifetime below 100 ps is reliable. It should be mentioned that above analysis is only applied to a single component system. In the case of multicomponent system, the limit of the lifetime resolution may be worse than this.

The lowest lifetime resolution limit was also be estimated by taking Raman scatter as sample and Rayleigh scattter as excitation flash in ATP neutral buffer solution. The analysis gave a fast lifetime of 60 ps, which indicates that 60 ps is the instrument response time.

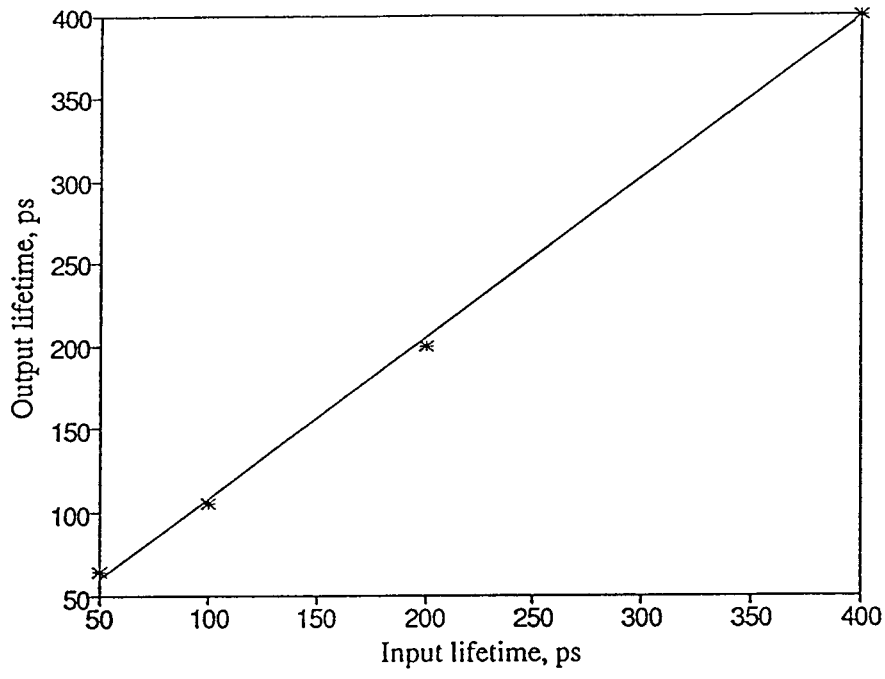

Figure VII Comparison of input and output values of lifetimes in single component system.

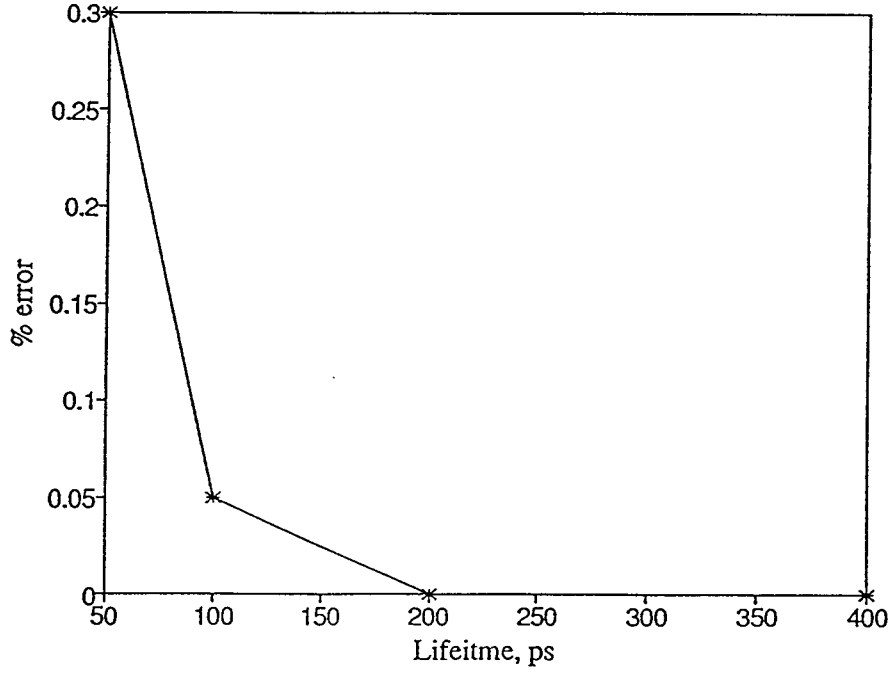

Figure VIII % error on lifetime analysis from simulated data.